Astro/Phys 224 Spring 2014

Origin and Evolution of the Universe

Week 6

Simulations

Joel Primack

University of California, Santa Cruz

TOP HAT
Max Expansion

VIOLENT RELAXATION

VIRIALIZED

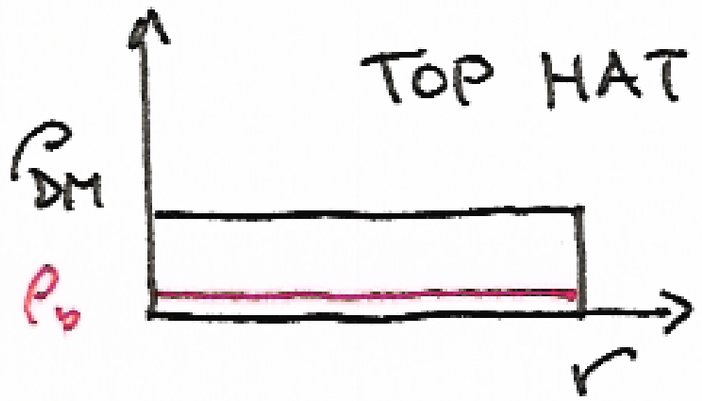

Virial Theorem: $\langle K \rangle = -\frac{1}{2}\langle W \rangle$

$-W_m = \frac{C}{r_m}$, so after virialization

$$-\frac{C}{r_m} = E = W + K = \frac{1}{2}\langle W \rangle = -\frac{C}{2r_v}$$

$$\Rightarrow r_v = \frac{1}{2} r_m, \quad \rho_v = 8\rho_m \approx 50\,\bar{\rho}(t_m)$$

$$\langle v^2 \rangle \approx \frac{GM}{r_v}$$

Spherical Collapse

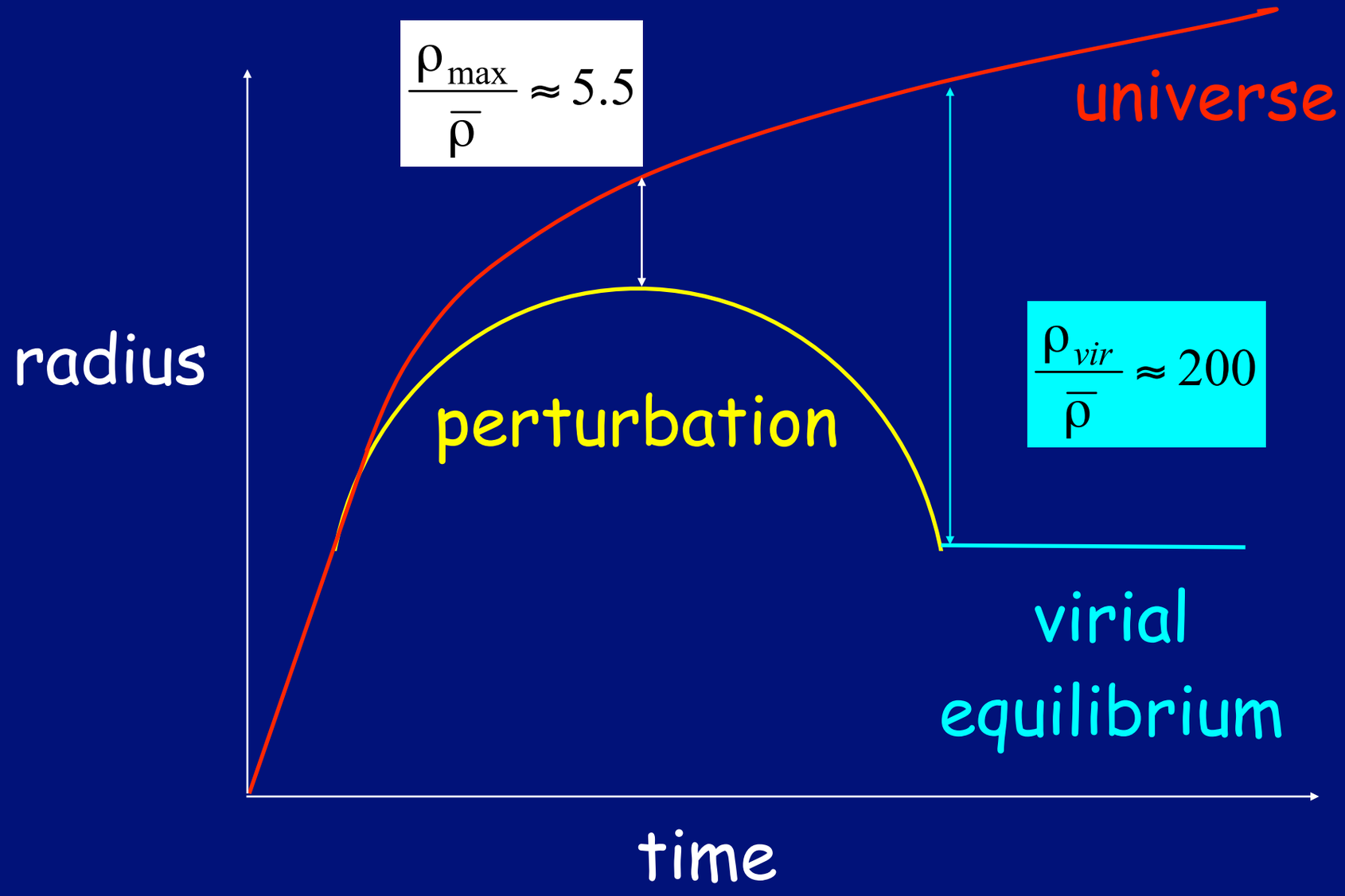

virial equilibrium: $E = -\frac{1}{2}\frac{GM}{R_{vir}} = -\frac{GM}{R_{\max}}$

Growth and Collapse of Fluctuations

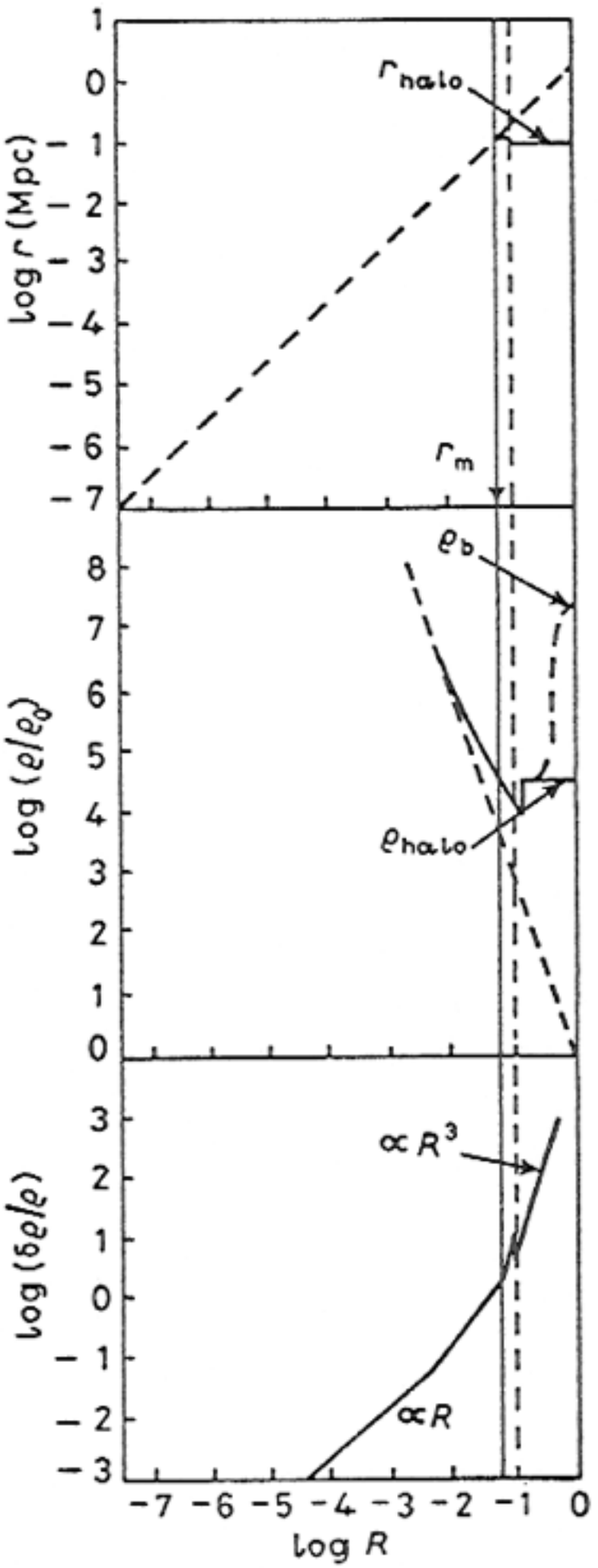

Schematic sketches of radius, density, and density contrast of an overdense fluctuation. It initially expands with the Hubble expansion, reaches a maximum radius (solid vertical line), and undergoes violent relaxation during collapse (dashed vertical line), which results in the dissipationless matter forming a stable halo. Meanwhile the ordinary matter ρ_b continues to dissipate kinetic energy and contract, thereby becoming more tightly bound, until dissipation is halted by star or disk formation, explaining the origin of galactic spheroids and disks.

(This was the simplified discussion of BFPR84; the figure is from my 1984 lectures at the Varenna school. Now we take into account halo growth by accretion, and the usual assumption is that spheroids form mostly as a result of galaxy mergers Toomre 1977. Also, we now know that most of the baryons in halos don't cool and fall to the center.)

Halo and Galaxy Merging and Spheroid Formation

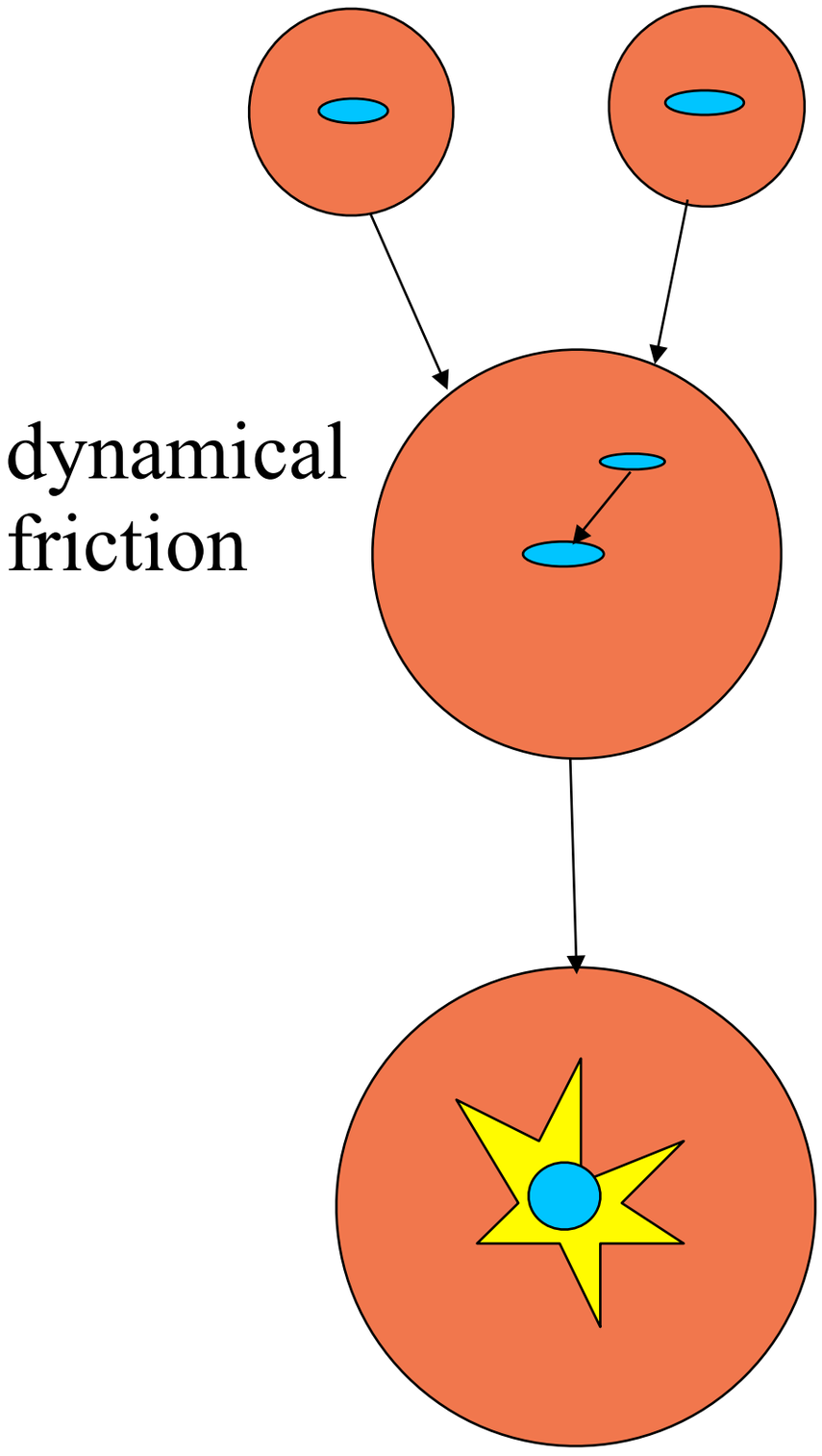

mergers can trigger starburst, forming spheroid

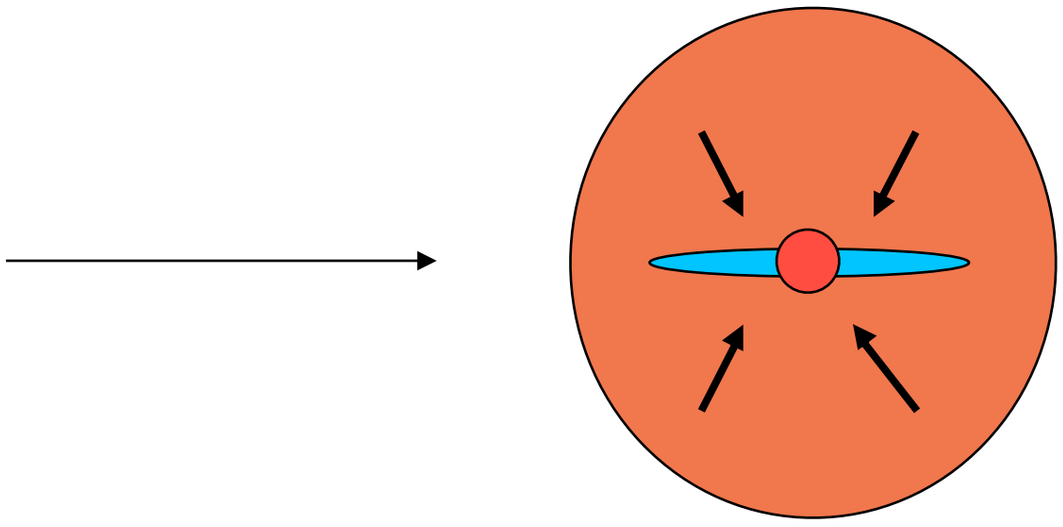

subsequent cooling forms disk

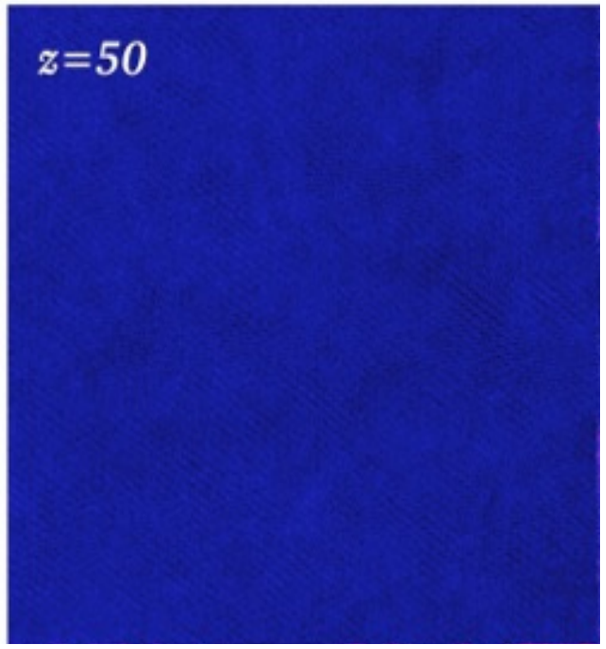

N-body simulation

ΛCDM

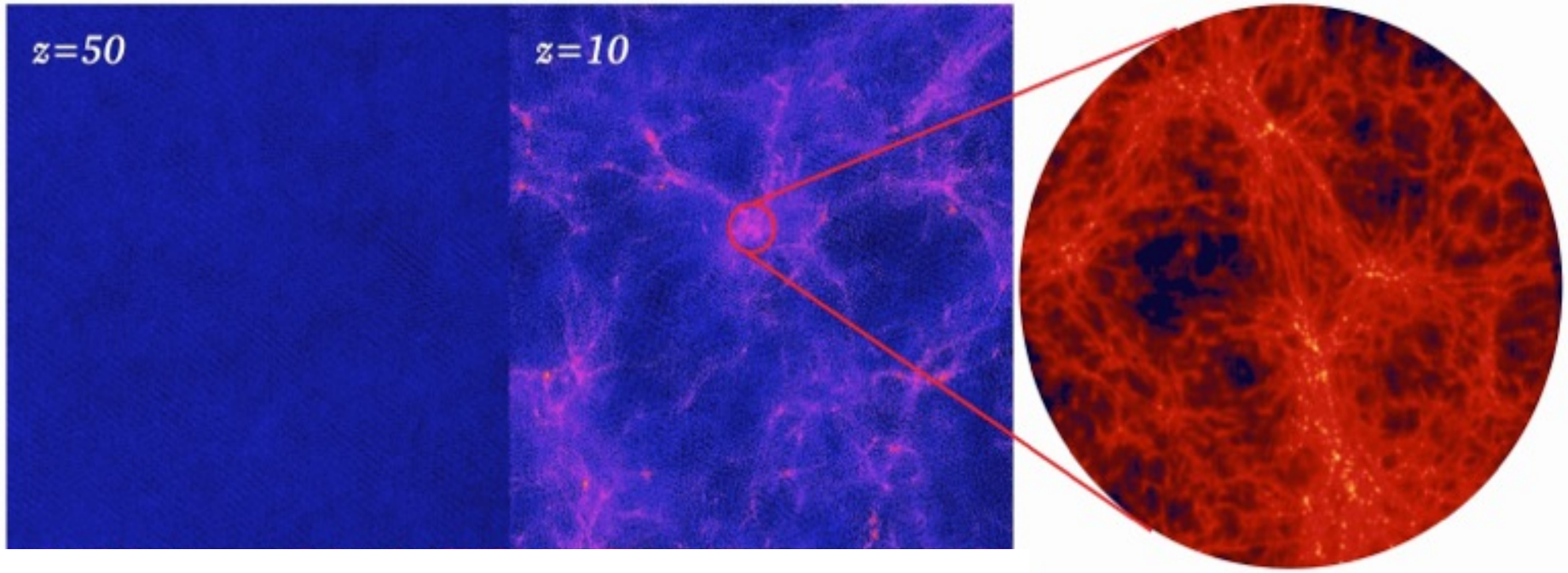
z=50
z=10

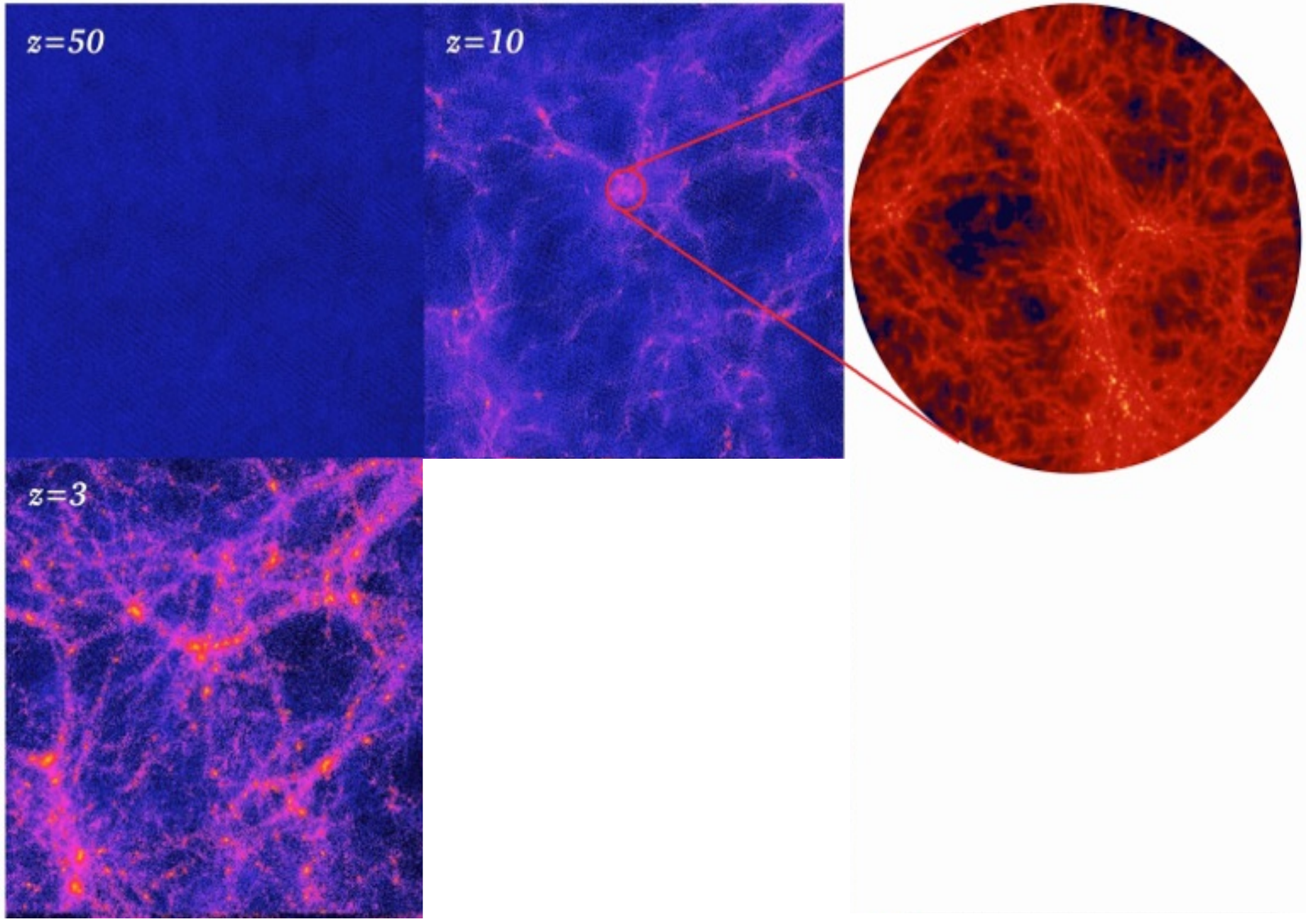
z=50
z=10
z=3

z=49.000

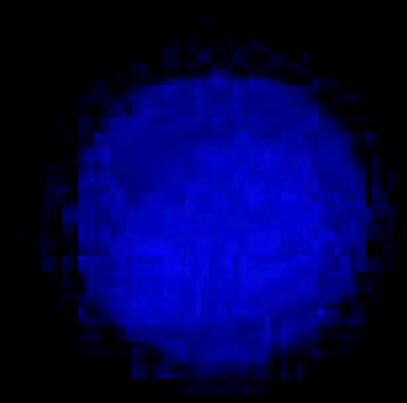

Expansion....

z=49.0t
=49 Myr

z=12.0
t=374Myr

z=2.95
t=2.23 Gyr

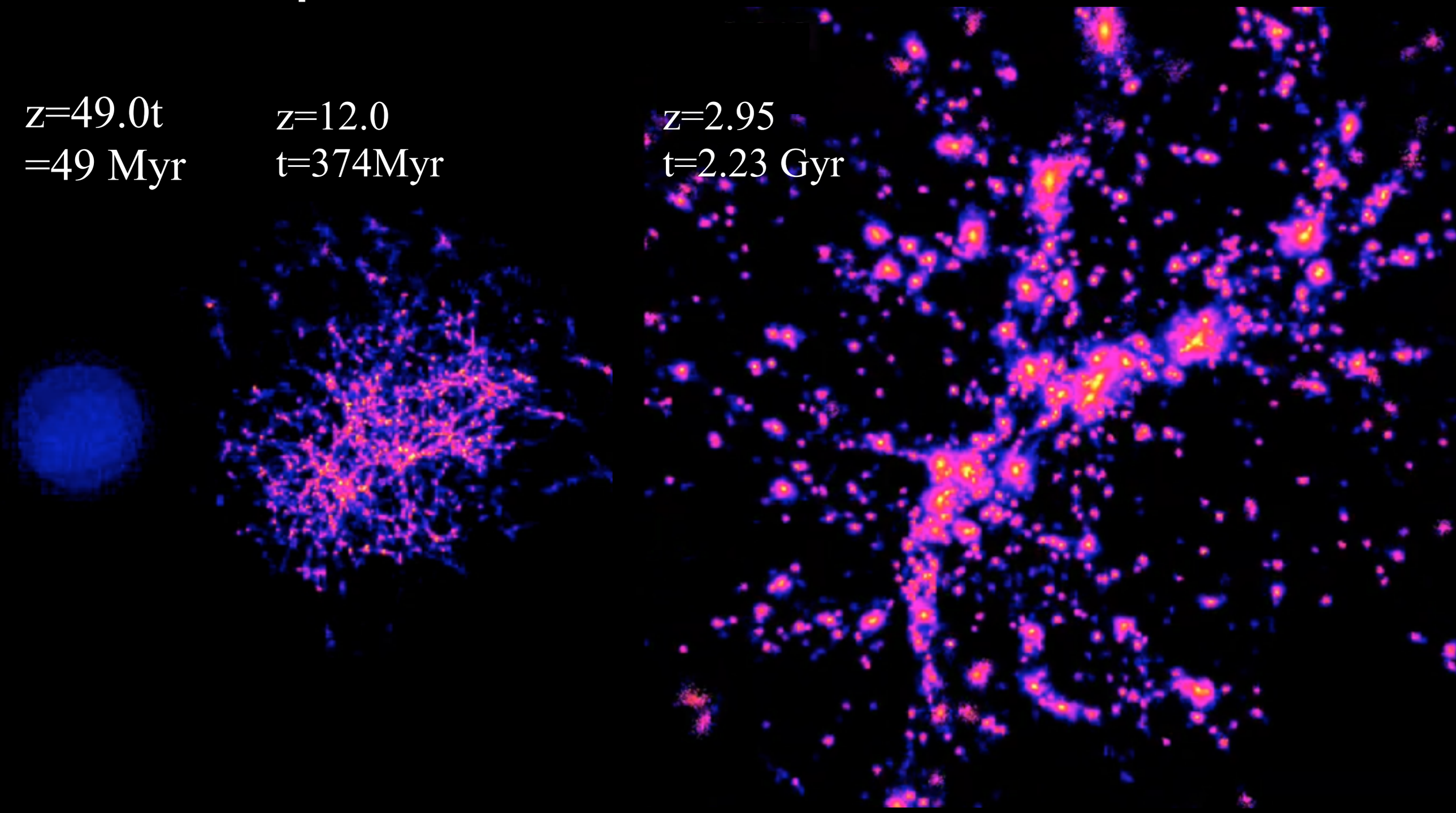

z=49.000 t= 6.66 Gyr

End of expansion
for this halo

z= 0.391 t= 9.48 Gyr

Wild
Space

Tame
Space

z= 0.391 t= 9.48 Gyr

Wild Space

Tame Space

z= 0.000 t= 13.7 Gyr (today)

Wild Space

Tame Space

Dark Matter Halo Structure

log ρ

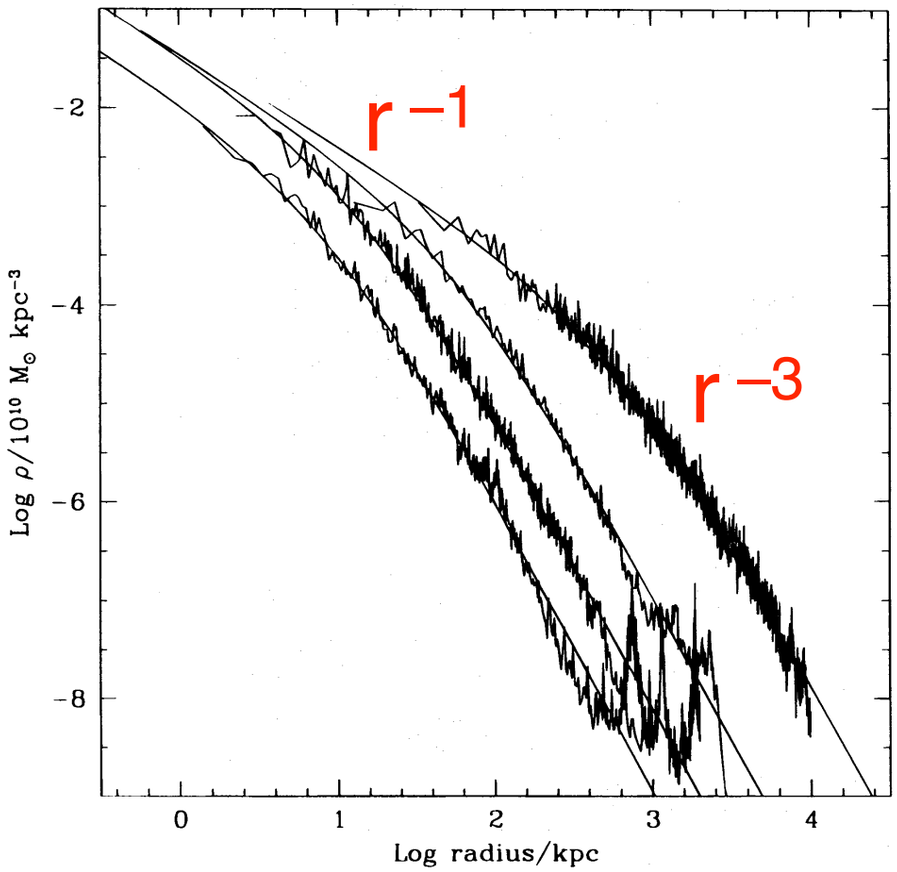

log r

log V_{circ}

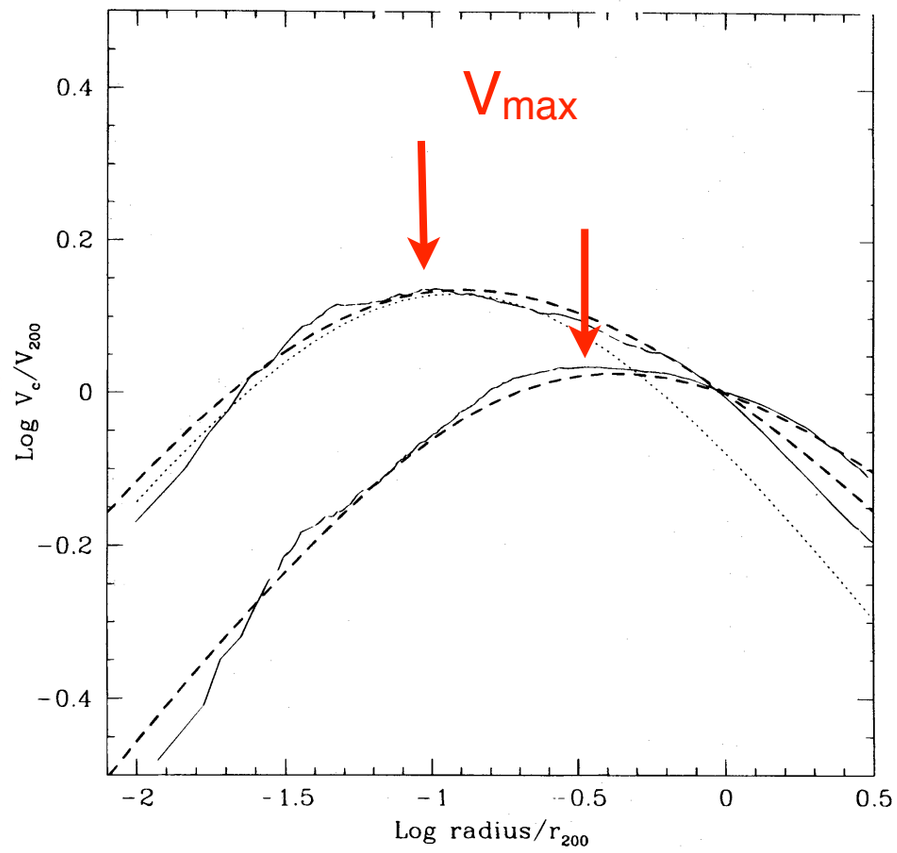

log r

1996 - Navarro, Frenk, & White: DM halo structure $\rho_{NFW}(r) = 4\ \rho_s\ (r/r_s)^{-1}(1+r/r_s)^{-2}$

2001 - Bullock et al.: concentration-mass-z relation for DM halos; universal angular momentum structure of DM halos

2002 - Wechsler et al.: halo concentration from mass assembly history $M(z) = M_0\ e^{-\alpha z}$

2003-present - Large Scale Structure surveys, WMAP and Planck CMB observations confirm ΛCDM predictions with increasing precision

Dark Matter Halo Structure

Navarro, Frenk, White

1996 1997 →

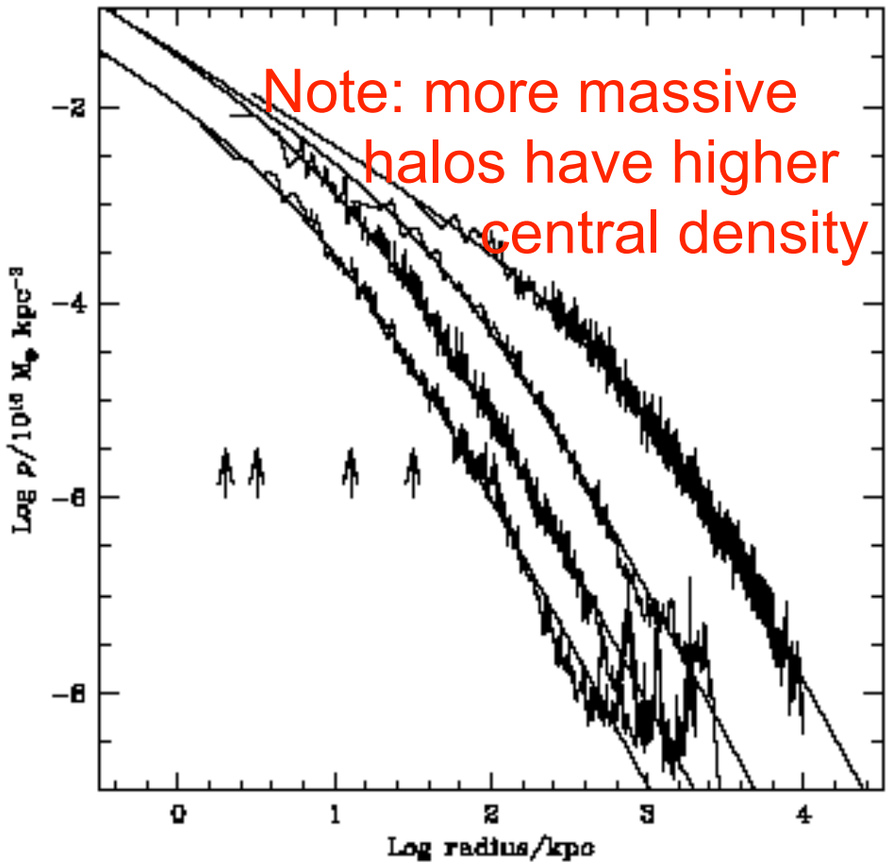

Note: more massive halos have higher central density

Fig. 3.— Density profiles of four halos spanning four orders of magnitude in mass. The arrows indicate the gravitational softening, h_g, of each simulation. Also shown are fits from eq.3. The fits are good over two decades in radius, approximately from h_g out to the virial radius of each system.

$$\frac{\rho(r)}{\rho_{crit}} = \frac{\delta_c}{(r/r_s)(1+r/r_s)^2}, \qquad (3)$$

NFW is a good approximation for <u>all</u> cosmologies

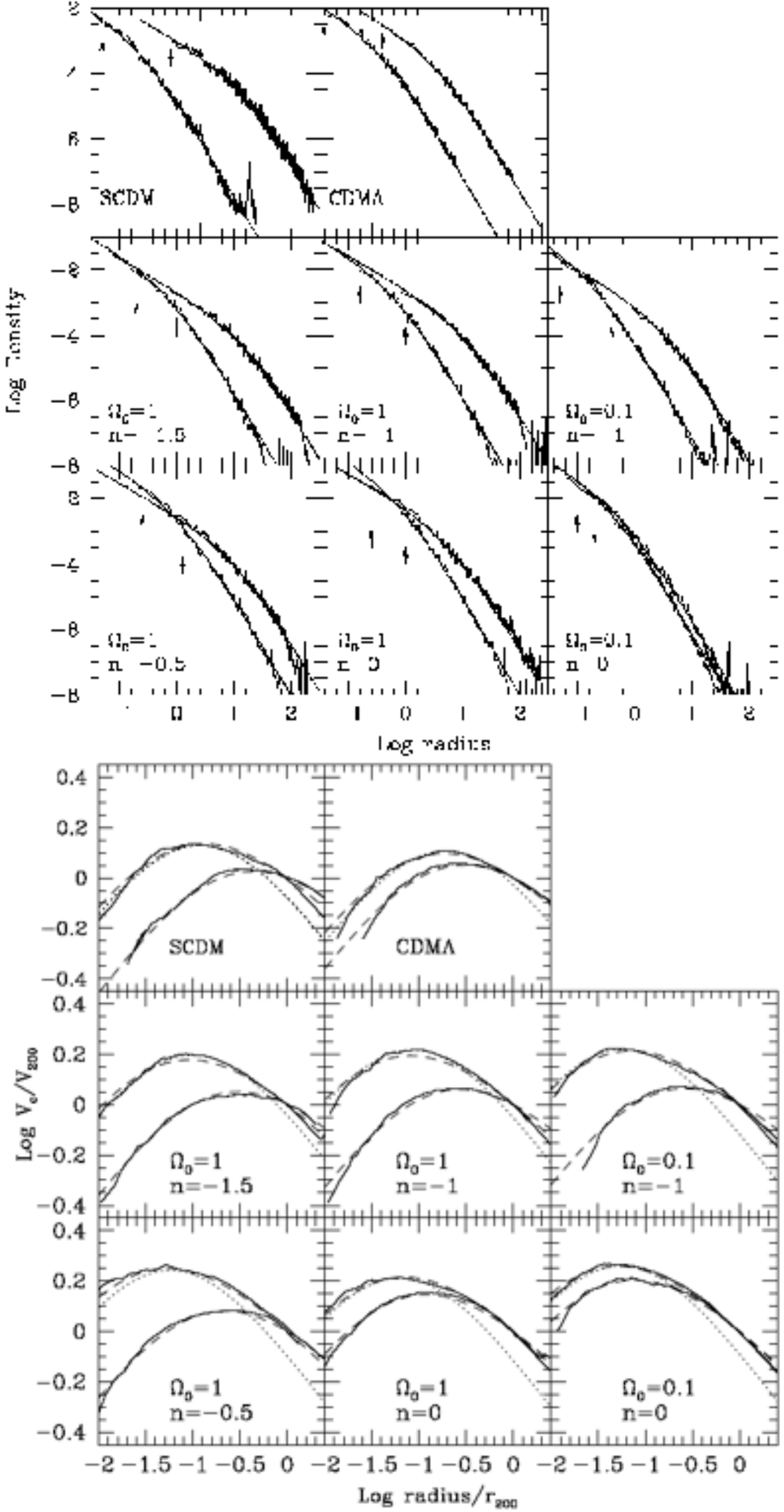

Dark Matter Halo Radial Profile

Comparison of NFW and Moore et al. profiles

Parameter	NFW	Moore et al.
Density $x = r/r_s$	$\rho = \frac{\rho_s}{x(1+x)^2}$ $\rho \propto x^{-3}$ for $x \gg 1$ $\rho \propto x^{-1}$ for $x \ll 1$ $\rho/\rho_s = 1/4$ at $x = 1$	$\rho = \frac{\rho_s}{x^{1.5}(1+x)^{1.5}}$ $\rho \propto x^{-3}$ for $x \gg 1$ $\rho \propto x^{-1.5}$ for $x \ll 1$ $\rho/\rho_s = 1/2$ at $x = 1$
Mass $M = 4\pi\rho_s r_s^3 f(x)$ $= M_{\rm vir} f(x)/f(C)$ $M_{\rm vir} = \frac{4\pi}{3}\rho_{\rm cr}\Omega_0\delta_{\rm top-hat} r_{\rm vir}^3$	$f(x) = \ln(1+x) - \frac{x}{1+x}$	$f(x) = \frac{2}{3}\ln(1+x^{3/2})$
Concentration $C = r_{\rm vir}/r_s$	$C_{\rm NFW} = 1.72 C_{\rm Moore}$ for halos with the same $M_{\rm vir}$ and $r_{\rm max}$ $C_{1/5} \approx \frac{C_{\rm NFW}}{0.86 f(C_{\rm NFW}) + 0.1363}$ error less than 3% for $C_{\rm NFW}$ =5-30 $C_{\gamma=-2} = C_{\rm NFW}$	$C_{\rm Moore} = C_{\rm NFW}/1.72$ $C_{1/5} = \frac{C_{\rm Moore}}{[(1+C_{\rm Moore}^{3/2})^{1/5} - 1]^{2/3}}$ $\approx \frac{C_{\rm Moore}}{[C_{\rm Moore}^{3/10} - 1]^{2/3}}$ $C_{\gamma=-2} = 2^{3/2} C_{\rm Moore}$ $\approx 2.83 C_{\rm Moore}$
Circular Velocity $v_{\rm circ}^2 = \frac{GM_{\rm vir}}{r_{\rm vir}}\frac{C}{x}\frac{f(x)}{f(C)}$ $= v_{\rm max}^2 \frac{x_{\rm max}}{x}\frac{f(x)}{f(x_{\rm max})}$ $v_{\rm vir}^2 = \frac{GM_{\rm vir}}{r_{\rm vir}}$	$x_{\rm max} \approx 2.15$ $v_{\rm max}^2 \approx 0.216 v_{\rm vir}^2 \frac{C}{f(C)}$ $\rho/\rho_s \approx 1/21.3$ at $x = 2.15$	$x_{\rm max} \approx 1.25$ $v_{\rm max}^2 \approx 0.466 v_{\rm vir}^2 \frac{C}{f(C)}$ $\rho/\rho_s \approx 1/3.35$ at $x = 1.25$

Klypin, Kravtsov, Bullock & Primack 2001

Micro-Macro Connection

Cold Dark Matter

Hot Dark Matter

ν

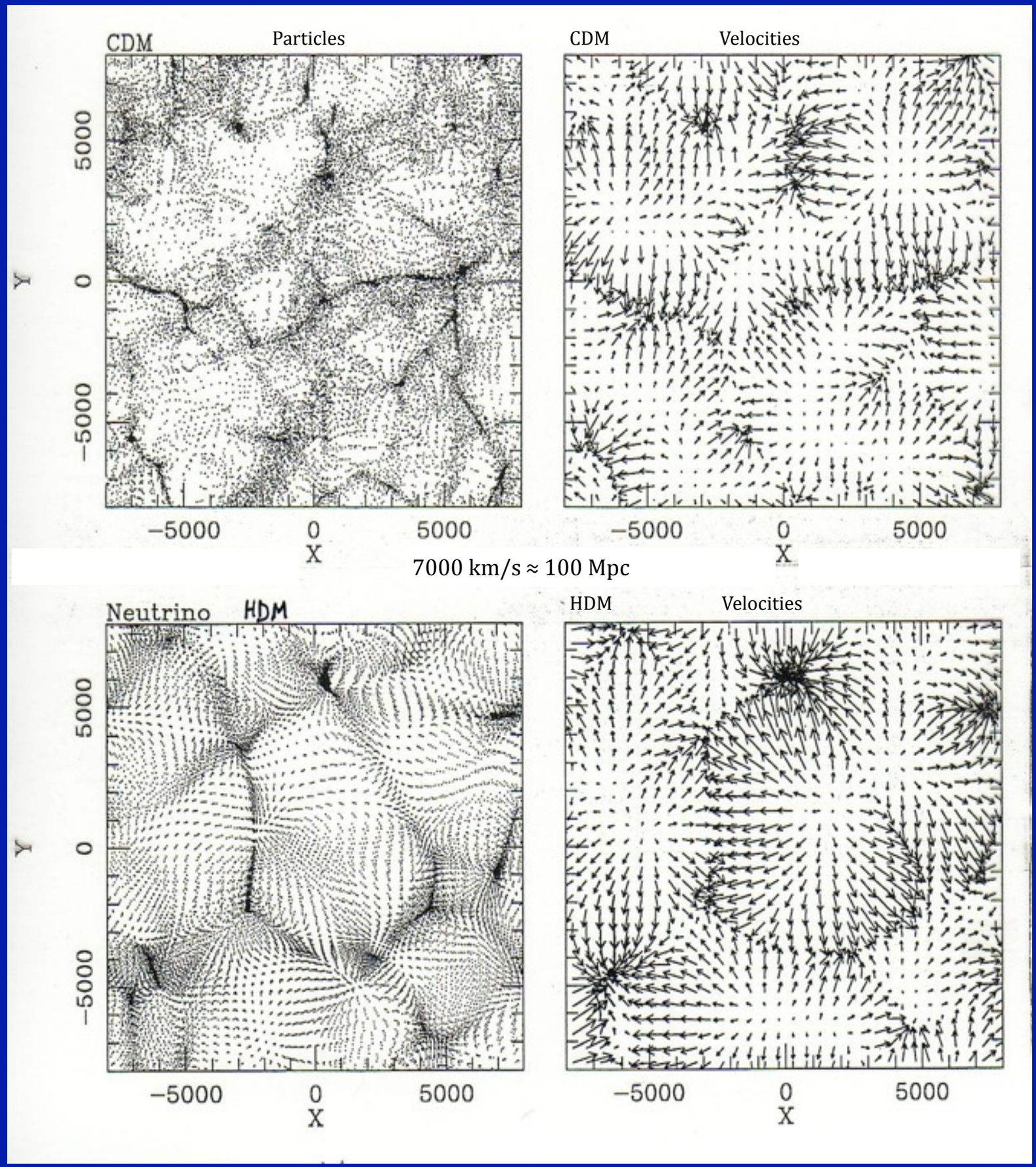

Cosmological Simulations

Astronomical observations represent snapshots of moments in time. It is the role of astrophysical theory to produce movies -- both metaphorical and actual -- that link these snapshots together into a coherent physical theory.

Cosmological dark matter simulations show large scale structure, growth of structure, and dark matter halo properties

Hydrodynamic galaxy formation simulations: evolution of galaxies, formation of galactic spheroids via mergers, galaxy images in all wavebands including stellar evolution and dust

CONSTRAINED LOCAL UNIVERSE SIMULATION

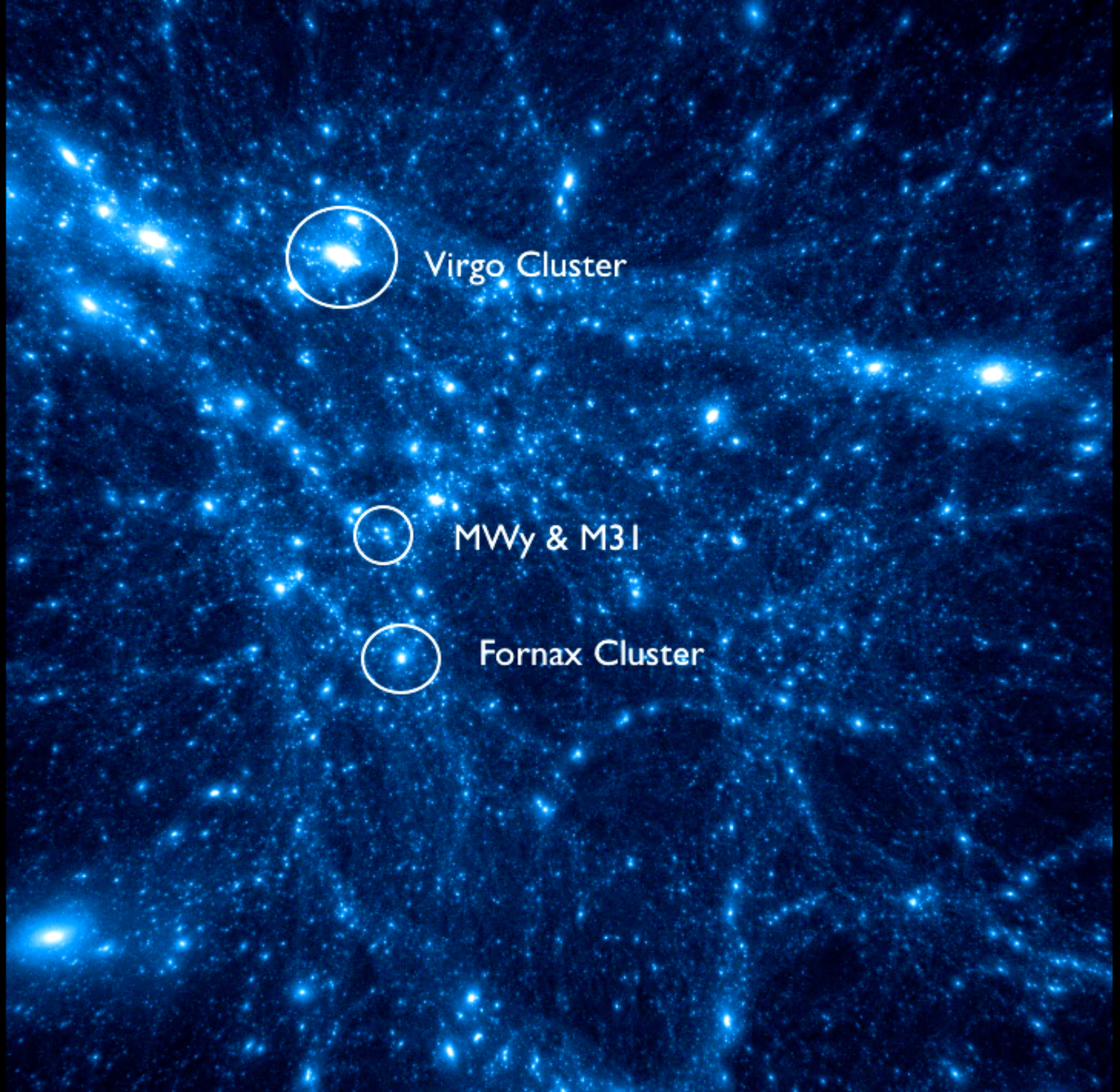
Virgo Cluster
MWy & M31
Fornax Cluster

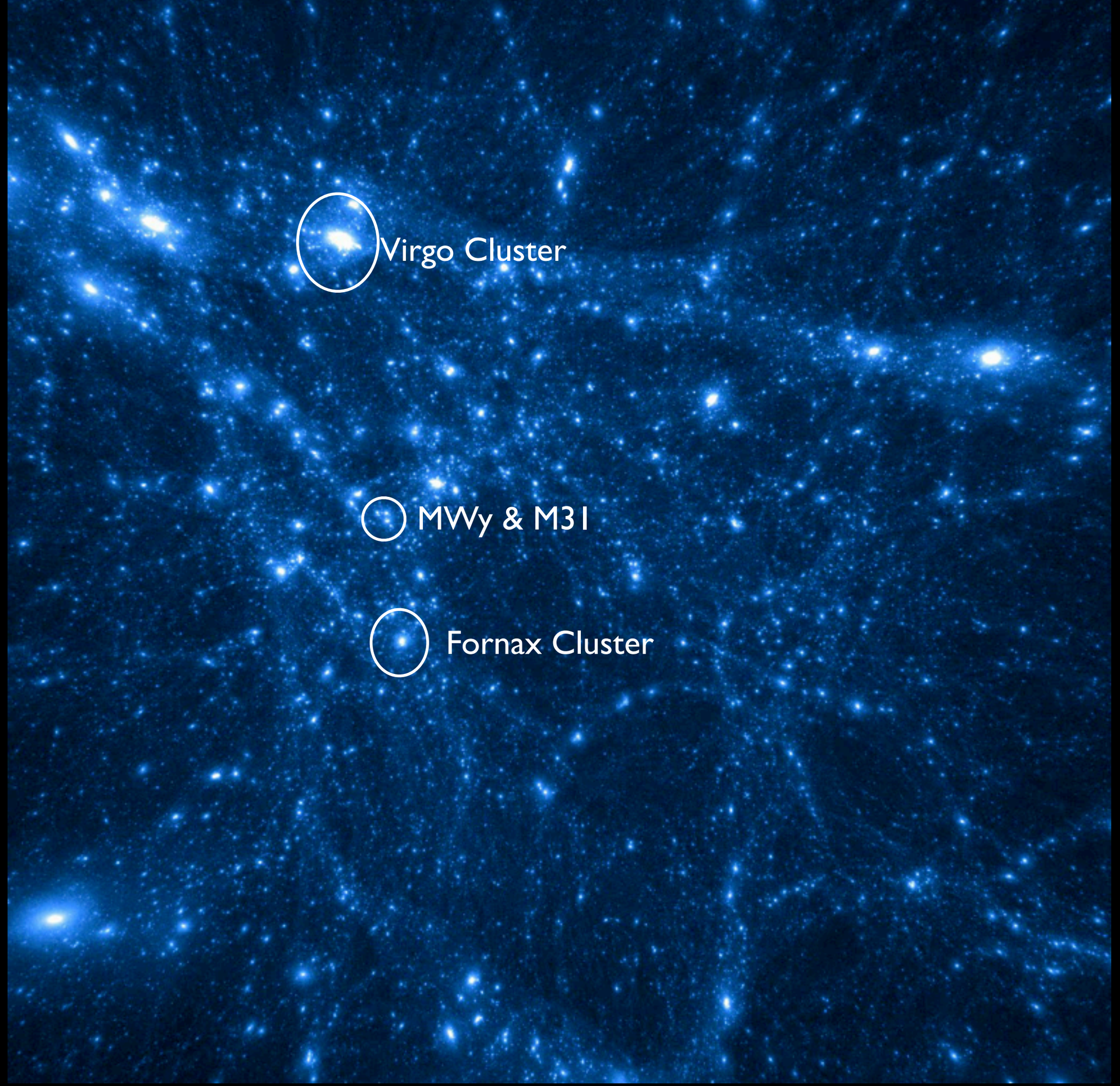
Virgo Cluster
MWy & M31
Fornax Cluster

Aquarius Simulation: Formation of a Milky-Way-size Dark Matter Halo

Diameter of Milky Way Dark Matter Halo
1.6 million light years

Aquarius Simulation

Milky Way
100,000 Light Years

Milky Way Dark Matter Halo
1,500,000 Light Years

Bolshoi Cosmological Simulation

1 Billion Light Years

IEEE Spectrum - October 2012

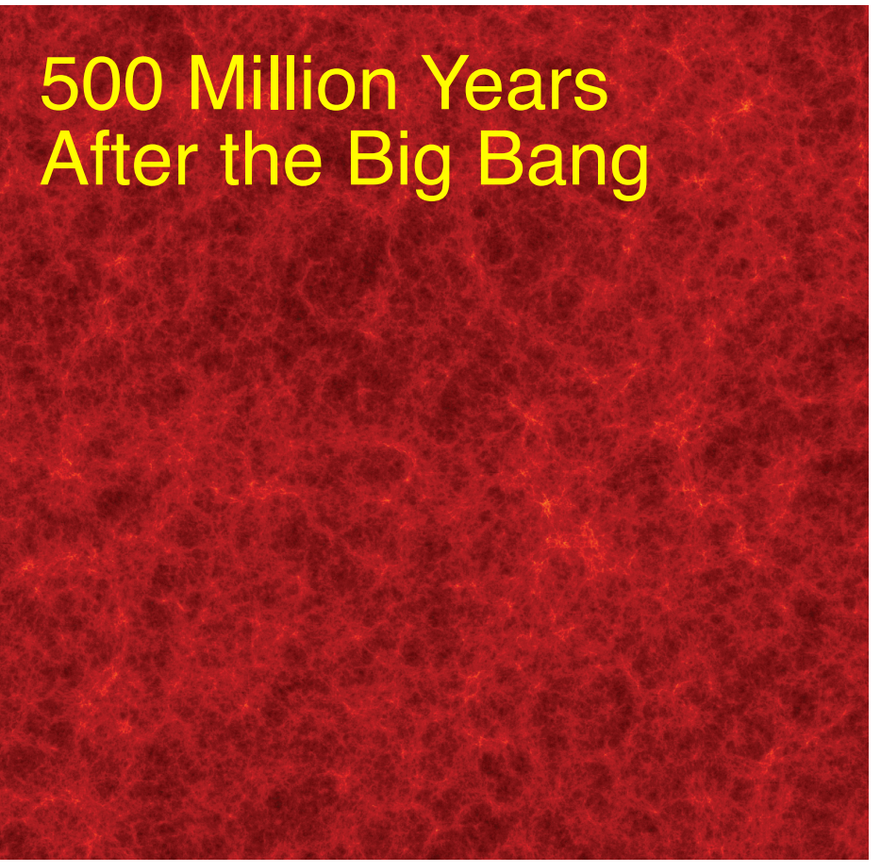

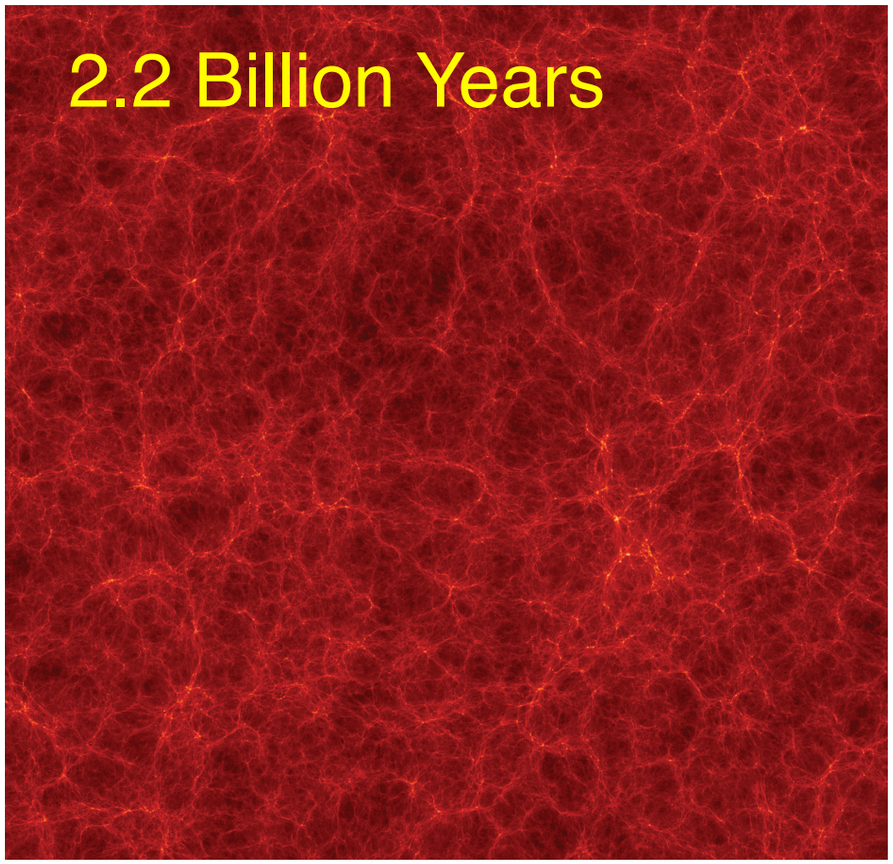

COSMIC WEB: The Bolshoi simulation models the evolution of dark matter, which is responsible for the large-scale structure of the universe. Here, snapshots from the simulation show the dark matter distribution at 500 million and 2.2 billion years [top] and 6 billion and 13.7 billion years [bottom] after the big bang. These images are 50-million-light-year-thick slices of a cube of simulated universe that today would measure roughly 1 billion light-years on a side and encompass about 100 galaxy clusters.

SOURCES: SIMULATION, ANATOLY KLYPIN AND JOEL R. PRIMACK; VISUALIZATION, STEFAN GOTTLÖBER/LEIBNIZ INSTITUTE FOR ASTROPHYSICS POTSDAM

THE UNIVERSE IN A SUPERCOMPUTER

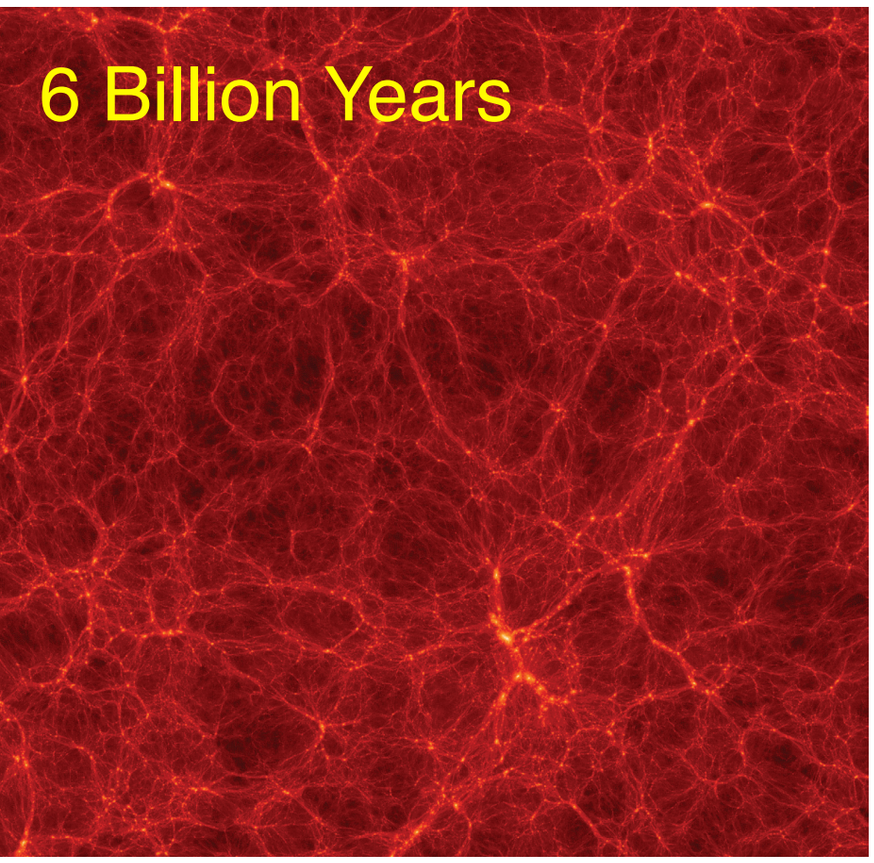

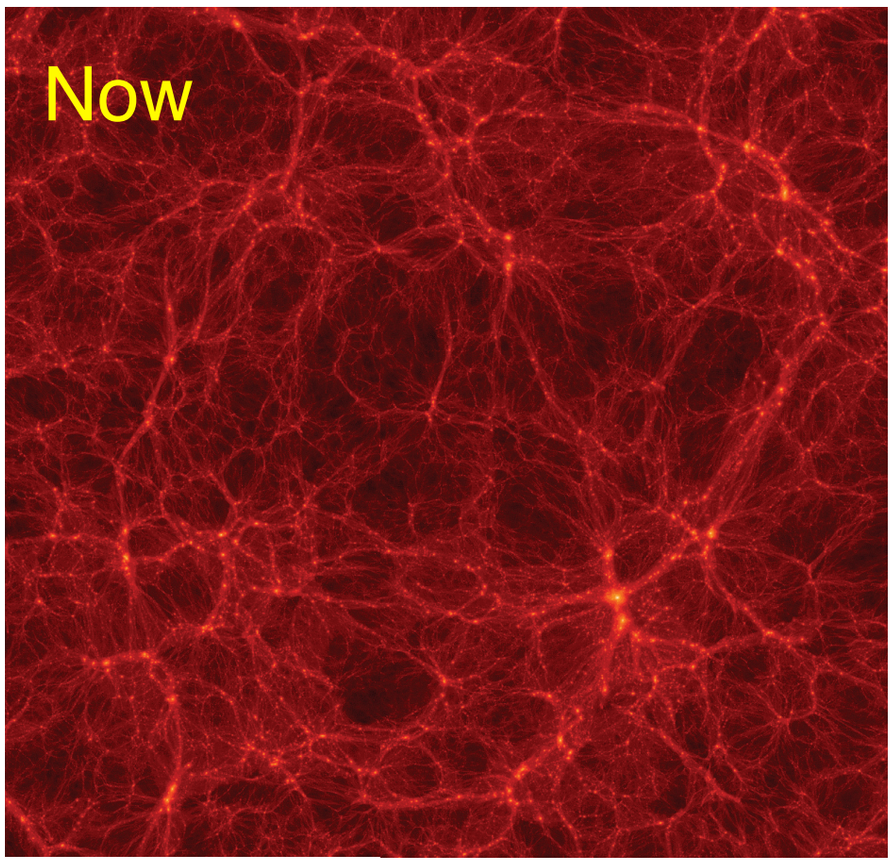

6 Billion Years

To understand the cosmos, we must evolve it all over again

By Joel R. Primack

WHEN IT COMES TO RECONSTRUCTING THE PAST, you might think that astrophysicists have it easy. After all, the sky is awash with evidence. For most of the universe's history, space has been largely transparent, so much so that light emitted by distant galaxies can travel for billions of years before finally reaching Earth. It might seem that all researchers have to do to find out what the universe looked like, say, 10 billion years ago is to build a telescope sensitive enough to pick up that ancient light.

Actually, it's more complicated than that. Most of the ordinary matter in the universe—the stuff that makes up all the atoms, stars, and galaxies astronomers can see—is invisible, either sprinkled throughout intergalactic space in tenuous forms that emit and absorb little light or else swaddled inside galaxies in murky clouds of dust and gas. When astronomers look out into the night sky with their most powerful telescopes, they can see no more than about 10 percent of the ordinary matter that's out there.

To make matters worse, cosmologists have discovered that if you add up all the mass and energy in the universe, only a small fraction is composed of ordinary matter. A good 95 percent of the cosmos is made up of two very different kinds of invisible and as-yet-unidentified stuff that is "dark," meaning that it emits and absorbs no light at all. One of these mysterious components, called dark matter, seems immune to all fundamental forces except gravity and perhaps the weak interaction, which is responsible for

250 Mpc/h Bolshoi

BOLSHOI SIMULATION ZOOM-IN

Anatoly Klypin, Stefan Gottloeber, Joel Primack

Bolshoi Cosmological Simulation

100 Million Light Years

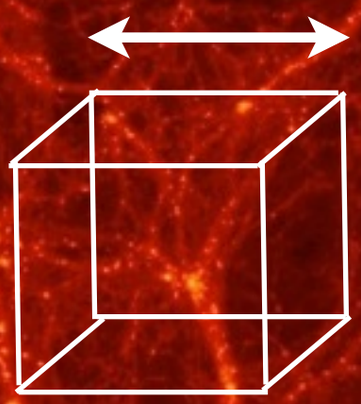

1 Billion Light Years

BOLSHOI SIMULATION FLY-THROUGH

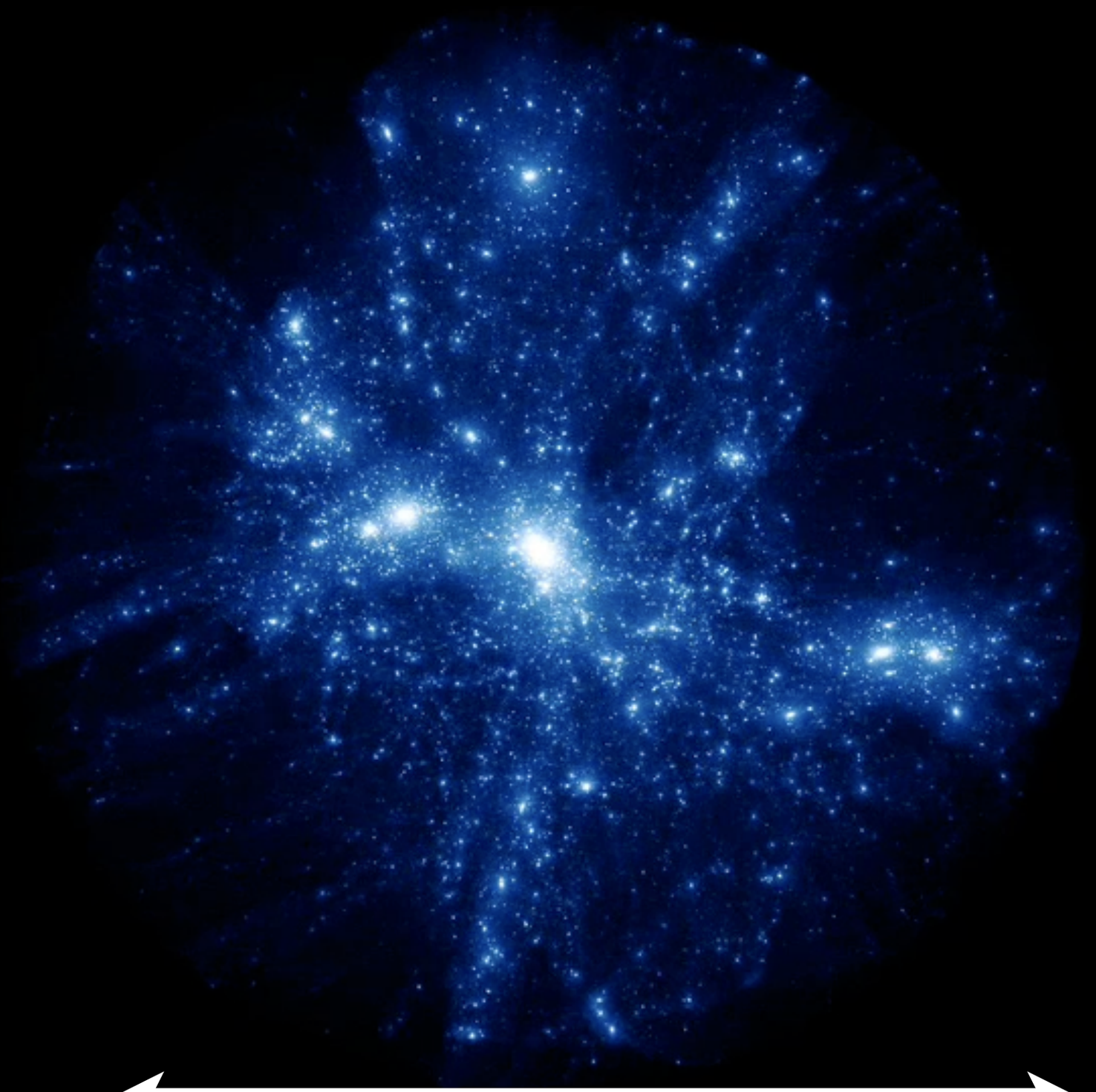

$<10^{-3}$
of the
Bolshoi
Simulation
Volume

Bolshoi Cosmological Simulation

100 Million Light Years

Bjork "Dark Matter"
Biophilia

Bolshoi-Planck Cosmological Simulation

Merger Tree of a Large Halo

Merger Tree: Peter Behroozi

Visualization: Alex Bogert

Bolshoi-Planck Cosmological Simulation

Anatoly Klypin & Joel Primack
NASA Ames Research Center

8.6×10^9 particles 1 kpc resolution

Filamentary Structure: Zel'dovich Approximation

displacement from initial position: $x(q,t) = q - D(t)\,\nabla\phi(q)$

Growth Factor

continuity: $\rho(x,t)\,d^3x = \rho_q d^3q \quad \rightarrow$

$$\rightarrow \rho(x,t) = \rho_q \,/\, \| \partial\vec{x} / \partial\vec{q} \|$$

$$= \frac{\rho_q}{(1-D(t)\lambda_1)(1-D(t)\lambda_2)(1-D(t)\lambda_3)}$$

eigenvalues of deformation tensor: $\lambda_i \equiv \frac{\partial^2\phi}{\partial^2 q_i}, \quad \lambda_1 \geq \lambda_2 \geq \lambda_3$

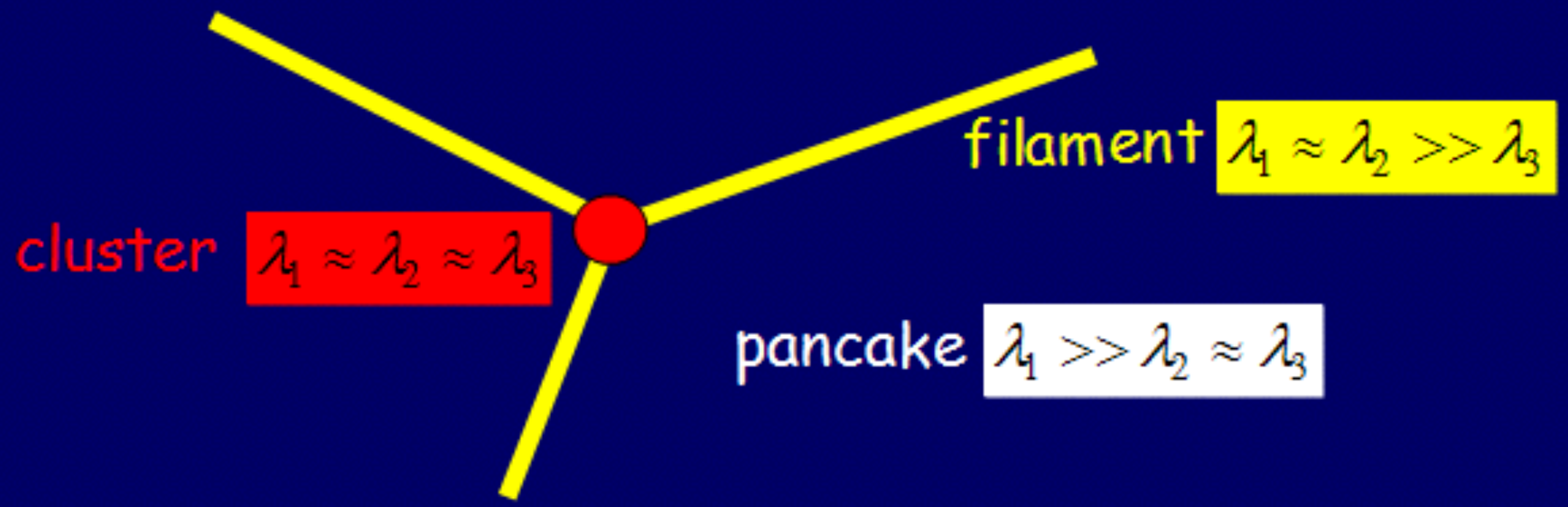

Mass Function of Distinct Halos

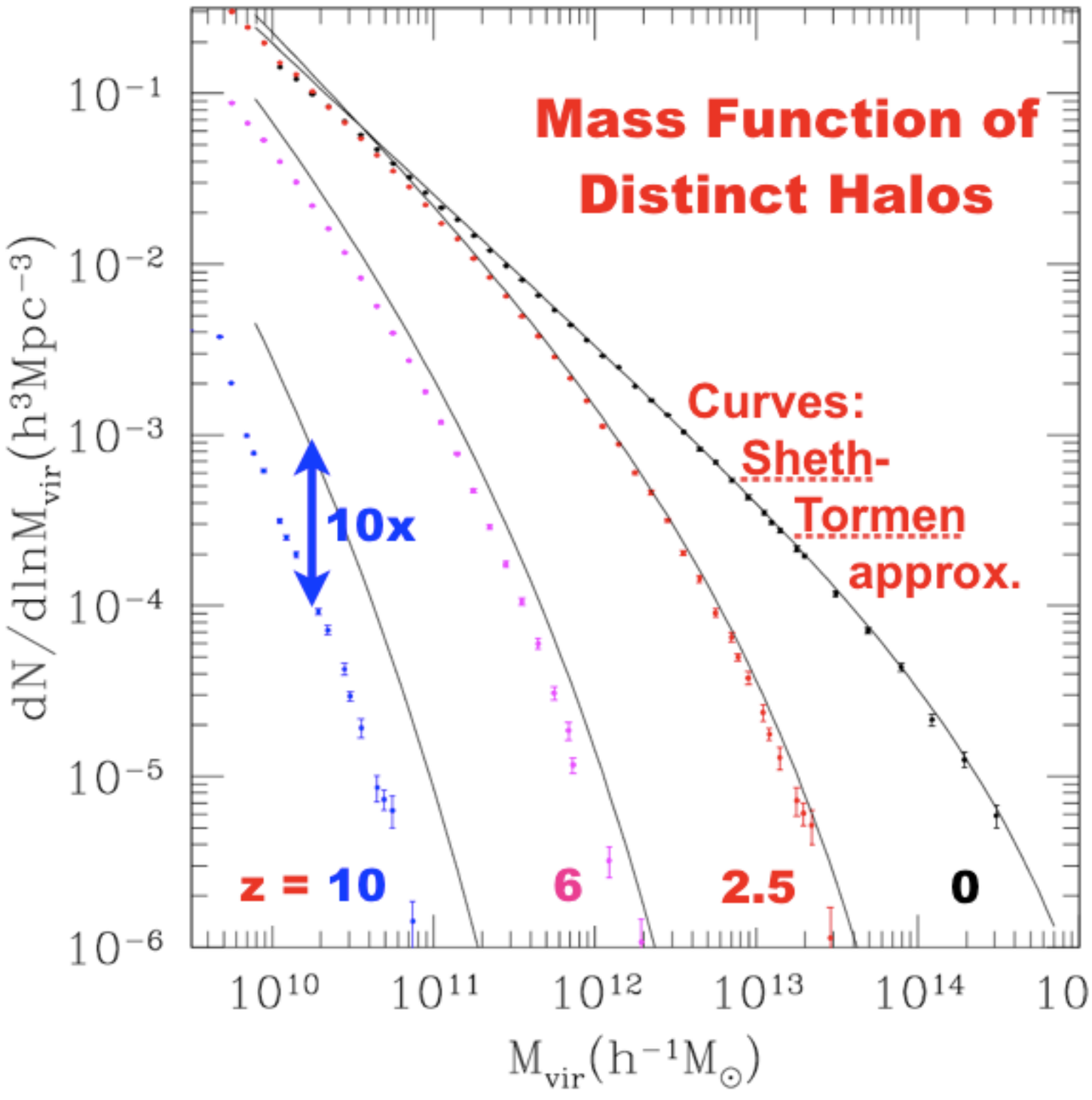

Sheth-Tormen Fails at High Redshifts

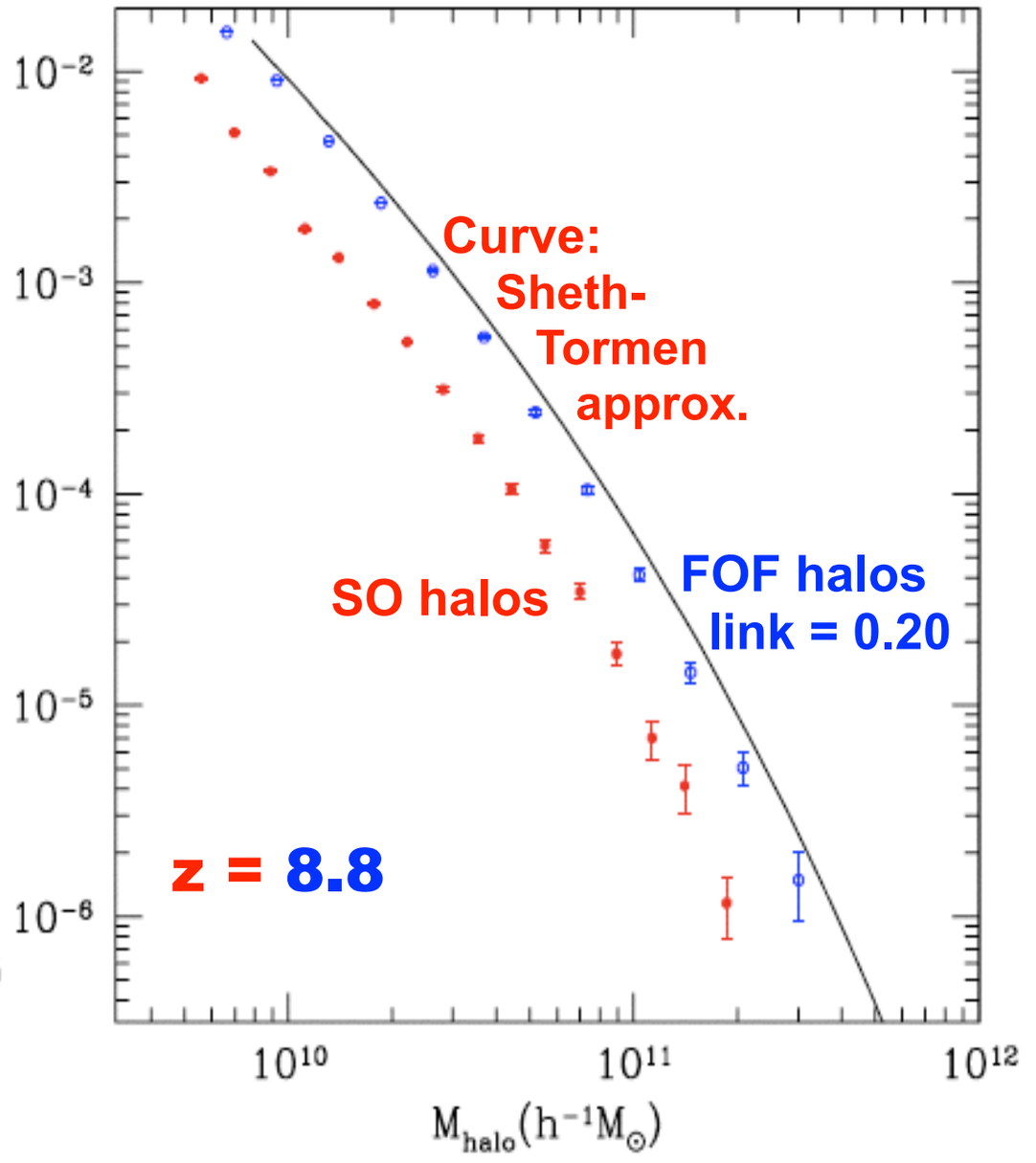

Sheth-Tormen approximation with the same WMAP5 parameters used for Bolshoi simulation very accurately agrees with abundance of halos at low redshifts, but increasingly overpredicts bound spherical overdensity halo abundance at higher redshifts.

Klypin, Trujillo, & Primack, arXiv: 1002.3660v3

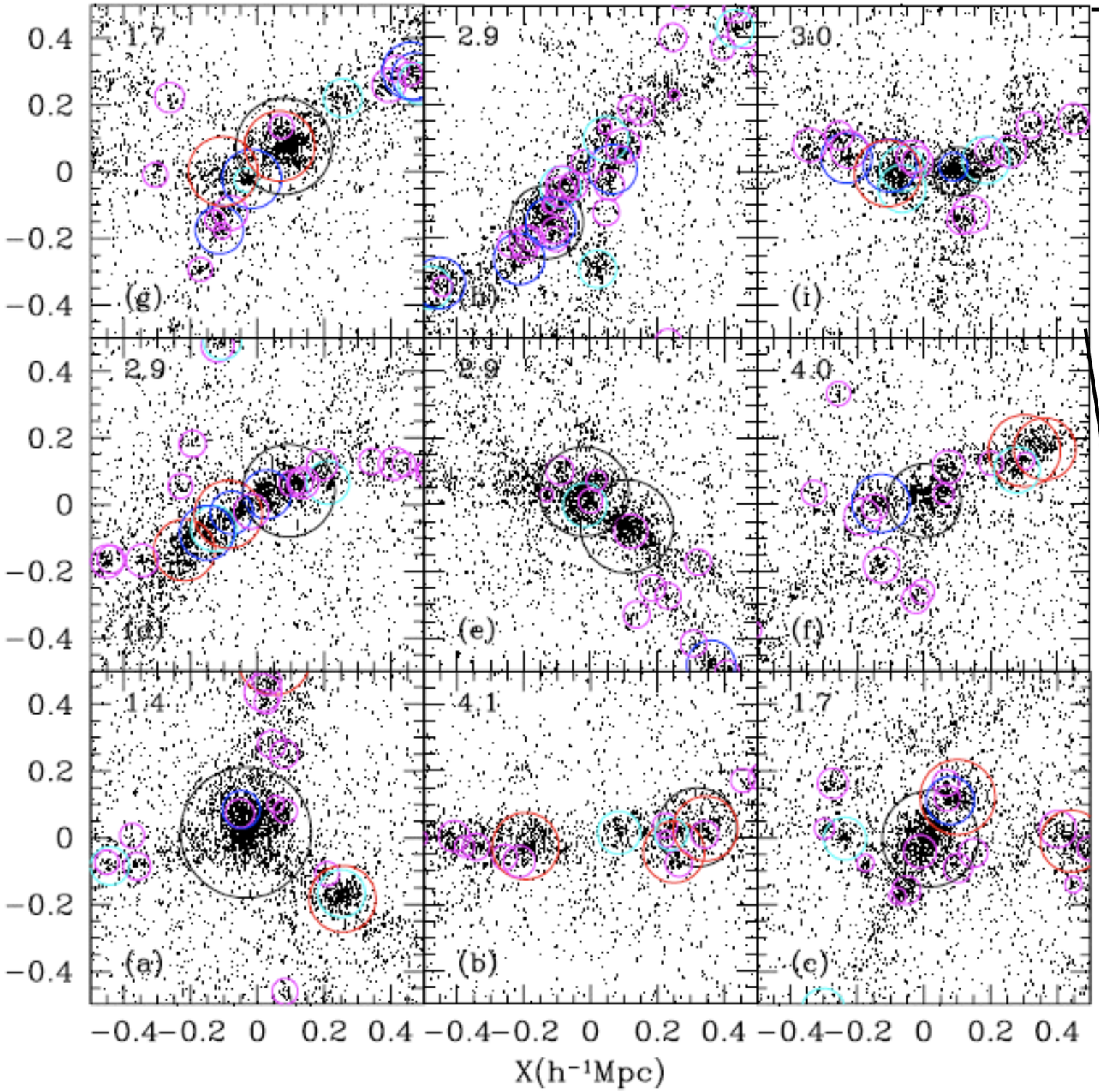

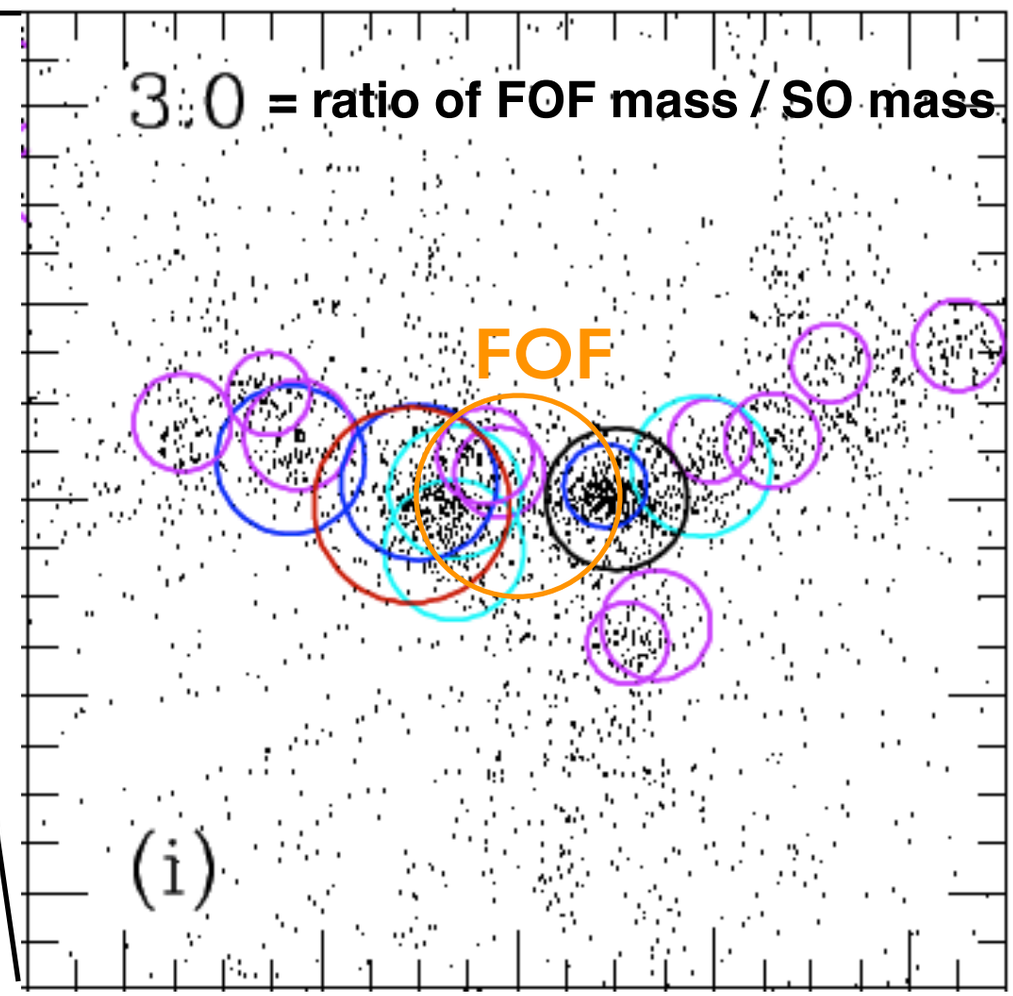

FOF linked together a chain of halos that formed in long and dense filaments (also in panels b, d, f, h; e = major merger)

Each panel shows 1/2 of the dark matter particles in cubes of $1h^{-1}$ Mpc size. The center of each cube is the exact position of the center of mass of the corresponding FOF halo. The effective radius of each FOF halo in the plots is 150 – 200 h^{-1} kpc. Circles indicate virial radii of distinct halos and subhalos identified by the spherical overdensity algorithm BDM.

Klypin, Trujillo, & Primack, arXiv: 1002.3660v3

Matter Distribution Agrees with ΛCDM

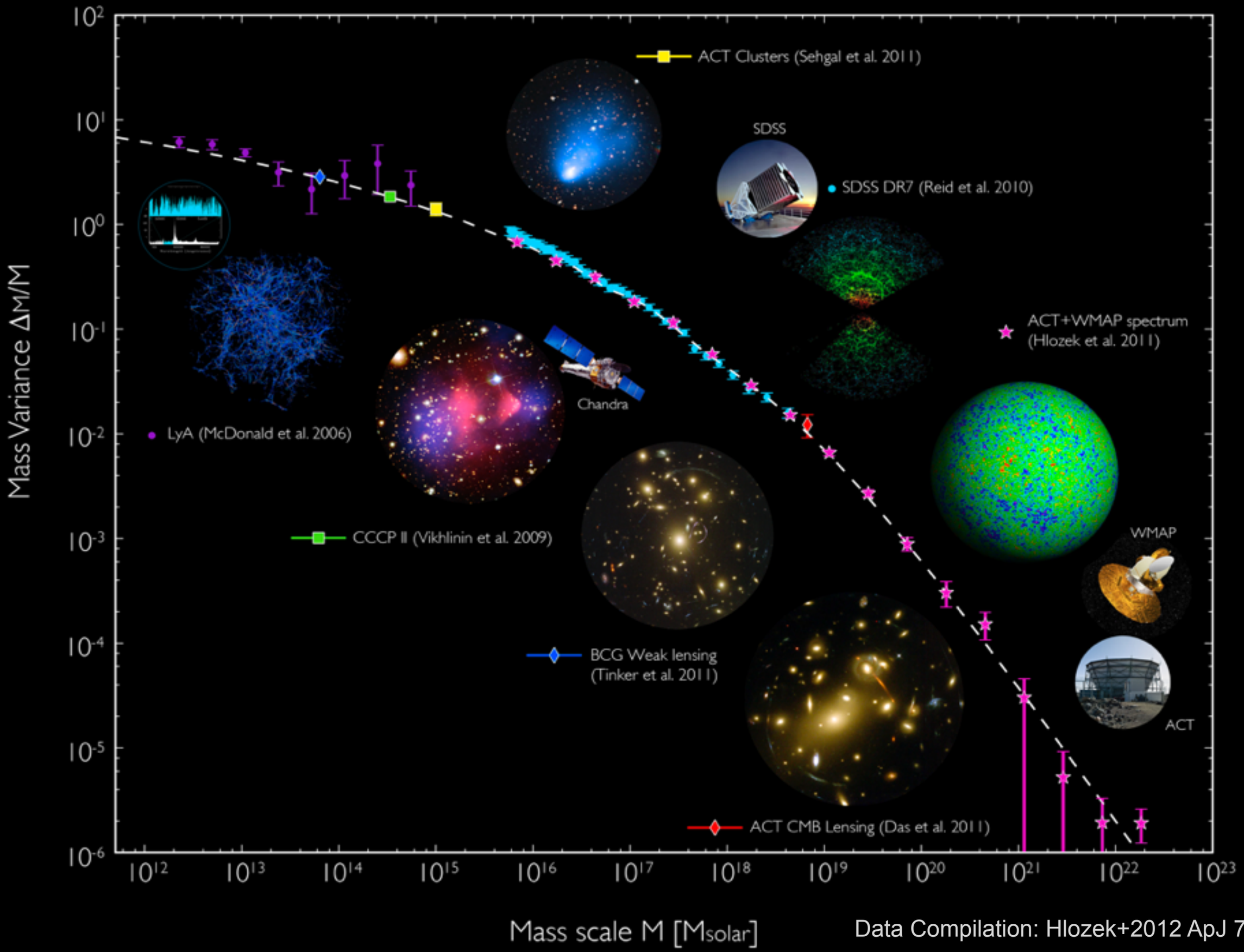

Data Compilation: Hlozek+2012 ApJ 749, 90

Halo Abundance Matching

Trujillo-Gomez, Klypin, Primack, & Romanowsky ApJ 2011

To investigate the statistics of galaxies and their relation to host DM halos as predicted by the LCDM model, we predicted the properties of our model galaxies using the following Halo Abundance Matching (HAM) procedure:

1. Using the merger tree of each DM halo and subhalo, obtain V_{acc} = the peak value of the circular velocity over the history of the halo (this is typically the maximum circular velocity of the halo when the halo is first accreted). Perform abundance matching of the velocity function of the halos to the LF of galaxies to obtain the luminosity of each model galaxy.

2. Perform abundance matching of the velocity function to the stellar mass function of galaxies to obtain the stellar mass of each model galaxy.

3. Use the observed gas-to-stellar mass ratio as a function of stellar mass to assign cold gas masses to our model galaxies. The stellar mass added to the cold gas mass becomes the total baryonic mass.

4. Using the density profiles of the DM halos, obtain the circular velocity at 10 kpc (V_{10}) from the center of each halo. Multiply the DM mass, as it comes from simulations, by the factor $(1 - f_{bar})$, where f_{bar} is the cosmological fraction of baryons. This is the dark-matter-only contribution. Add the contribution to V_{10} of the baryon mass from step 3 assuming it is enclosed within a radius of 10 kpc.

5. Optionally implement the BlumenthalFaberFloresPrimack86 correction to V_{10} due to the adiabatic contraction of the DM halos from the infall of the baryon component to the center.

Bolshoi $w_p(r_p)$ by Halo Abundance Matching vs. SDSS Observations

Angular correlation function of SDSS galaxies vs. Bolshoi galaxies using halo abundance matching, with scatter using our stochastic abundance matching method. This results in a better than 20% agreement with SDSS. *Top left:* correlation functinon in three magnitude bins, showing Poisson uncertainties as thin lines. *Remaining panels:* correlation function in each luminosity bin compared with SDSS galaxies (points with error bars: Zehavi et al. 2010).

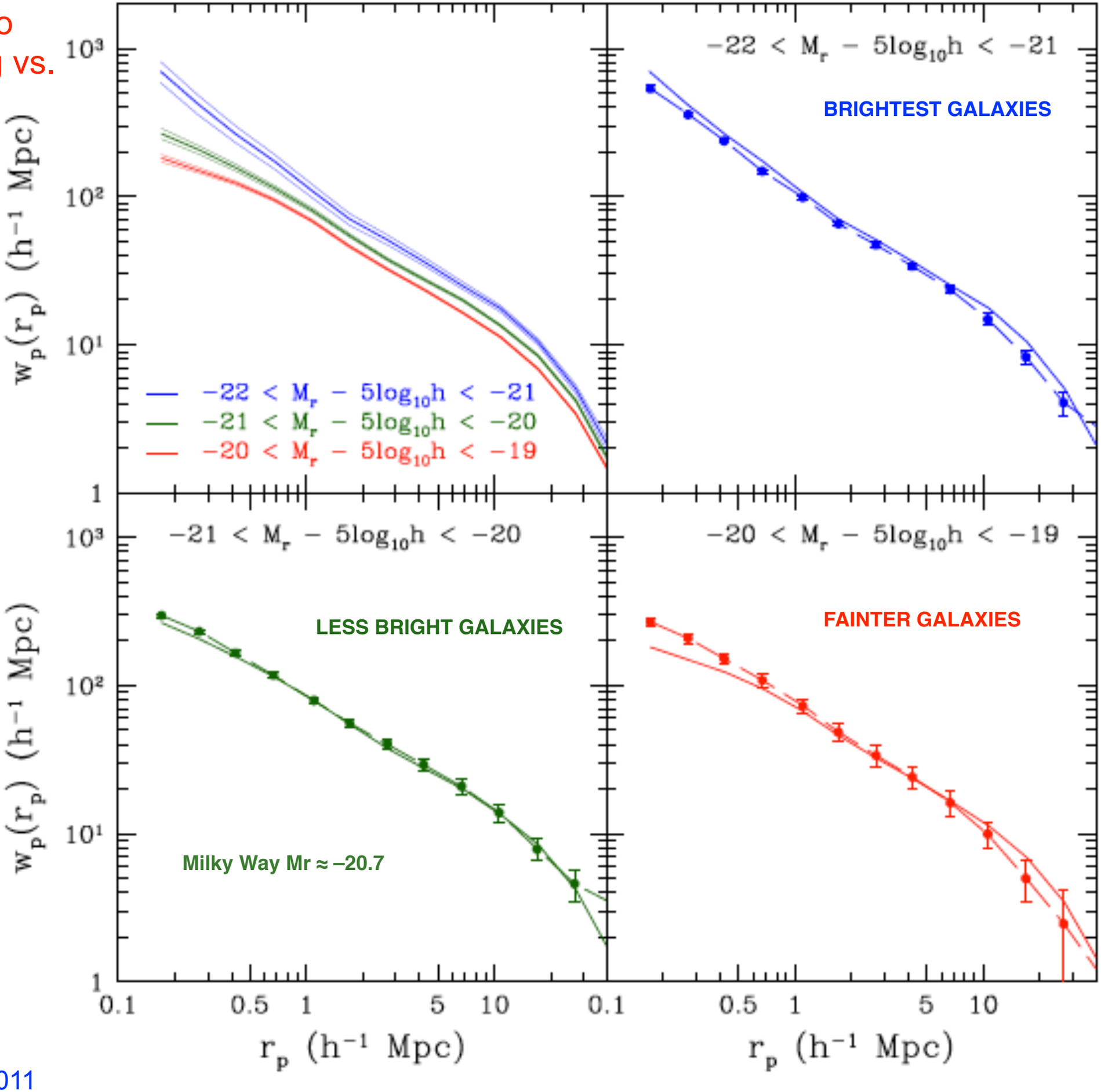

Trujillo-Gomez, Klypin, Primack, & Romanowsky 2011

ΛCDM PREDICTS EVOLUTION IN THE GALAXY CORRELATION FUNCTION

$\xi_{gg}(r)$

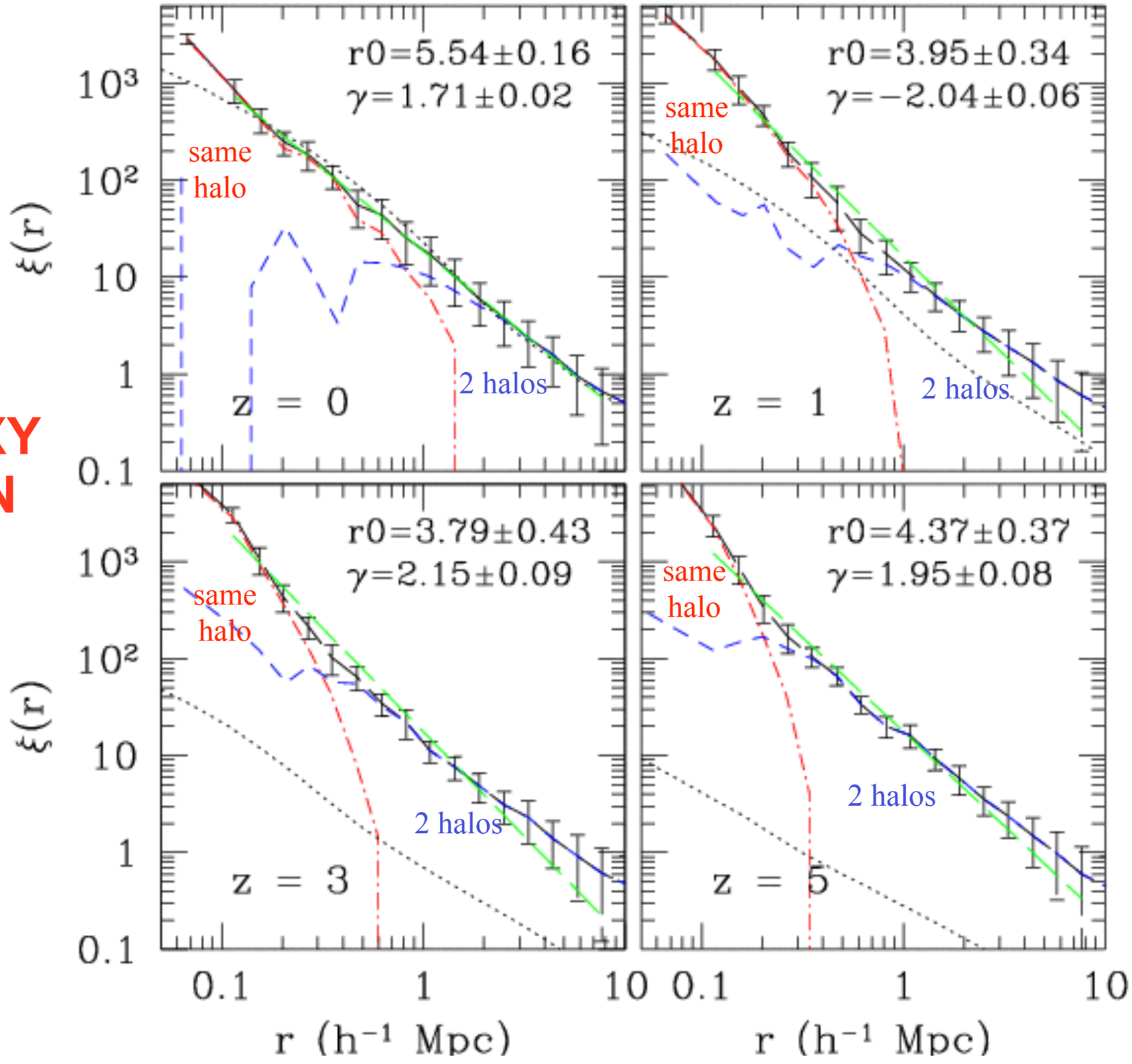

FIG. 8.— Evolution of the two-point correlation function in the $80h^{-1}$ Mpc simulation. The solid line with error bars shows the clustering of halos of the fixed number density $n = 5.89 \times 10^{-3}h^3$ Mpc^{-3} at each epoch. The error-bars indicate the "jack-knife" one sigma errors and are larger than the Poisson error at all scales. The dot-dashed and dashed lines show the corresponding one- and two-halo term contributions. The long-dashed lines show the power-law fit to the correlation functions in the range of $r = [0.1 - 8h^{-1}$ Mpc$]$. Although the correlation functions can be well fit by the power law at $r \gtrsim 0.3h^{-1}$ Mpc in each epoch, at $z > 0$ the correlation function steepens significantly at smaller scales due to the one-halo term.

Kravtsov, Berlind, Wechsler, Klypin, Gottloeber, Allgood, & Primack 2004

Galaxy clustering in SDSS at z~0 agrees with ΛCDM simulations

$n(>V_{\mathrm{max,acc}})=n(>L)$

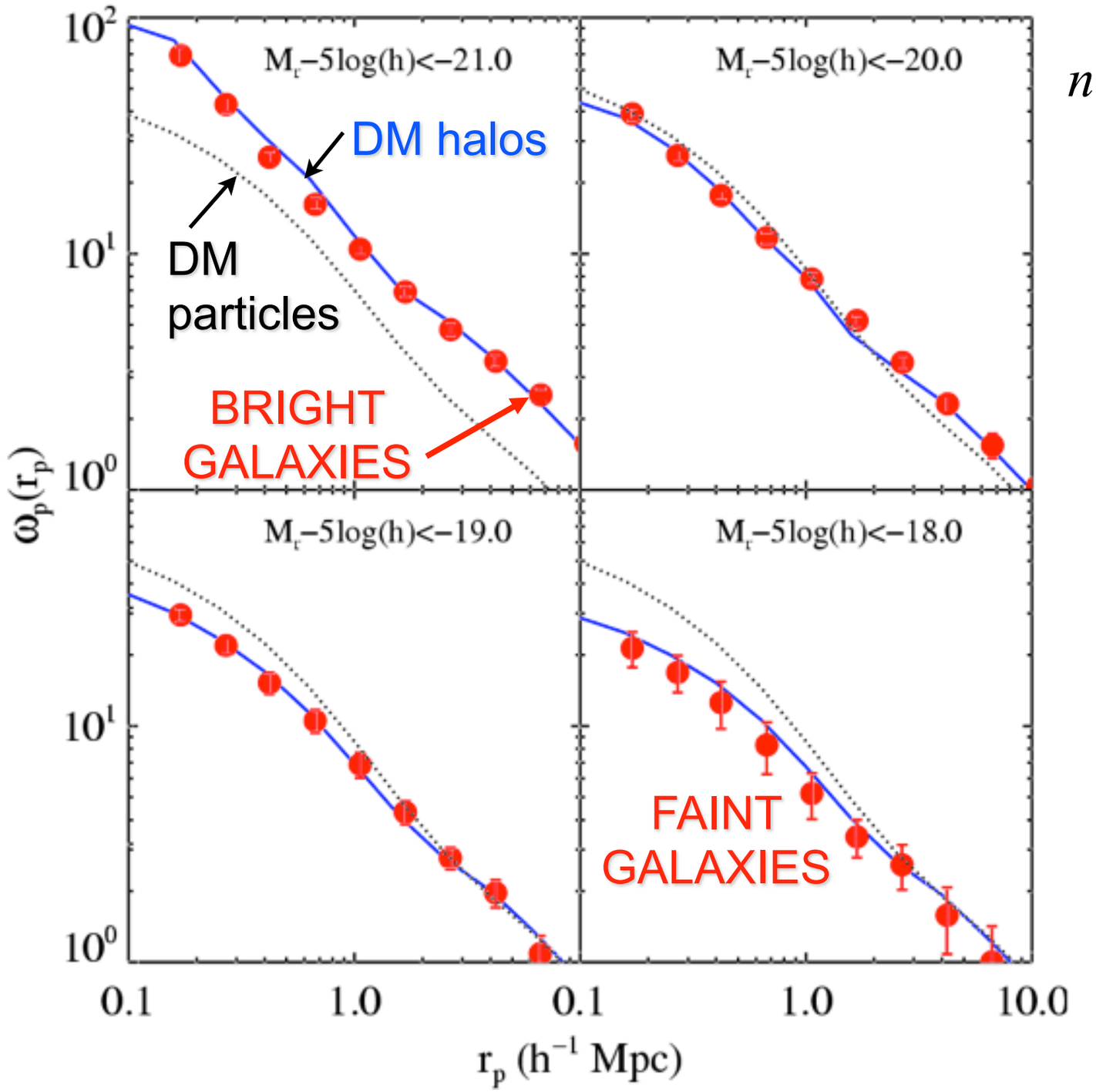

projected 2-point correlation function

Conroy, Wechsler & Kravtsov 2006, ApJ 647, 201

and at redshift z~1 (DEEP2)

$$n(>V_{\mathrm{max,acc}})=n(>L)$$

projected 2-point correlation function

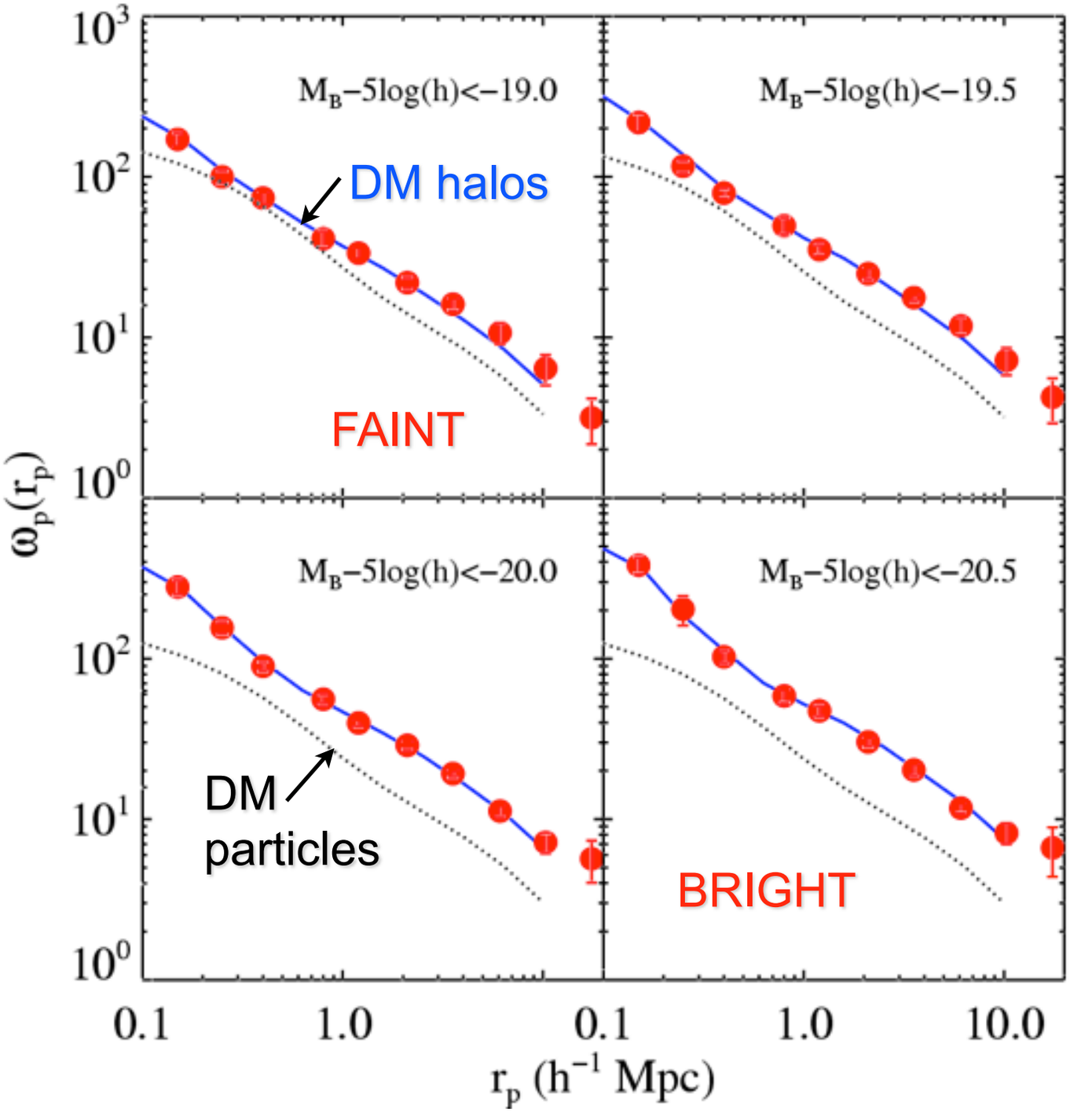

projected separation

Conroy, Wechsler & Kravtsov 06

and at z~4-5 (LBGs, Subaru)!

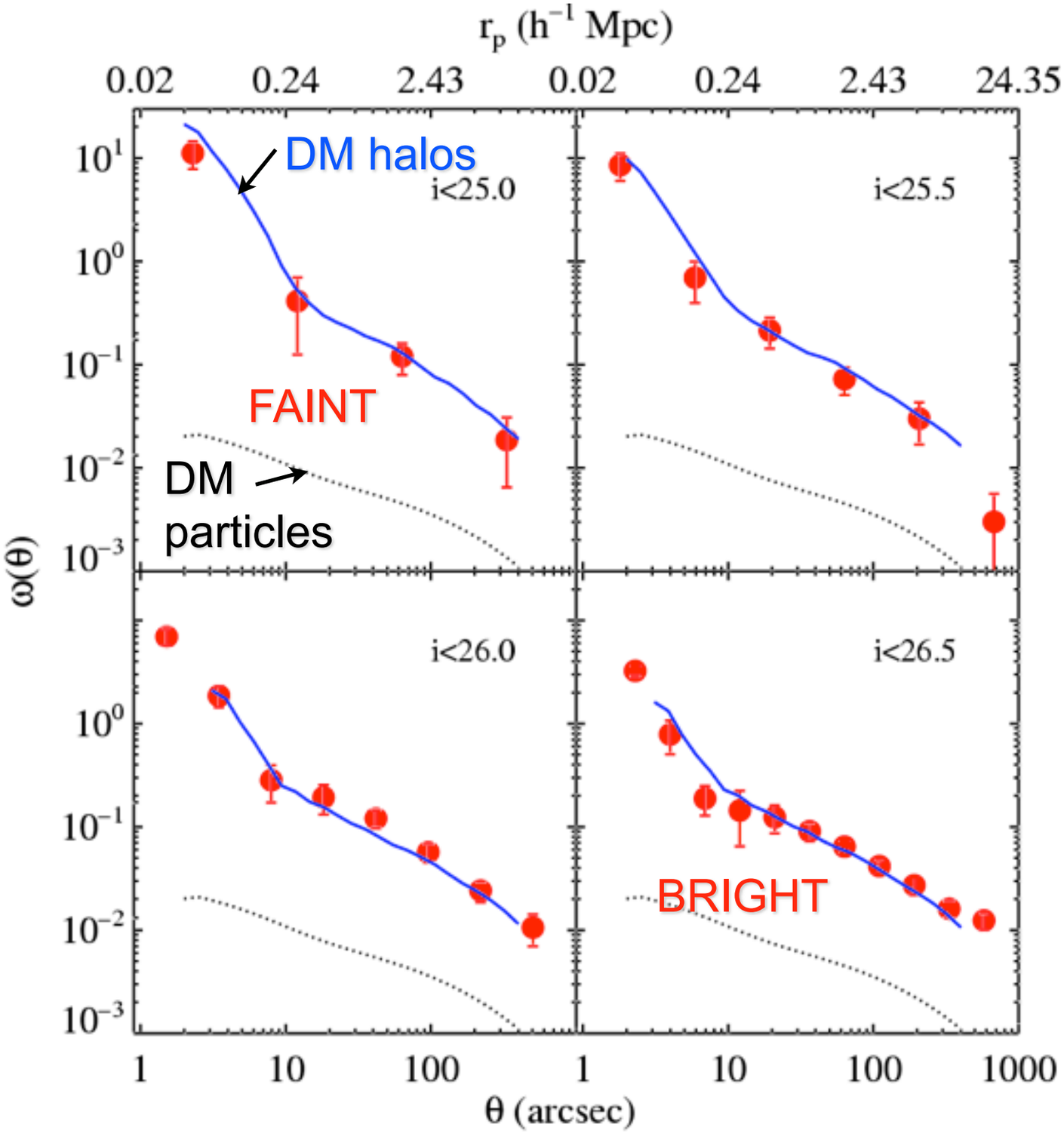

$n(>V_{\mathrm{max,acc}})=n(>L)$

angular 2-point correlation function

projected separation

Conroy, Wechsler & Kravtsov 06

The dark side of galaxy colour

Andrew P. Hearin & Douglas F. Watson MNRAS 435, 1313–132

ABSTRACT

We present *age distribution matching*, a theoretical formalism for predicting how galaxies of luminosity L and colour C occupy dark matter haloes. Our model supposes that there are just two fundamental properties of a halo that determine the colour and brightness of the galaxy it hosts: the maximum circular velocity V_{max} and the redshift z_{starve} that correlates with the epoch at which the star formation in the galaxy ceases. The halo property z_{starve} is intended to encompass physical characteristics of halo mass assembly that may deprive the galaxy of its cold gas supply and, ultimately, quench its star formation. The new, defining feature of the model is that, at fixed luminosity, galaxy colour is in monotonic correspondence with z_{starve}, with the larger values of z_{starve} being assigned redder colours. We populate an N-body simulation with a mock galaxy catalogue based on age distribution matching and show that the resulting mock galaxy distribution accurately describes a variety of galaxy statistics. Our model suggests that halo and galaxy assembly are indeed correlated. We make publicly available our low-redshift, Sloan Digital Sky Survey $M_r < -19$ mock galaxy catalogue, and main progenitor histories of all $z = 0$ haloes, at http://logrus.uchicago.edu/~aphearin

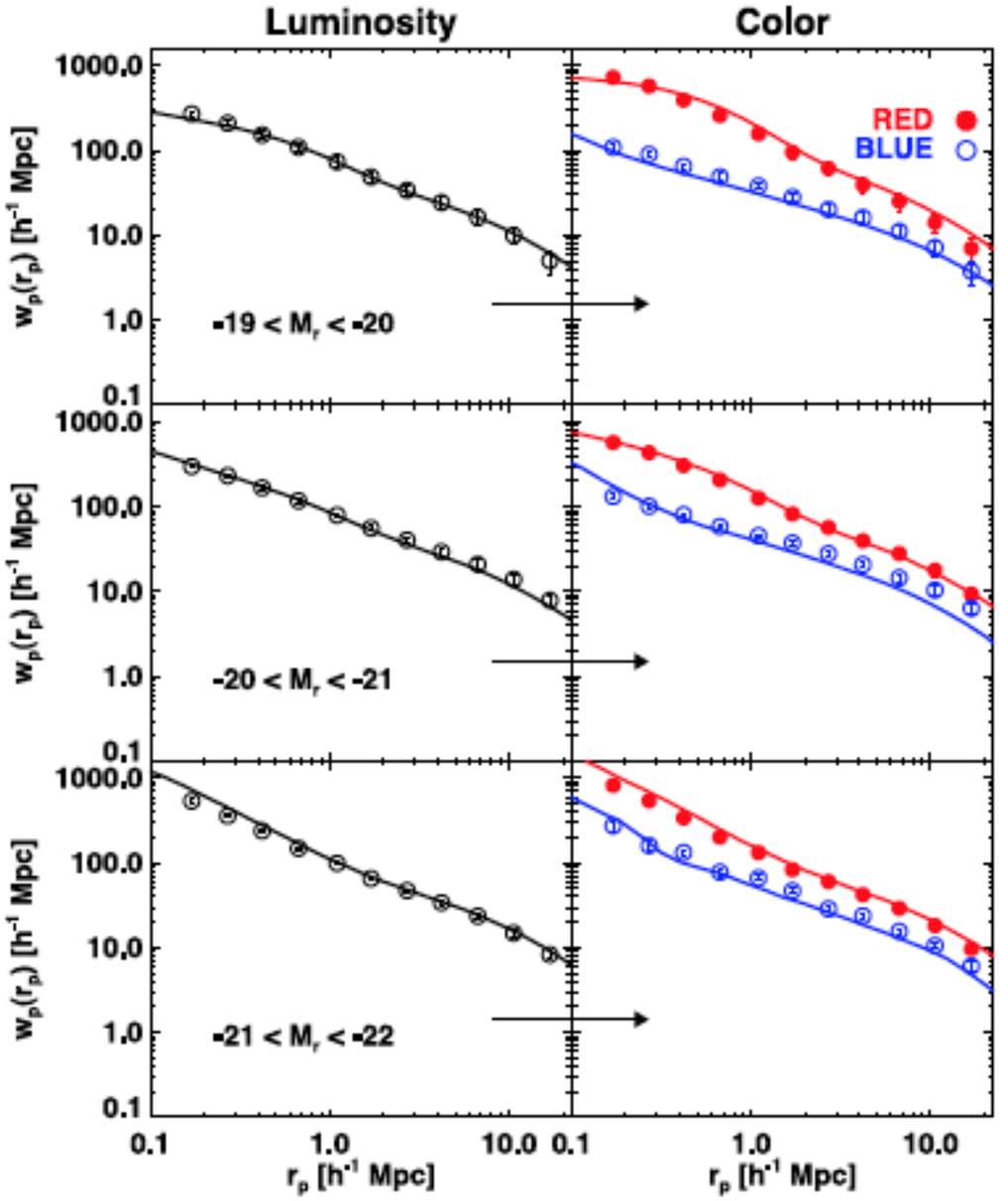

Hearin and Watson 2013 showed that by extending the traditional abundance matching formalism to consider an additional halo property beyond V_{max}, the observed spatial distribution of galaxies as a function of luminosity and color could be accurately reproduced. Specifically, the authors considered the redshift, dubbed z_{starve}, that correlates with the epoch at which the star formation in the galaxy is likely stifled, ultimately leading to the quenching of the galaxy.

By using merger trees to map the full mass assembly history (MAH) of halos, a halo's z_{starve} value is determined by whichever of the following three events happens first in its MAH: (1) the epoch a halo accretes onto a larger halo, thus becoming a subhalo, (2) the epoch a halo reaches a characteristic mass1, and (3) the epoch a halo transitioned from the fast- to slow-accretion regime. Under the simple assumption that z_{starve} correlates with g – r color at fixed luminosity, the age matching technique was able to accurately predict color-dependent clustering in the Sloan Digital Sky Survey (SDSS) and a variety of galaxy group statistics. The success of the model supported the idea that the assembly history of galaxies and halos are correlated.

Observational Data

Sloan Digital Sky Survey

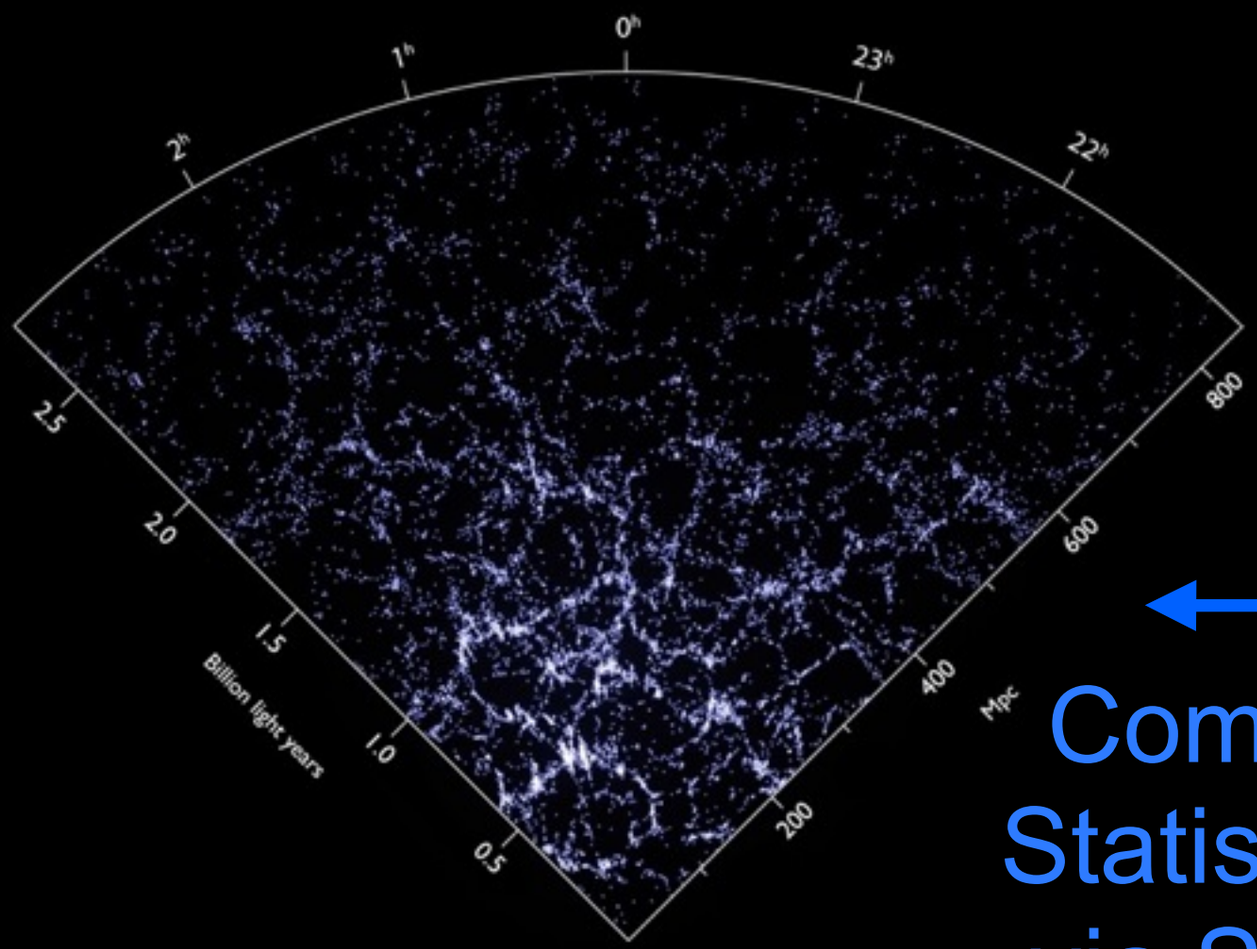

Bolshoi Simulation

Anatoly Klypin, Joel Primack, Peter Behroozi
Risa Wechsler, Ralf Kahler, Nina McCurdy

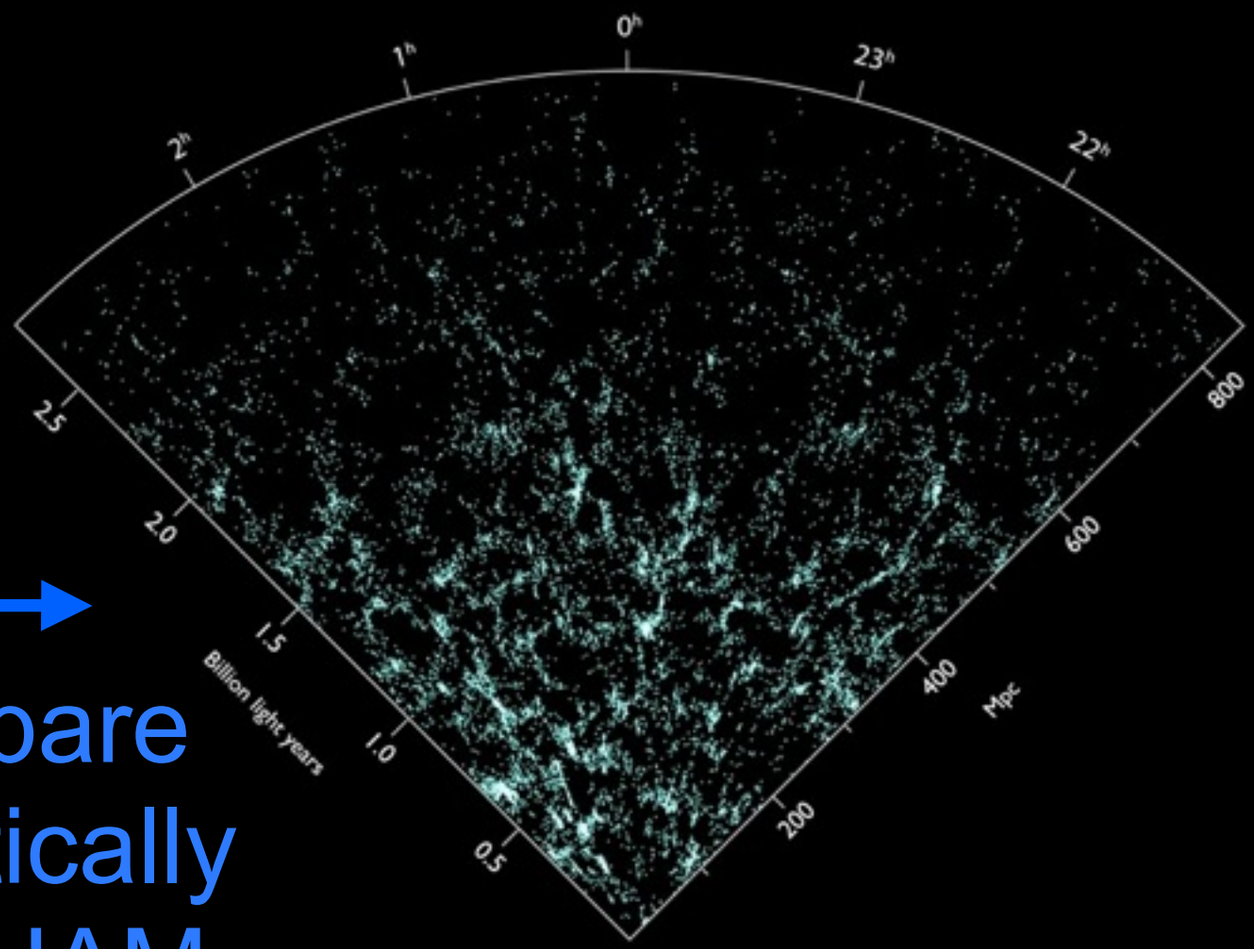

Compare Statistically via SHAM
(SubHalo Abundance Matching)

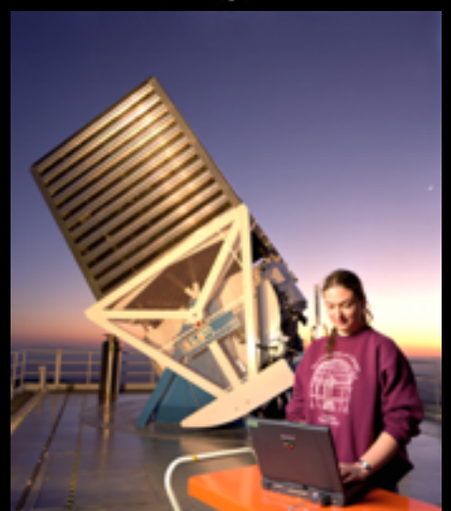

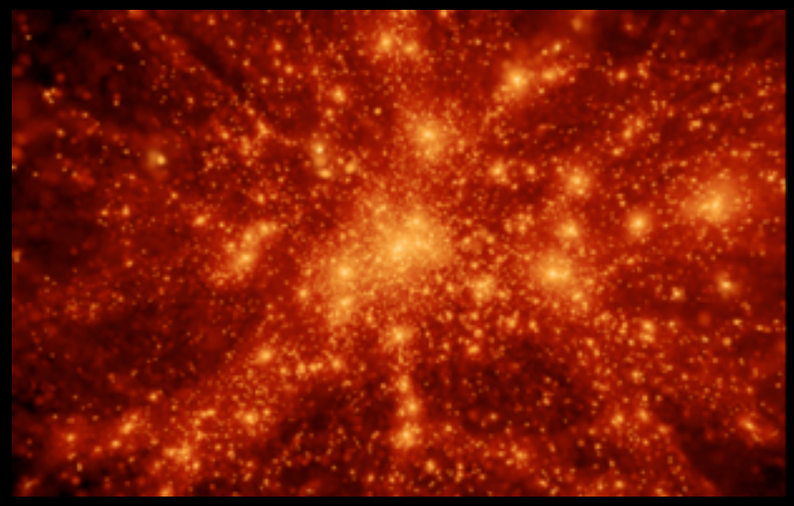

The Milky Way has two large satellite galaxies,
the small and large Magellanic Clouds

How common is this?

The Bolshoi simulation + sub-halo abundance matching predict the likelihood of 0, 1, 2, 3, ... large satellites

SDSS sky

Bolshoi simulation

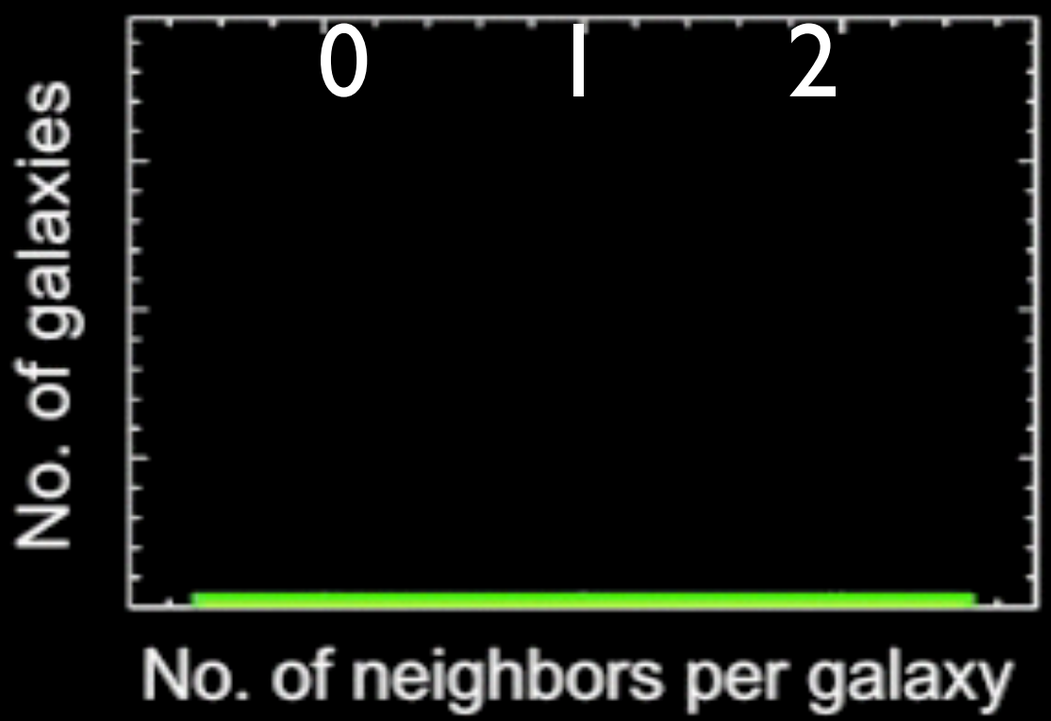

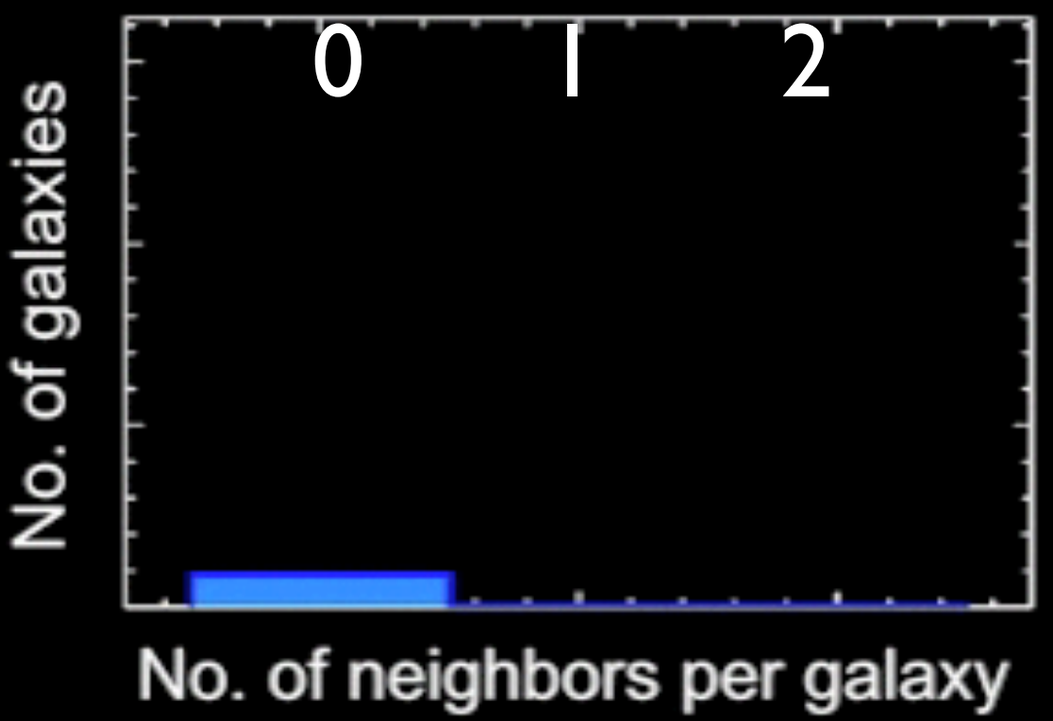

Statistics of MW bright satellites:

Sloan Digital Sky Survey data vs. Bolshoi simulation

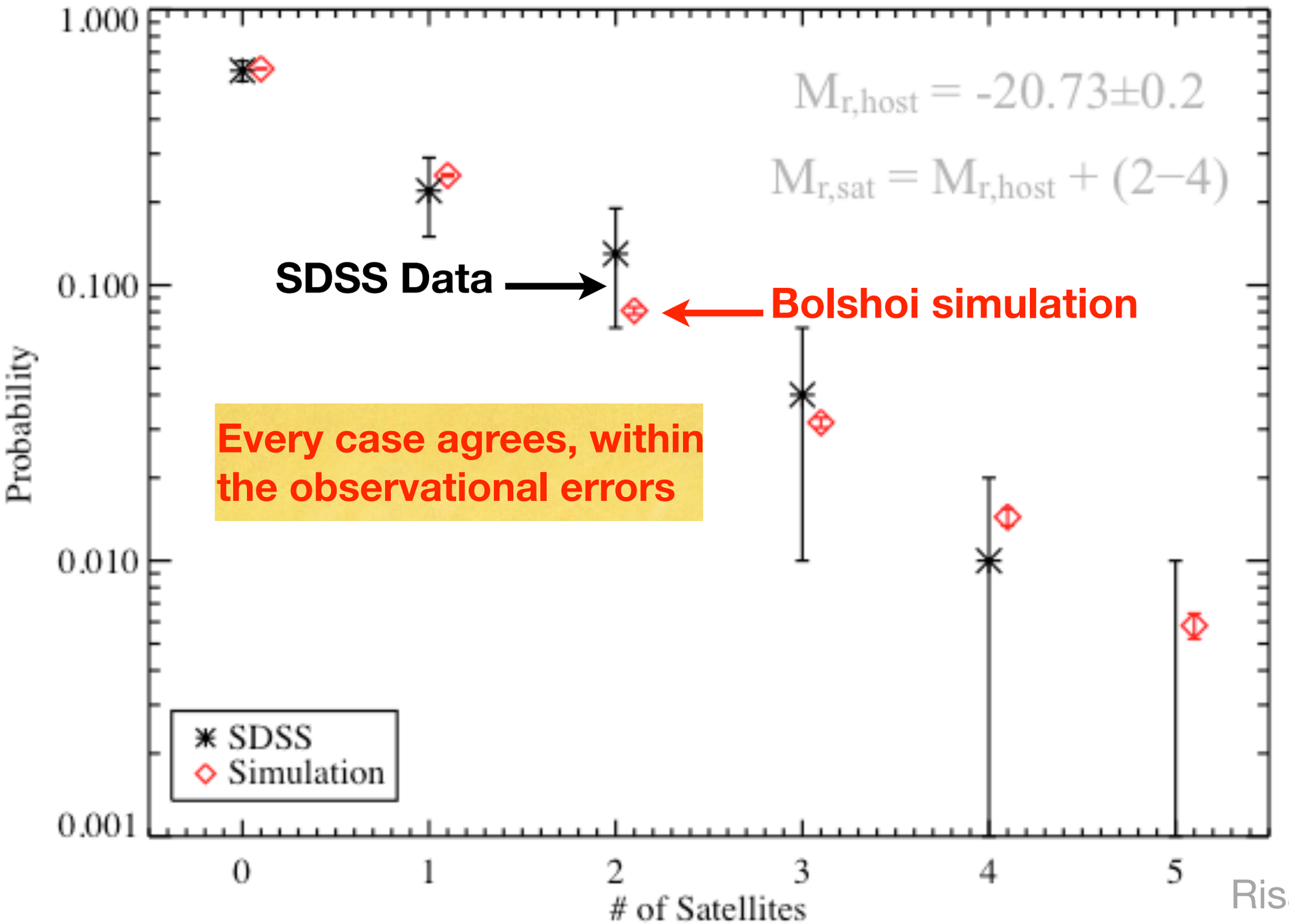

Risa Wechsler

Busha et al. 2011 ApJ
Liu et al. 2011 ApJ

Dark Matter Only simulations on Cosmic, Cluster, & Galactic scales

Name	Code	L_{box} [h^{-1} Mpc]	N_p [10^9]	m_p [h^{-1} $M_\odot$]	ε_{soft} [h^{-1} kpc]
Cosmic					
DEUS FUR	Ramses-Deus	21,000	550	1.2×10^{12}	40.0[a]
Horizon Run 3	GotPM	10,815	370	2.5×10^{11}	150.0
Millennium-XXL	Gadget-3	3000	300	6.2×10^{9}	10.0
Horizon-4Π	Ramses	2000	69	7.8×10^{9}	7.6[a]
Millennium	Gadget-2	500	10	8.6×10^{8}	5.0
Millennium-II	Gadget-3	100	10	6.9×10^{6}	1.0
MultiDark Run1	Art	1000	8.6	8.7×10^{9}	7.6[a]
Bolshoi	Art	250	8.6	1.4×10^{8}	1.0[a]

Name	Code	L_{hires} [h^{-1} Mpc]	$N_{p,hires}$ [10^9]	$m_{p,hires}$ [h^{-1} $M_\odot$]	ε_{soft} [h^{-1} kpc]
Cluster					
Phoenix A-1	Gadget-3	41.2	4.1	6.4×10^{5}	0.15
Name	Code	L_{hires} [Mpc]	$N_{p,hires}$ [10^9]	$m_{p,hires}$ [$M_\odot$]	ε_{soft} [pc]
Galactic					
Aquarius A-1	Gadget-3	5.9	4.3×10^{9}	1.7×10^{3}	20.5
GHalo	Pkdgrav2	3.89	2.1×10^{9}	1.0×10^{3}	61.0
Via Lactea II	Pkdgrav2	4.86	1.0×10^{9}	4.1×10^{3}	40.0

[a] For AMR simulations (Ramses, Art) ε_{soft} refers to the highest resolution cell width.

Table 2 in Kuhlen, Vogelsberger, Angulo 2012, Dark Universe 1, 50-93

Dark Matter Only simulations on Cosmic, Cluster, & Galactic scales

Supercomputers and computational resources utilized for each simulation.

Simulation	Supercomputer	Type	Center	Country	Core-hours [10^6]	N_{cores}	Memory [TB]	Disk space [TB]
DEUS FUR	*Curie Thin Nodes*	Bullx B510	Très Grand Centre de Calcul (TGCC)	France	10	38,016	230	3000
Horizon Run 3	*Tachyon II*	Sun Blades B6275	KISTI Supercomputing Center	Korea	4	8240	21	400
Millennium-XXL	*JuRoPa*	Bull/Sun Blades	Forschungzentrum Jülich	Germany	2.86	12,288	28.5	100
Horizon-4II	*Platine*	Bull Novascale 3045	Commissariat a l'Energie Atomique	France	8	6144	14.7	300
Millennium	*p690*	IBM Power 4	Rechenzentrum Garching	Germany	0.35	512	1	20
Millennium-II	*VIP*	IBM Power 6	Rechenzentrum Garching	Germany	1.4	2048	8	35
MultiDark Run1	*Pleiades*	SGI Altix ICE	NASA Ames Research Center	USA	0.4	4000	8	20
Bolshoi	*Pleiades*	SGI Altix ICE	NASA Ames Research Center	USA	6	13,900	12	100
Phoenix A-1	*DeepComp 7000*	HS21/ x3950 Cluster	Chinese Academy of Science	China	1.9	1024	3	15
Aquarius A-1	*HLRB-II*	SGI Altix 4700	Leibniz Rechenzentrum Garching	Germany	3.5	1024	3	45
GHalo	*Marenostrum*	IBM JS21 Blades	Barcelona Supercomputing Center	Spain	2	1000	1	60
Via Lactea II	*Jaguar*	Cray XT4	Oak Ridge National Lab	USA	1.5	3000	0.3	20

Table 3 in Kuhlen, Vogelsberger, Angulo 2012, Dark Universe 1, 50-93

Determination of σ_8 and Ω_M from CMB+

WMAP+SN+Clusters Planck+WP+HighL+BAO

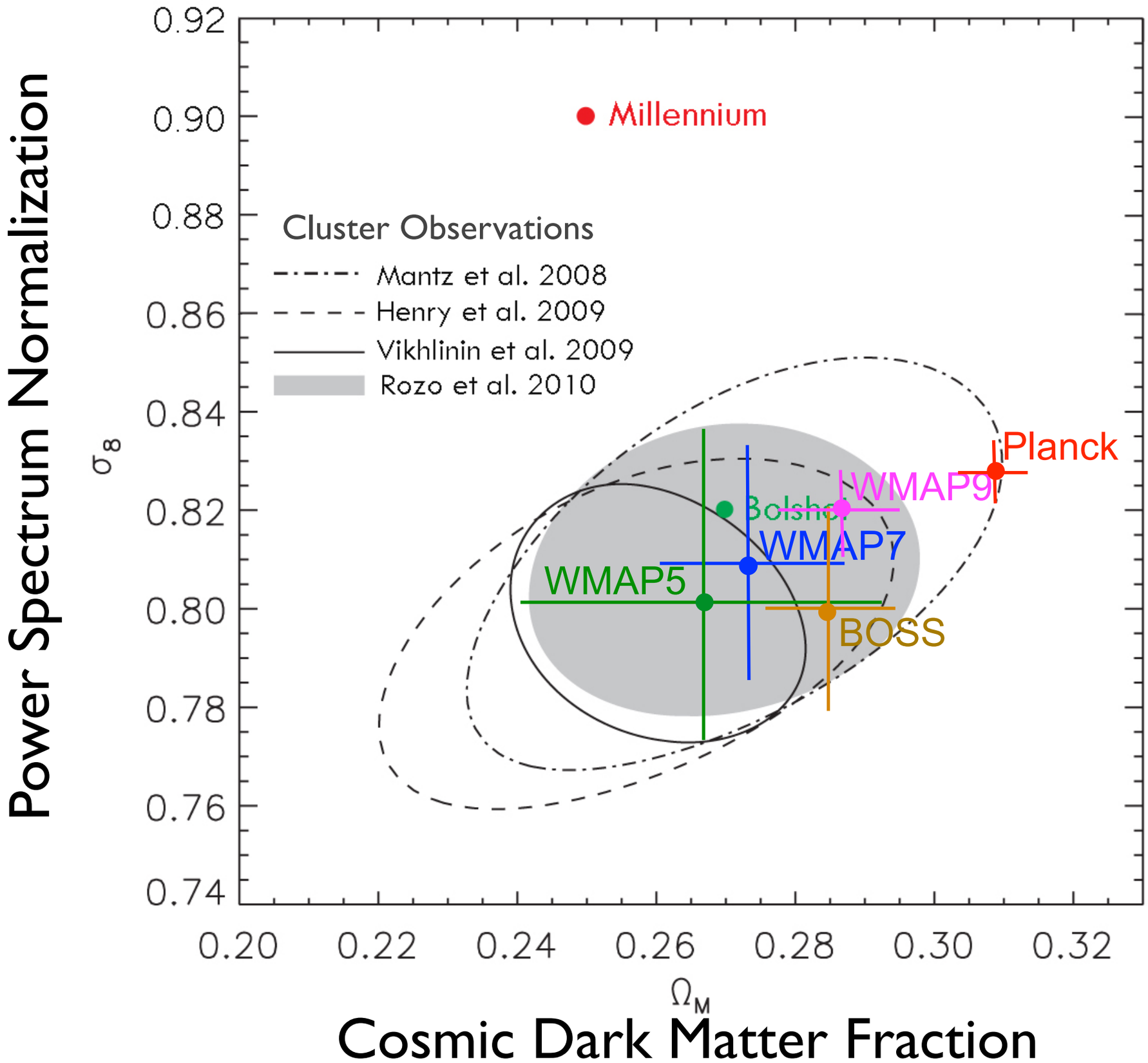

Bolshoi-Planck Cosmological Simulation

Anatoly Klypin & Joel Primack

Finished 6 Aug 2013 on Pleiades computer

at NASA Ames Research Center

8.6×10^8 particles 1 kpc resolution

Bolshoi-Planck has a lot more massive halos at high redshifts than Bolshoi!

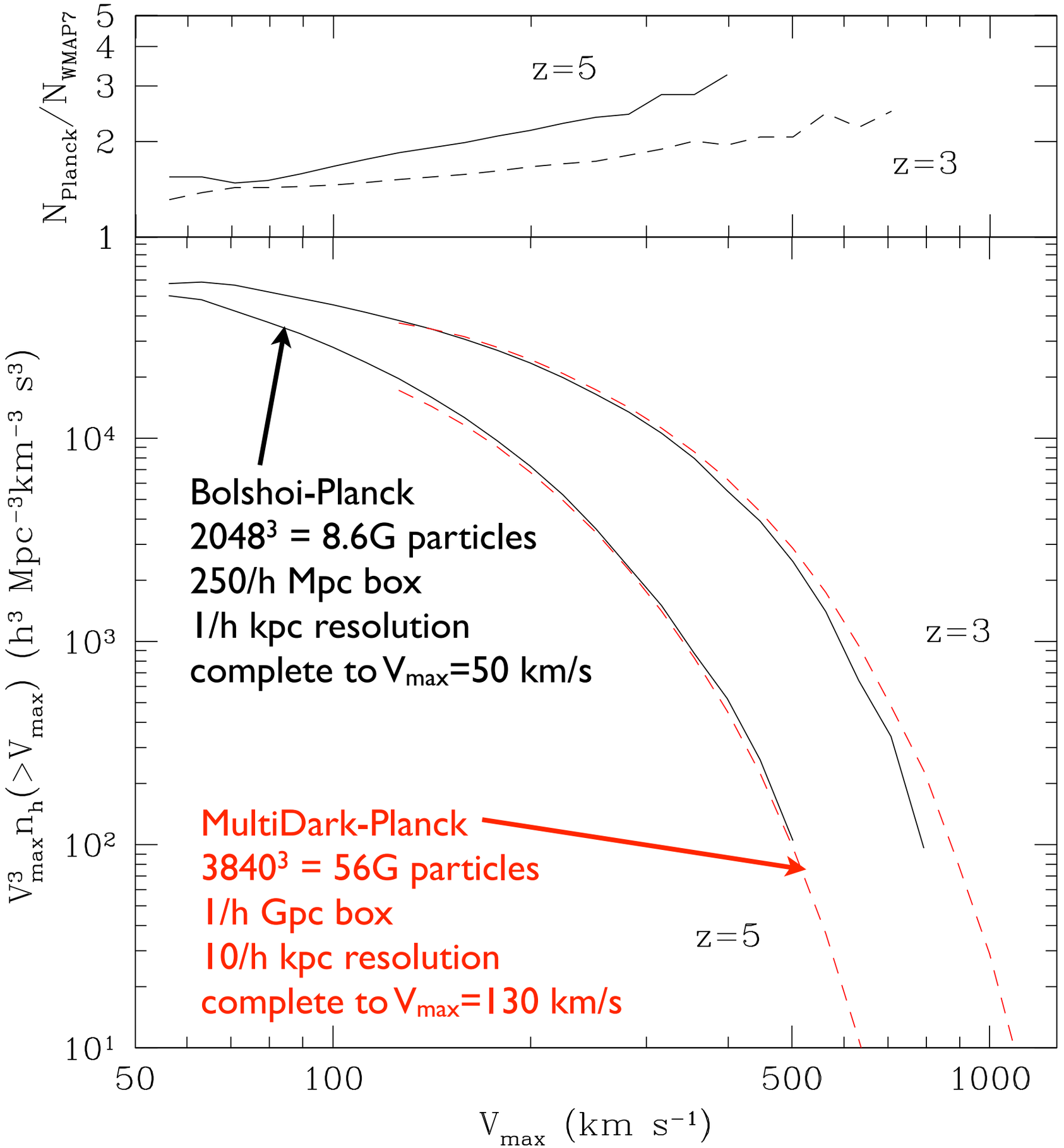

Mon. Not. R. Astron. Soc. **336,** 112–118 (2002)

The abundance and clustering of dark haloes in the standard ΛCDM cosmogony

H. J. Mo★ and S. D. M. White★

Max-Planck-Institute für Astrophysik, Karl-Schwarzschild-Strasse 1, 85740 Garching, Germany

Accepted 2002 May 27. Received 2002 May 27; in original form 2002 March 4

$\Omega_{\rm m,0}=0.3$, $\Omega_{\Lambda,0}=0.7$, $h=0.7$ and $\sigma_8=0.9$

ABSTRACT

Much evidence suggests that we live in a flat cold dark matter universe with a cosmological constant. Accurate analytic formulae are now available for many properties of the dark halo population in such a Universe. Assuming current 'concordance' values for the cosmological parameters, we plot halo abundance against redshift as a function of halo mass, halo temperature, the fraction of cosmic matter in haloes, halo clustering strength, and the clustering strength of the $z=0$ descendants of high-redshift haloes. These plots are useful for understanding how nonlinear structure grows in the model. They demonstrate a number of properties that may seem surprising, for example: 10^9 $M_\odot$ haloes are as abundant at $z=20$ as L_* galaxies are today; 10^6 K haloes are equally abundant at $z=8$ and at $z=0$; 10 per cent of all matter is currently in haloes hotter than 1 keV, while more than half is in haloes too cool to trap photo-ionized gas; 1 per cent of all matter at $z=15$ is in haloes hot enough to ionize hydrogen; haloes of given mass or temperature are more clustered at *higher* redshift; haloes with the abundance of present-day L_* galaxies are equally clustered at all $z<20$; the metals produced by star-formation at $z>10$ are more clustered at $z=0$ than are L_* galaxies.

H. J. Mo, S.D.M. White
MNRAS 336 (2002) 112

The abundance and clustering of dark haloes in the standard Lambda CDM cosmogony

We define the characteristic properties of a dark halo within a sphere of radius r_{200} chosen so that the mean enclosed density is 200 times the mean cosmic value. Then, with the Fourier transform of a radius R spherical top hat $\tilde{W}(x) = 3(\sin kR - kR\cos kR)/(kR)^3$

$$r_{200} = \left[\frac{GM}{100\Omega_{\rm m}(z)H^2(z)}\right]^{1/3}, \quad \text{and} \quad V_c = \left(\frac{GM}{r_{200}}\right)^{1/2}, \; R(M) \equiv \left(\frac{3M}{4\pi\bar{\rho}_0}\right)^{1/3}, \; \sigma^2(R) = \frac{1}{2\pi^2}\int_0^\infty k^3 P(k)\tilde{W}^2(kR)\frac{{\rm d}k}{k},$$

According to the argument first given by Press & Schechter (1974, hereafter PS), the abundance of haloes as a function of mass and redshift, expressed as the number of haloes per unit comoving volume at redshift z with mass in the interval $(M, M + dM)$, may be written as

$$n(M,z){\rm d}M = \sqrt{\frac{2}{\pi}}\frac{\bar{\rho}_0}{M}\frac{{\rm d}\nu}{{\rm d}M}\exp\left(-\frac{\nu^2}{2}\right){\rm d}M\,. \tag{9}$$

Here $\nu \equiv \delta_c/[D(z)\sigma(M)]$, where $\delta_c \approx 1.69$ and the growth factor is

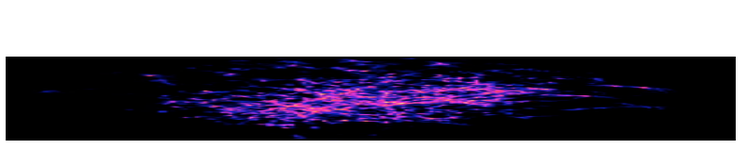

$$g(z) \approx \frac{5}{2}\Omega_{\rm m}\left[\Omega_{\rm m}^{4/7} - \Omega_\Lambda + (1+\Omega_{\rm m}/2)(1+\Omega_\Lambda/70)\right]^{-1},$$

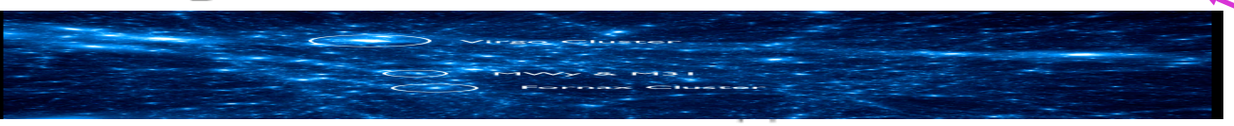

Lahav, Lilje, Primack, & Rees 1991

Press & Schechter derived the above mass function from the *Ansatz* that the fraction F of all cosmic mass which at redshift z is in haloes with masses exceeding M is *twice* the fraction of randomly placed spheres of radius $R(M)$ which have linear overdensity at that time exceeding δ_c, the value at which a spherical perturbation collapses. Since the linear fluctuation distribution is gaussian this hypothesis implies

$$F(>M,z) = {\rm erfc}\left(\frac{\nu}{\sqrt{2}}\right), \tag{12}$$

and equation (9) then follows by differentiation.

The PS formula is $$n(M,z)\mathrm{d}M = \sqrt{\frac{2}{\pi}}\frac{\overline{\rho}_0}{M}\frac{\mathrm{d}\nu}{\mathrm{d}M}\exp\left(-\frac{\nu^2}{2}\right)\mathrm{d}M \quad (9)$$

Numerical simulations show that although the scaling properties implied by the PS argument hold remarkably well for a wide variety of hierarchical cosmogonies, substantially better fits to simulated mass functions are obtained if the error function in equation (12) is replaced by a function of slightly different shape. Sheth & Tormen (1999) suggested the following modification of equation (9)

$$n(M,z)\mathrm{d}M = A\left(1+\frac{1}{\nu'^{2q}}\right)\sqrt{\frac{2}{\pi}}\frac{\overline{\rho}}{M}\frac{\mathrm{d}\nu'}{\mathrm{d}M}\exp\left(-\frac{\nu'^2}{2}\right)\mathrm{d}M, \quad (14)$$

where $\nu' = \sqrt{a}\nu$, $a = 0.707$, $A \approx 0.322$ and $q = 0.3$.

[See Sheth, Mo & Tormen (2001) and Sheth & Tormen (2002) for a justification of this formula in terms of an ellipsoidal model for perturbation collapse.] The fraction of all matter in haloes with mass exceeding M can be obtained by integrating equation (14). To good approximation,

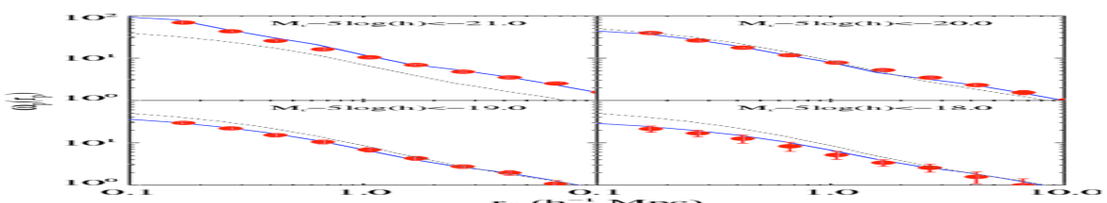

In a detailed comparison with a wide range of simulations, Jenkins et al. (2001) confirmed that this model is indeed a good fit provided haloes are defined at the same density contrast relative to the mean in all cosmologies. This is for FOF halo finding -- but Klypin, Trujillo, Primack 2010 find that the more physical Bound Density Maximum (BDM) halo finder results in 10x lower halo number density at z=10.

Comoving Halo Number Density $n(M_{halo})$

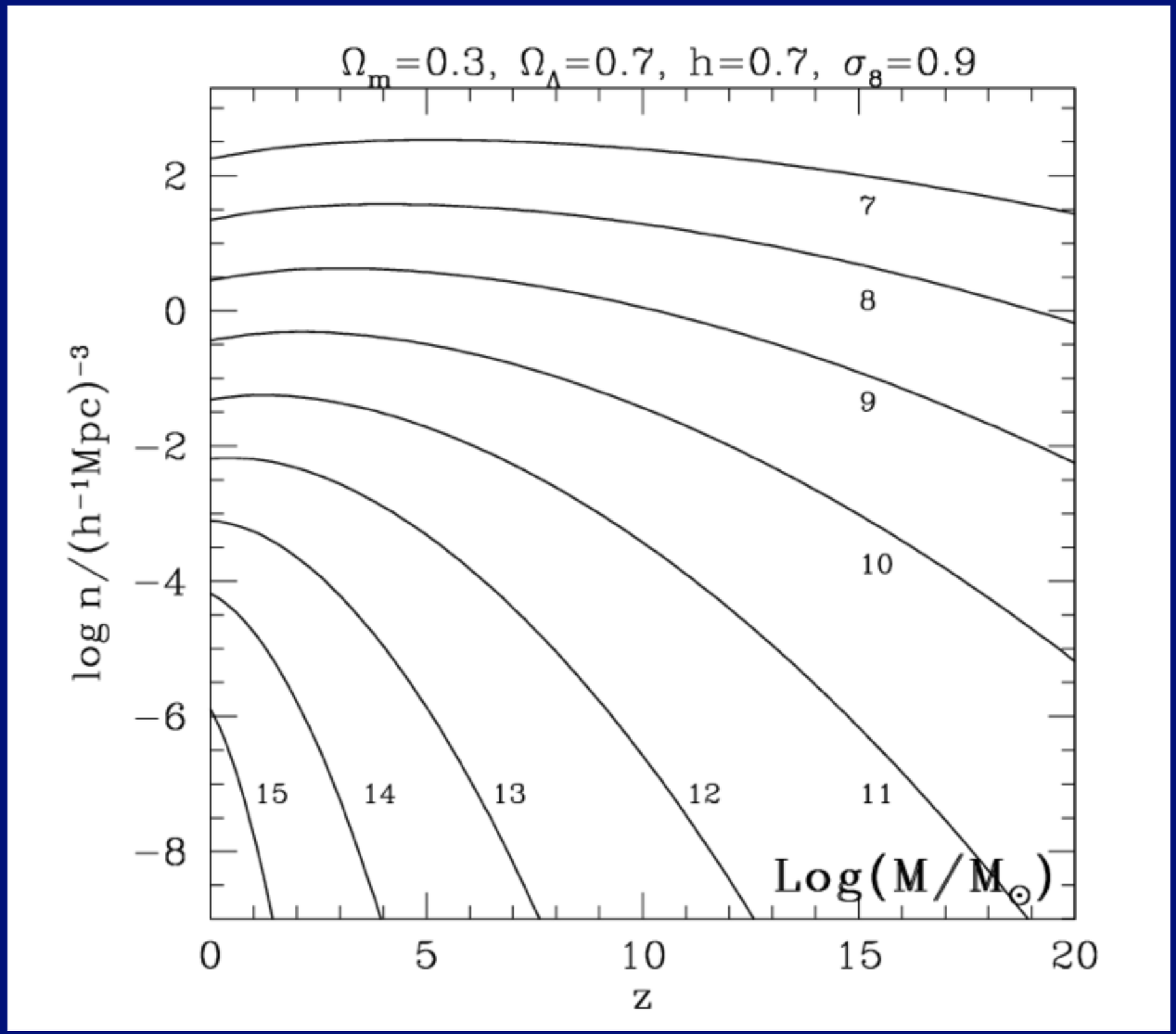

Mo & White 2002

Comoving Halo Number Density $n(M_{halo})$

Mo & White 2002

Standard LCDM

$\Omega_{m,0} = 0.3$, $\Omega_{\Lambda,0} = 0.7$, $h = 0.7$ and $\sigma_8 = 0.9$

About 1% of the mass is in halos with $M > 10^{15}\ M_\odot$ at $z = 0$, $M > 10^{12}\ M_\odot$ at $z = 5$, and $M > 10^{10}\ M_\odot$ at $z = 10$

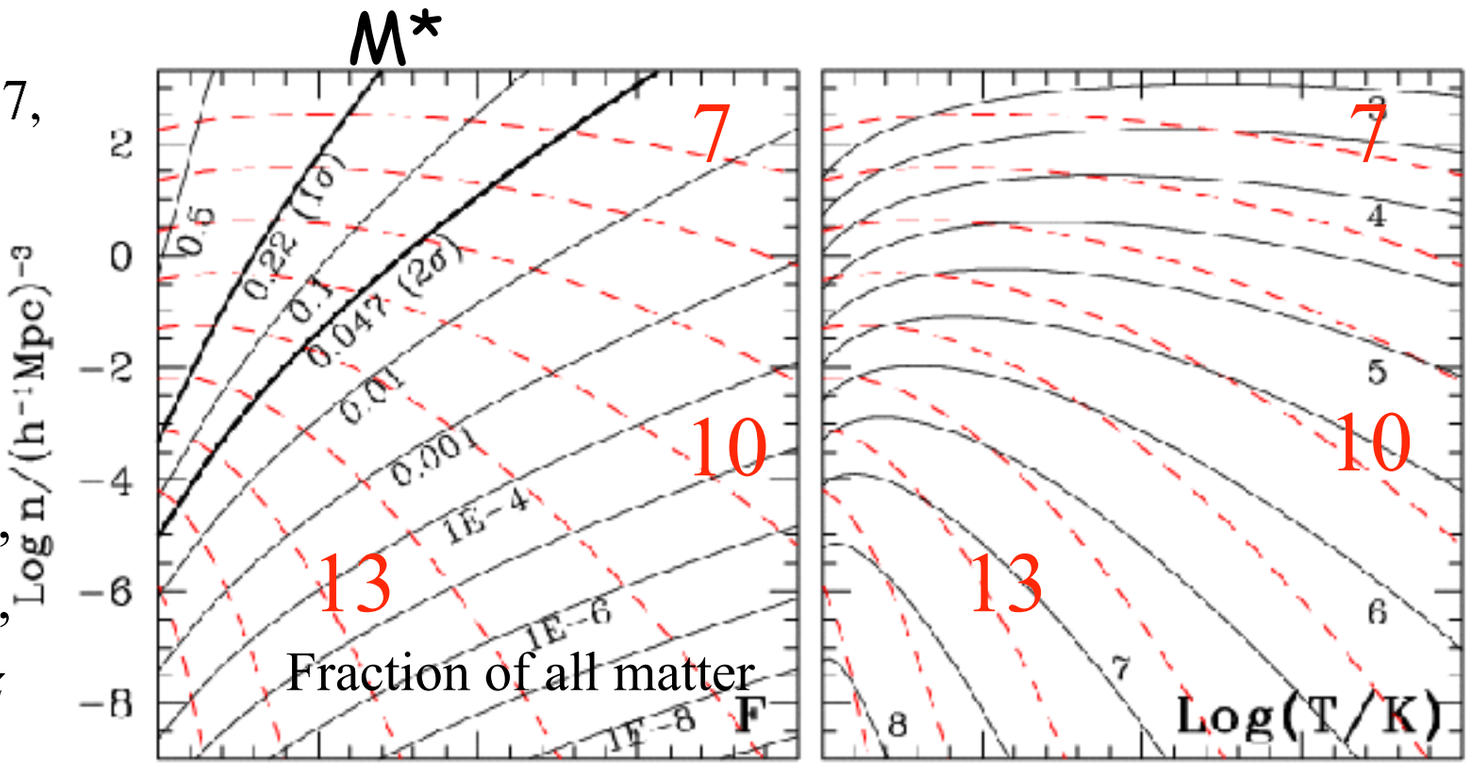

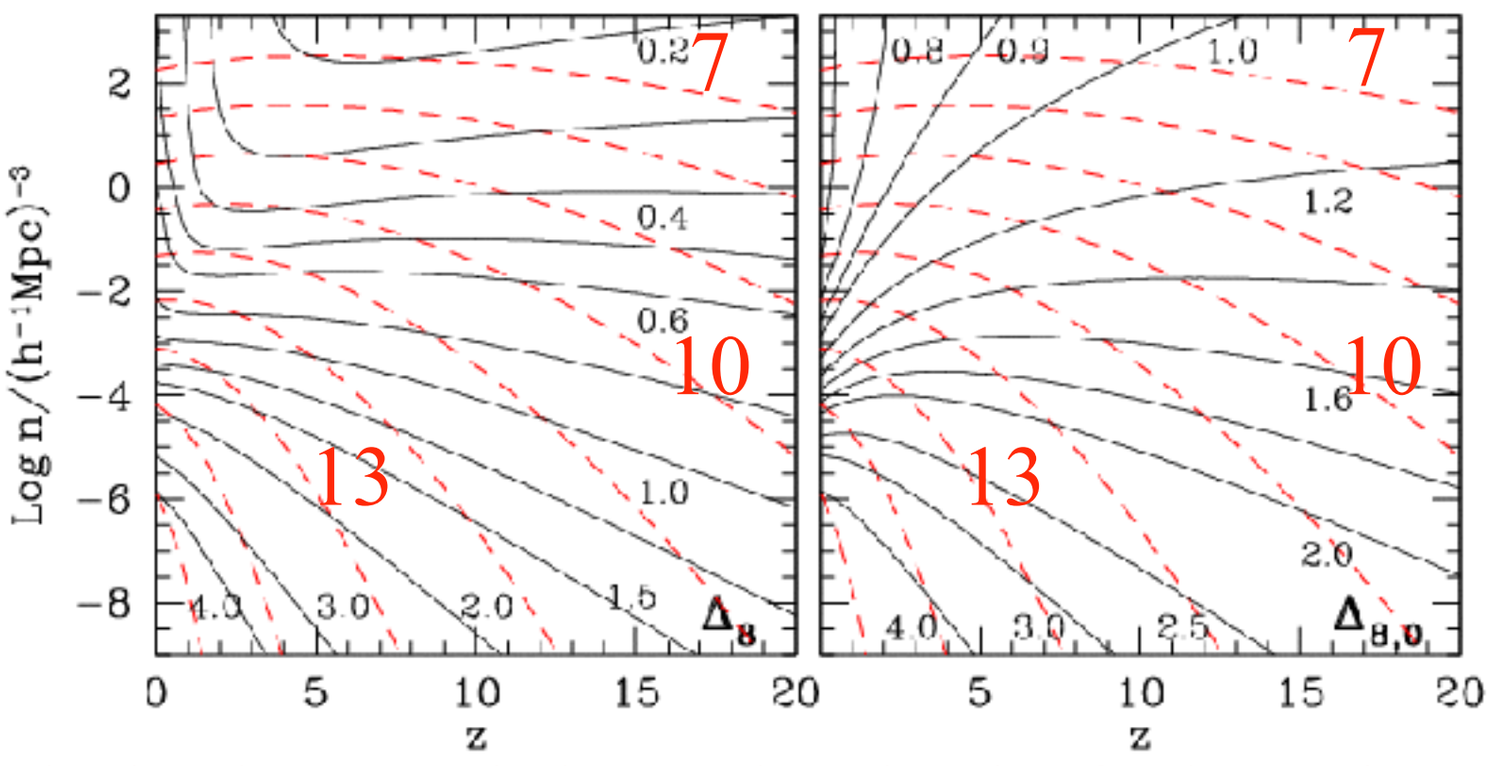

Δ_8 = "comoving clustering length of halos" = rms overdensity of halos > M at plotted redshift

A $10^{12}\ M_\odot$ halo now and a $2 \times 10^{10}\ M_\odot$ halo at $z = 20$ both have $T \sim 10^6$ K (i.e, $V_c \sim 200$ km/s)

T = virial temperature

$\Delta_{8,0}$ = comoving clustering length of halo descendants at $z = 0$

Dashed red curves: halo number density for log M/M_{sun}

Cosmological Simulation Methods

Dissipationless Simulations

Particle-Particle (PP) - Aarseth NbodyN, N=1,...,6
Particle Mesh (PM) - see Klypin & Holtzman 1997
Adaptive PM (P3M) - Efstathiou et al.
Tree - Barnes & Hut 1986, PKDGRAV Stadel
TreePM - GADGET2, Springel 2005
Adaptive Mesh Refinement (AMR) - Klypin (ART)

Hydrodynamical Simulations

Fixed grid - Cen & Ostriker
Smooth Particle Hydrodynamics (SPH) - GADGET2, Springel 2005
- Gasoline, Wadsley, Stadel, & Quinn
Adaptive grid - ART+hydro - Klypin & Kravtsov; ENZO - Norman et al.;
- RAMSES - Teyssier

Initial Conditions

Standard: Gaussian P(k) realized uniformly, Zel'dovich displacement
Multimass - put lower mass particles in a small part of sim volume
Constrained realization - small scale: simulate individual halos (NFW)
large scale: simulate particular region

Reviews

Bertschinger ARAA 1998; Klypin lectures 2002; U Washington website http://www-hpcc.astro.washington.edu/; UC-HiPACC 2010 summer school at UCSC http://hipacc.ucsc.edu/html/2010SummerSchool_archive.html

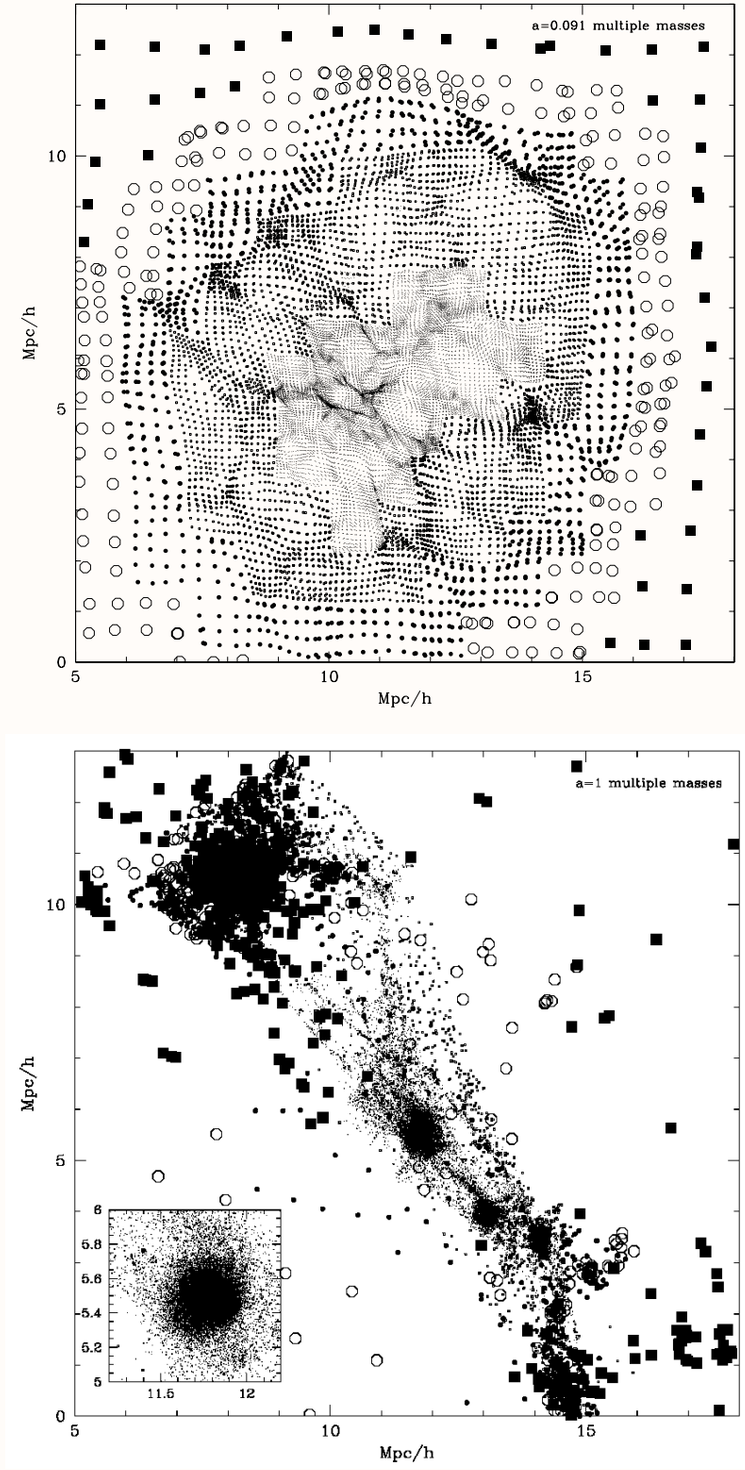

Fig. 2.— Distribution of particles of different masses in a thin slice through the center of halo A_1 (see Table 1) at $z = 10$ (top panel) and at $z = 0$ (bottom panel). To avoid crowding of points the thickness of the slice is made smaller in the center (about $30h^{-1}$kpc) and larger ($1h^{-1}$Mpc) in the outer parts of the forming halo. Particles of different mass are shown with different symbols: tiny dots, dots, large dots, squares, and open circles.

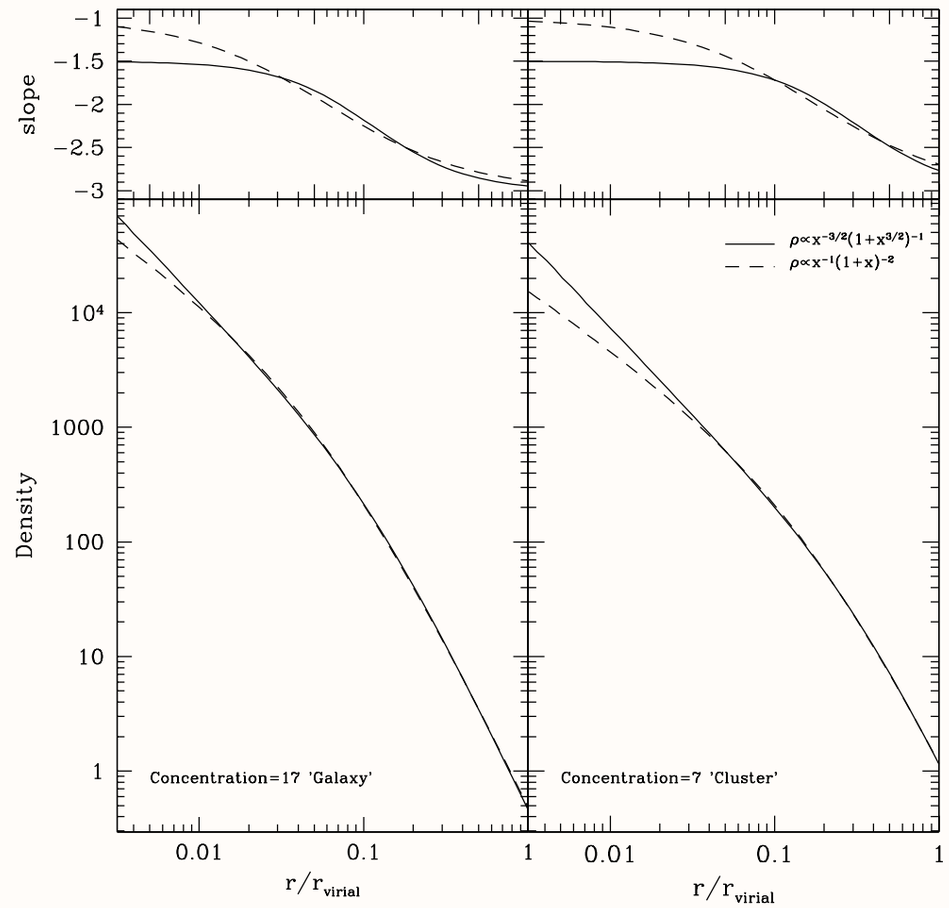

Fig. 3.— Comparison of the Moore et al. and the NFW profiles. Each profile is normalized to have the same virial mass and the same radius of the maximum circular velocity. *Left panels:* High-concentration halo typical of small galaxy-size halos $C_{\rm NFW} = 17$. *Right panels:* Low-concentration halo typical of cluster-size halos. The deviations are very small ($< 3\%$) for radii $r > r_s/2$. Top panels show the local logarithmic slope of the profiles. Note that for the high concentration halo the slope of the profile is significantly larger than the asymptotic value -1 even at very small radii $r \approx 0.01 r_{\rm vir}$.

Klypin, Kravtsov, Bullock & Primack 2001

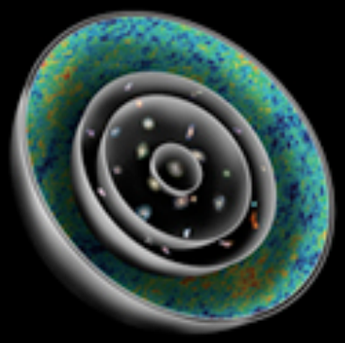

The New Universe and the Human Future

How a Shared Cosmology Could Transform the World

Nancy Ellen Abrams and Joel R. Primack

Click to view videos

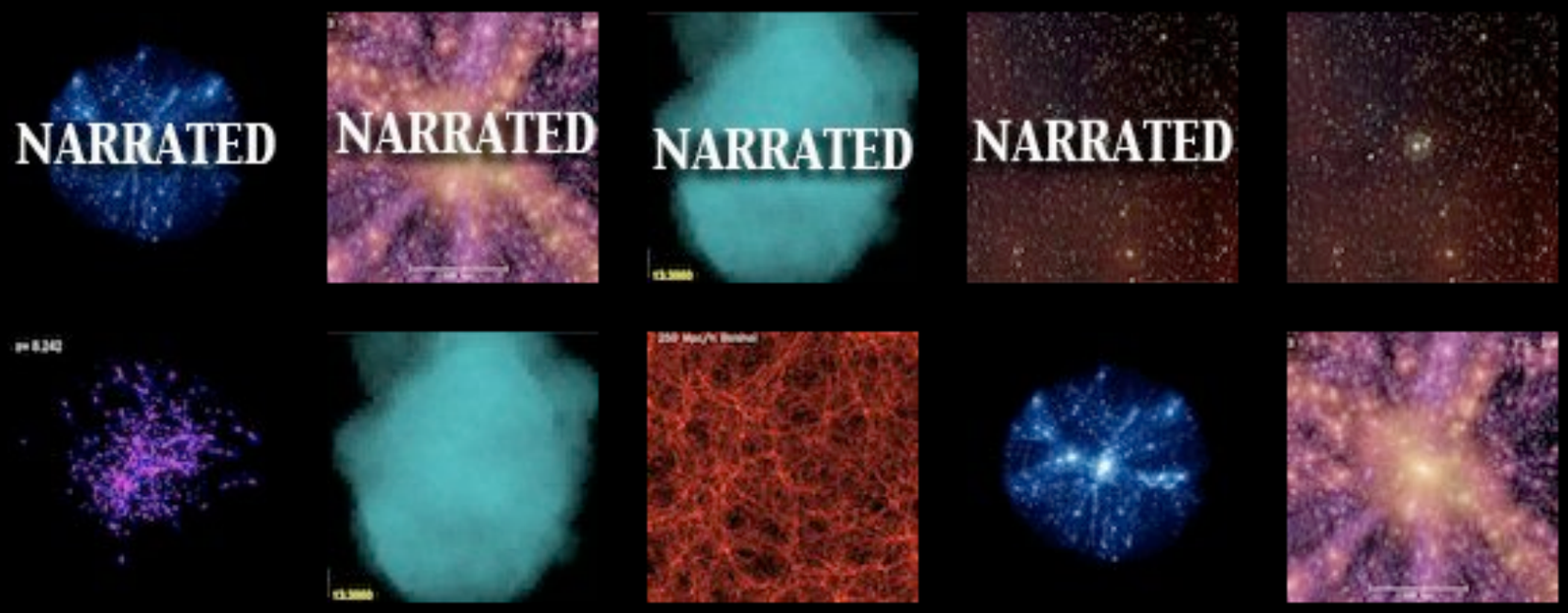

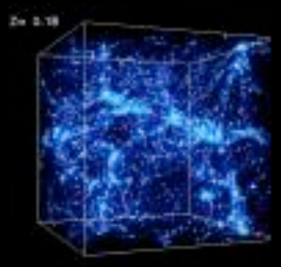

Extra Videos

Many relevant videos can be found at this URL:
http://new-universe.org/zenphoto/Chapter3/Videos/

Particle number in cosmological N-body simulations vs. pub date

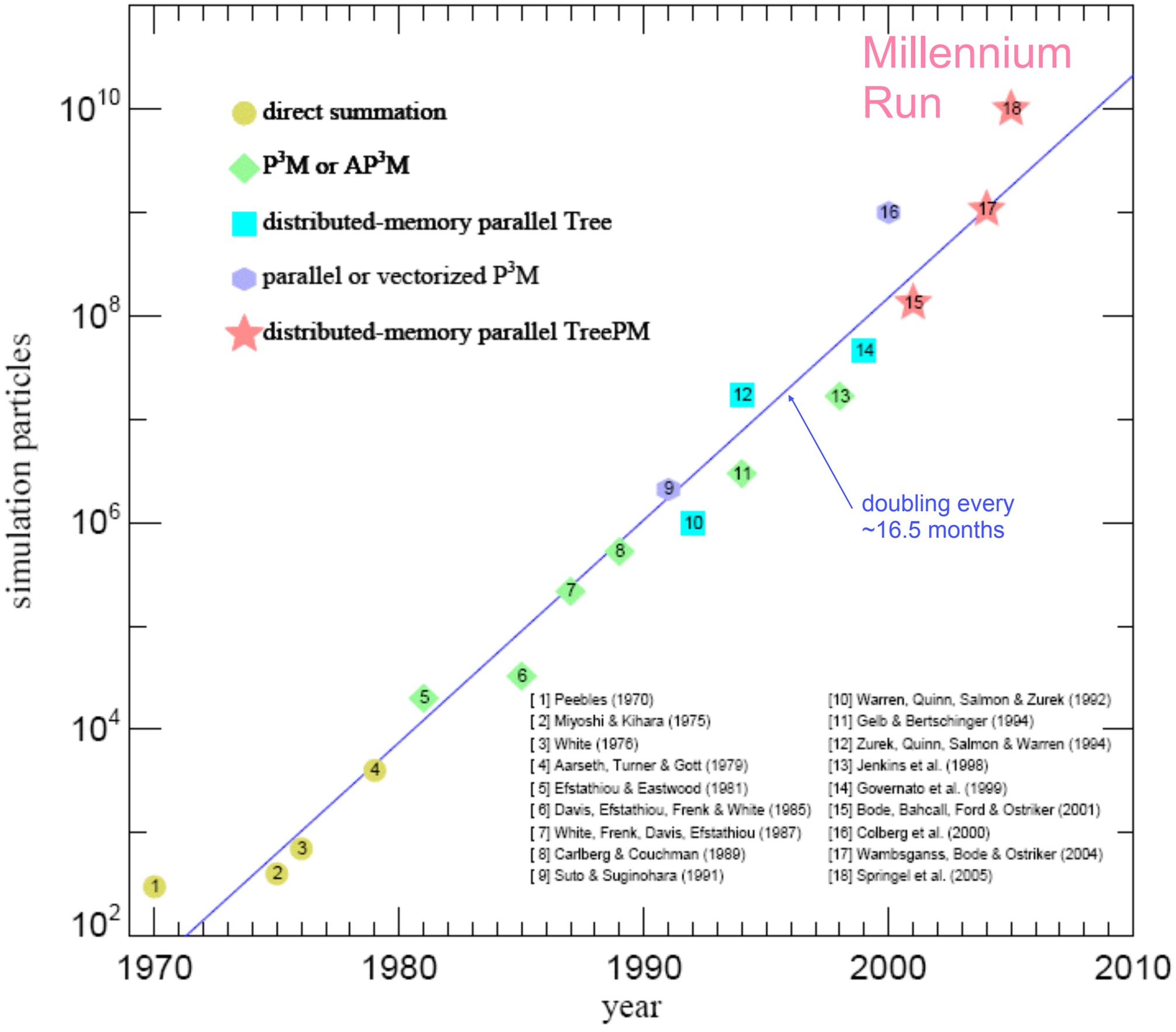

Particle number in cosmological N-body simulations vs. pub date

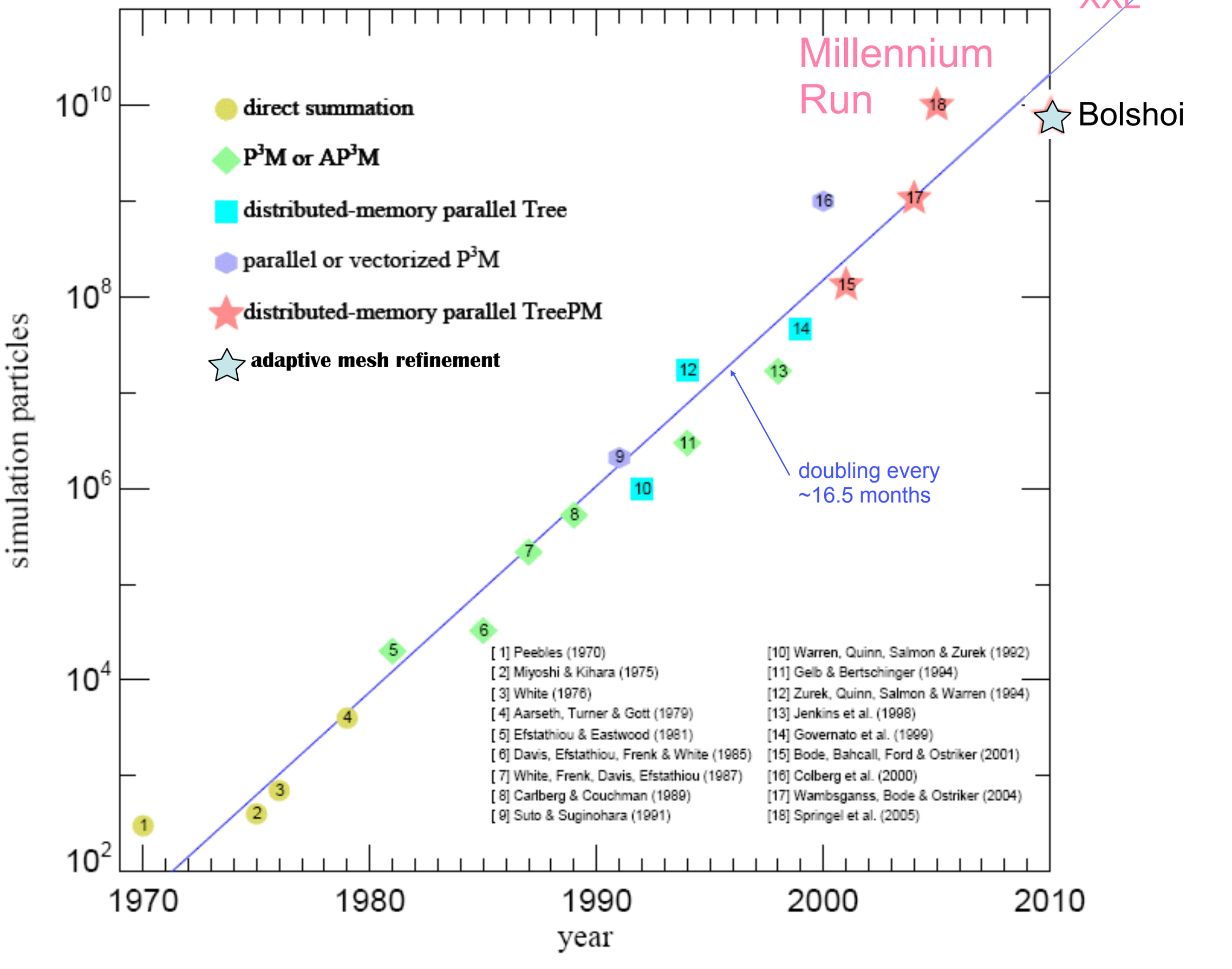

WMAP-only Determination of σ_8 and Ω_M

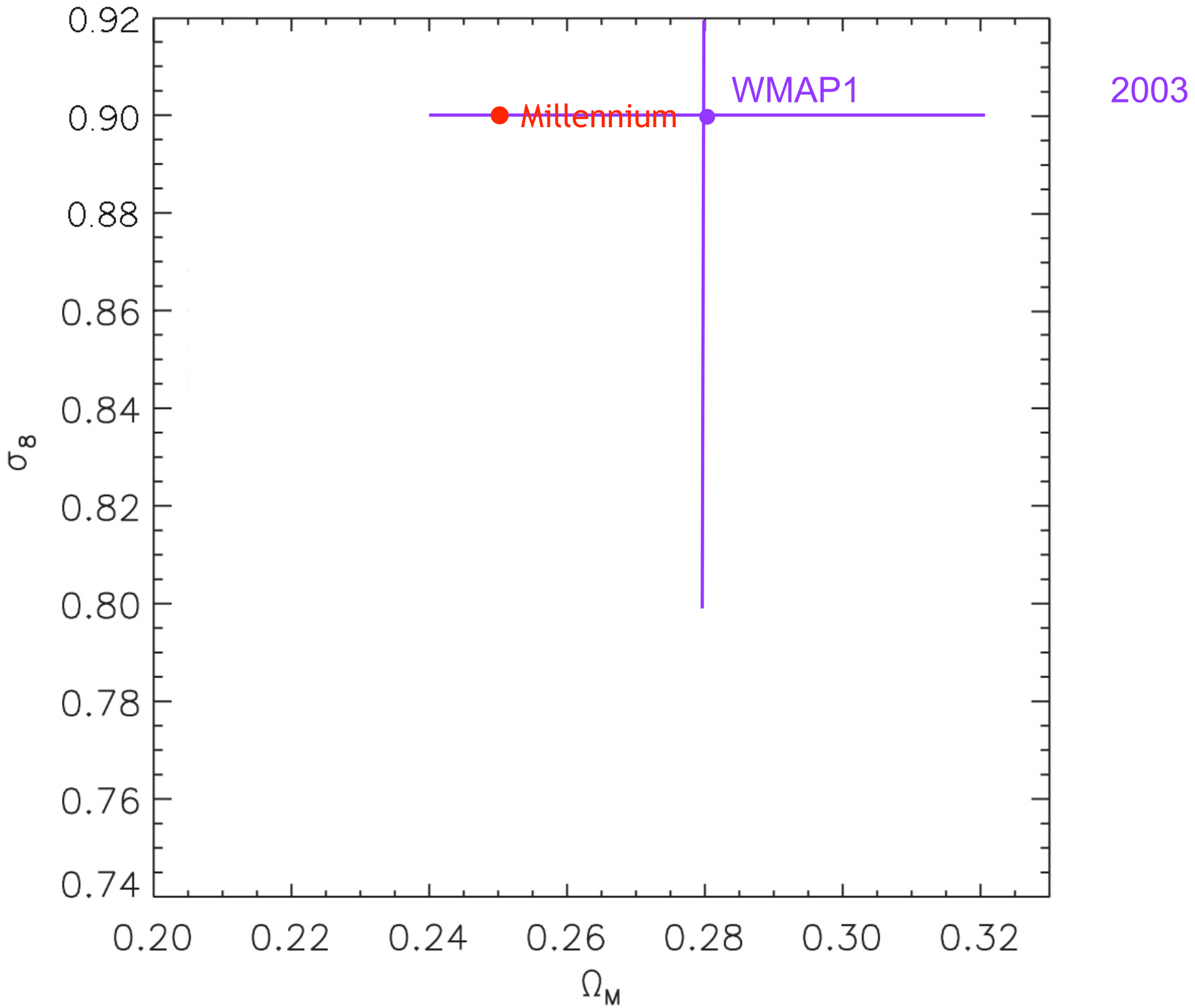

The Millennium Run

• **properties of halos** (radial profile, concentration, shapes)
• **evolution of the number density of halos**, essential for normalization of Press-Schechter-type models
• **evolution of the distribution and clustering of halos** in real and redshift space, for comparison with observations
• **accretion history of halos**, assembly bias (variation of large-scale clustering with as- sembly history), and correlation with halo properties including angular momenta and shapes
• **halo statistics** including the mass and velocity functions, angular momentum and shapes, subhalo numbers and distribution, and correlation with environment

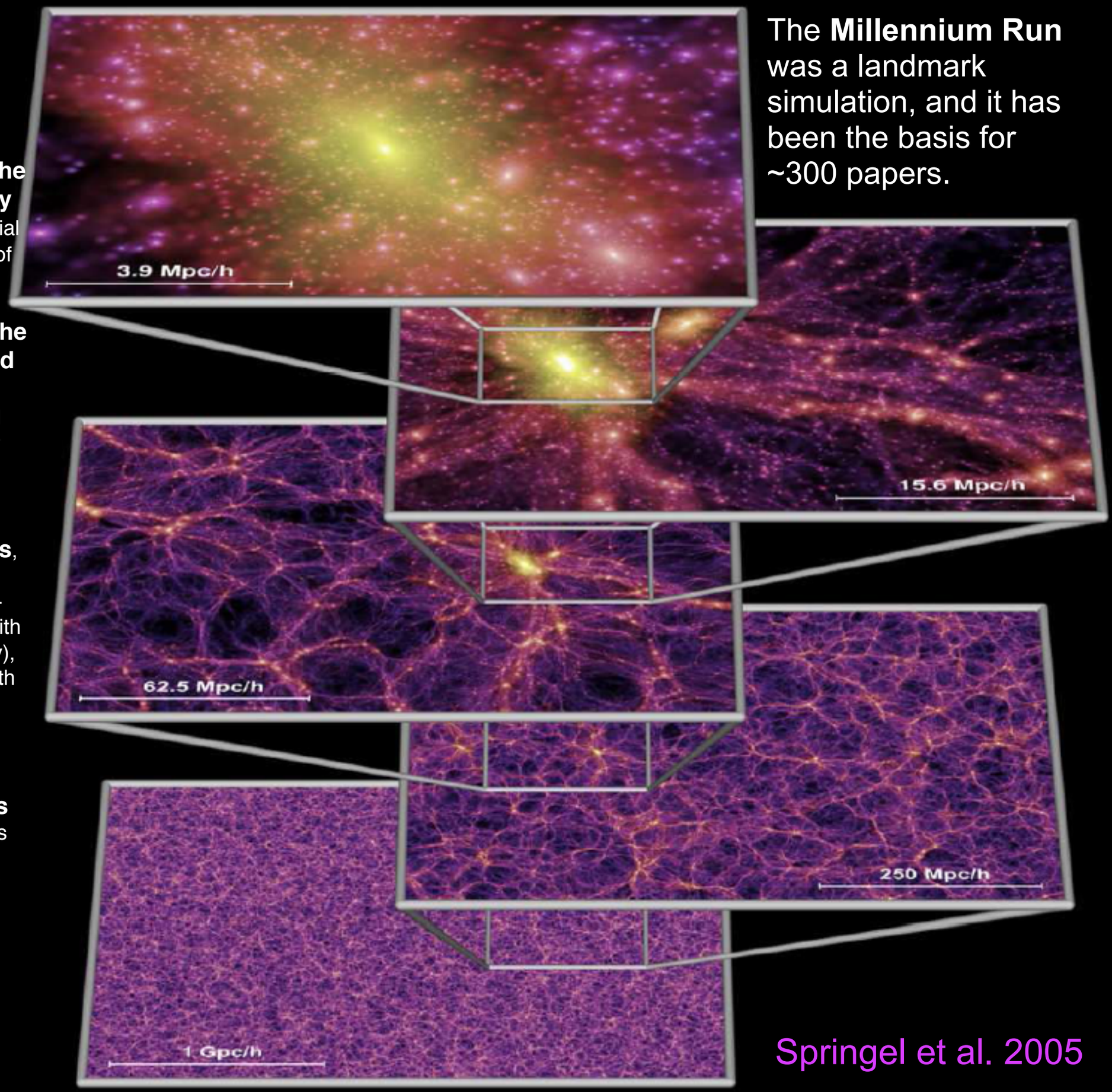

The **Millennium Run** was a landmark simulation, and it has been the basis for ~300 papers.

Springel et al. 2005

• **void statistics**, including sizes and shapes and their evolution, and the orientation of halo spins around voids
• quantitative descriptions of the evolving **cosmic web**, including applications to weak gravitational lensing
• preparation of **mock catalogs**, essential for analyzing SDSS and other survey data, and for preparing for new large surveys for dark energy etc.
• **merger trees**, essential for **semi-analytic modeling** of the evolving galaxy population, including models for the galaxy merger rate, the history of star formation and galaxy colors and morphology, the evolving AGN luminosity function, stellar and AGN feedback, recycling of gas and metals, etc.

WMAP-only Determination of σ_8 and Ω_M

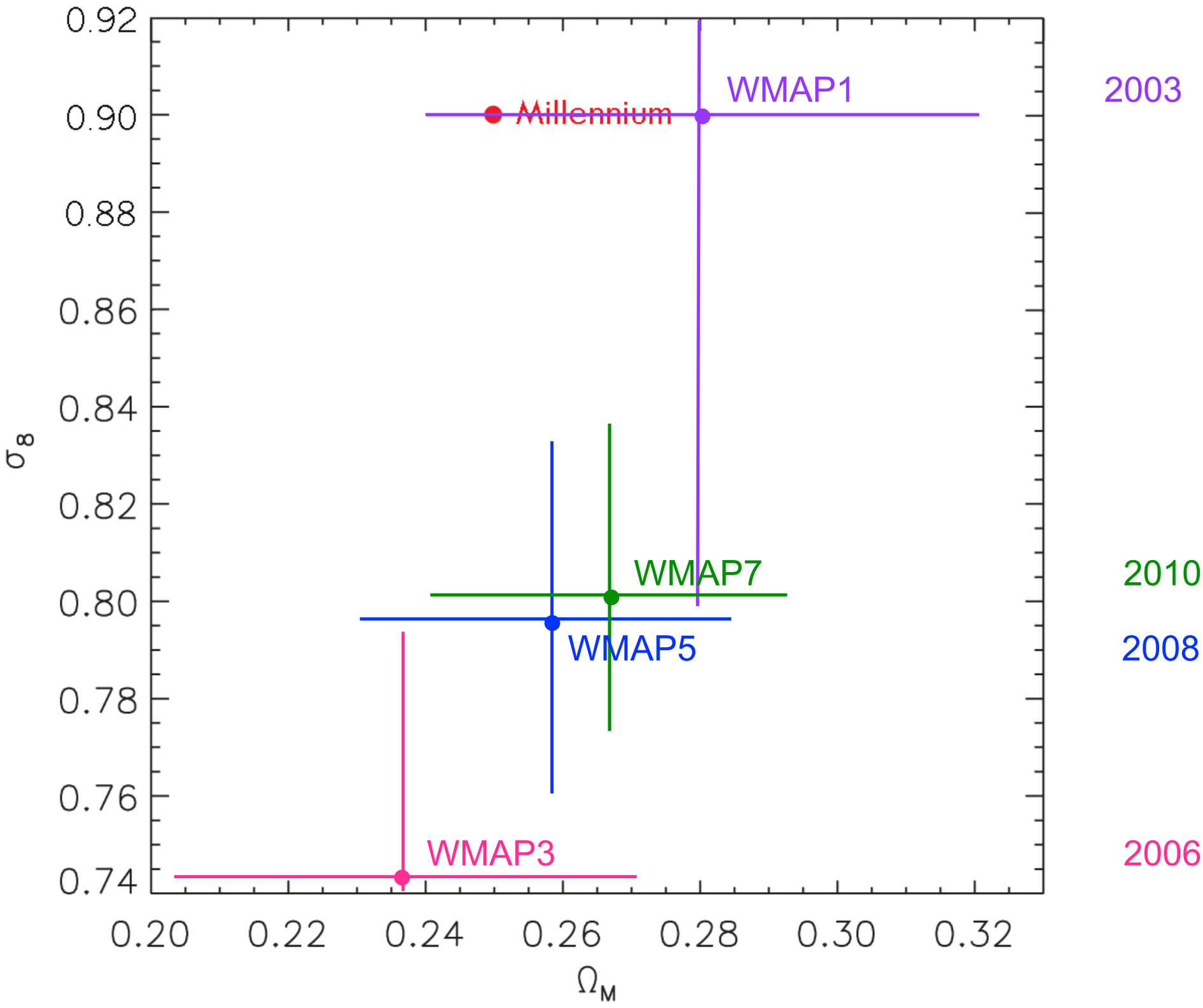

WMAP+SN+Clusters Determination of σ_8 and Ω_M

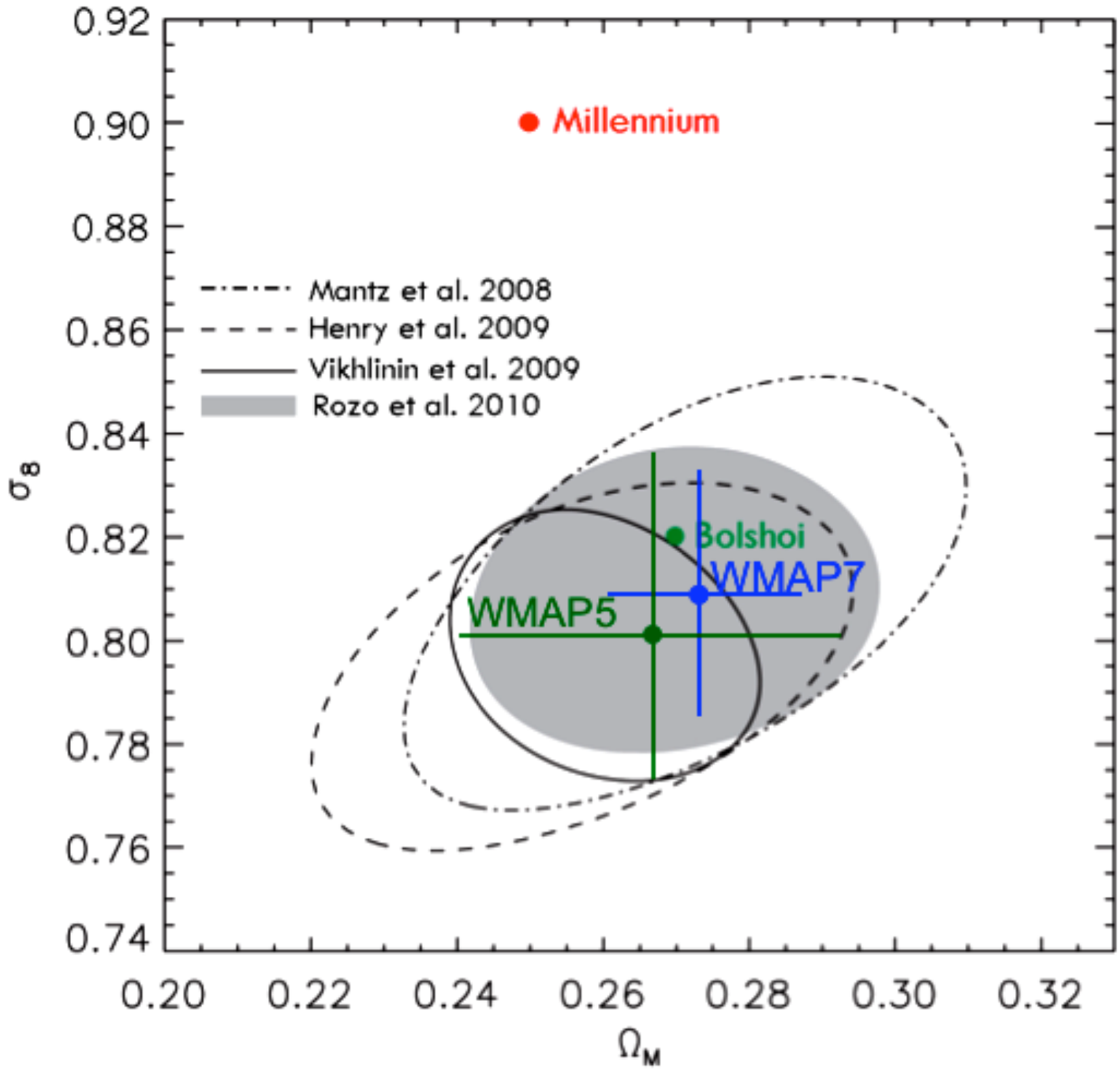

The Bolshoi simulation

ART code

250Mpc/h Box
LCDM

σ_8 = 0.82
h = 0.70

8G particles
1kpc/h force resolution
1e8 Msun/h mass res

dynamical range 262,000
time-steps = 400,000

NASA AMES
supercomputing center
Pleiades computer
13824 cores
12TB RAM
75TB disk storage
6M cpu hrs
18 days wall-clock time

Cosmological parameters are consistent with the latest observations

Force and Mass Resolution are nearly an order of magnitude better than Millennium-I

Force resolution is the same as Millennium-II, in a volume 16x larger

Halo finding is complete to $V_{circ} > 50$ km/s, using both BDM and ROCKSTAR halo finders

Bolshoi and MultiDark halo catalogs were released in September 2011 at Astro Inst Potsdam; Merger Trees will soon be available

Bolshoi Sub-Halo Abundance Matching

Luminosity-Velocity Relation

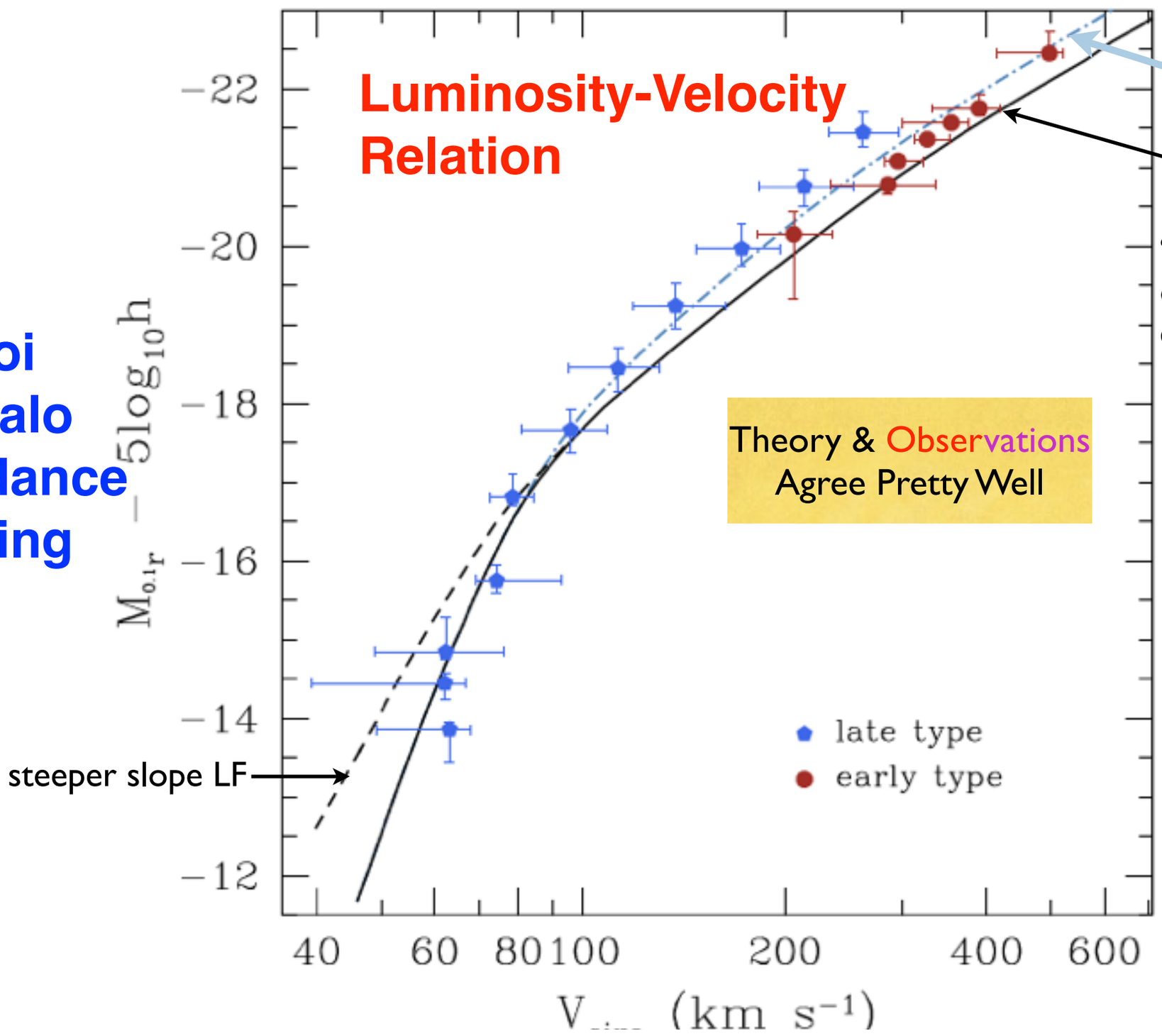

median Vcirc without AC

median Vcirc with AC

"AC" = Adiabatic Contraction of dark matter halos when baryons cool & condense to halo centers, following Blumenthal, Faber, Flores, & Primack 1986

Theory & Observations Agree Pretty Well

Trujillo-Gomez, Klypin, Primack, & Romanowsky ApJ 2011

Fig. 4.— Comparison of the observed LuminosityVelocity relation with the predictions of the ΛCDM model. The solid curve shows the median values of $^{0.1}r$-band luminosity vs. circular velocity for the model galaxy sample. The circular velocity for each model galaxy is based on the peak circular velocity of its host halo over its entire history, measured at a distance of 10 kpc from the center including the cold baryonic mass and the standard correction due to adiabatic halo contraction. The dashed curve show results for a steeper ($\alpha = -1.34$) slope of the LF. The dot-dashed curve shows predictions after adding the baryon mass but without adiabatic contraction. Points show representative observational samples.

Bolshoi Sub-Halo Abundance Matching

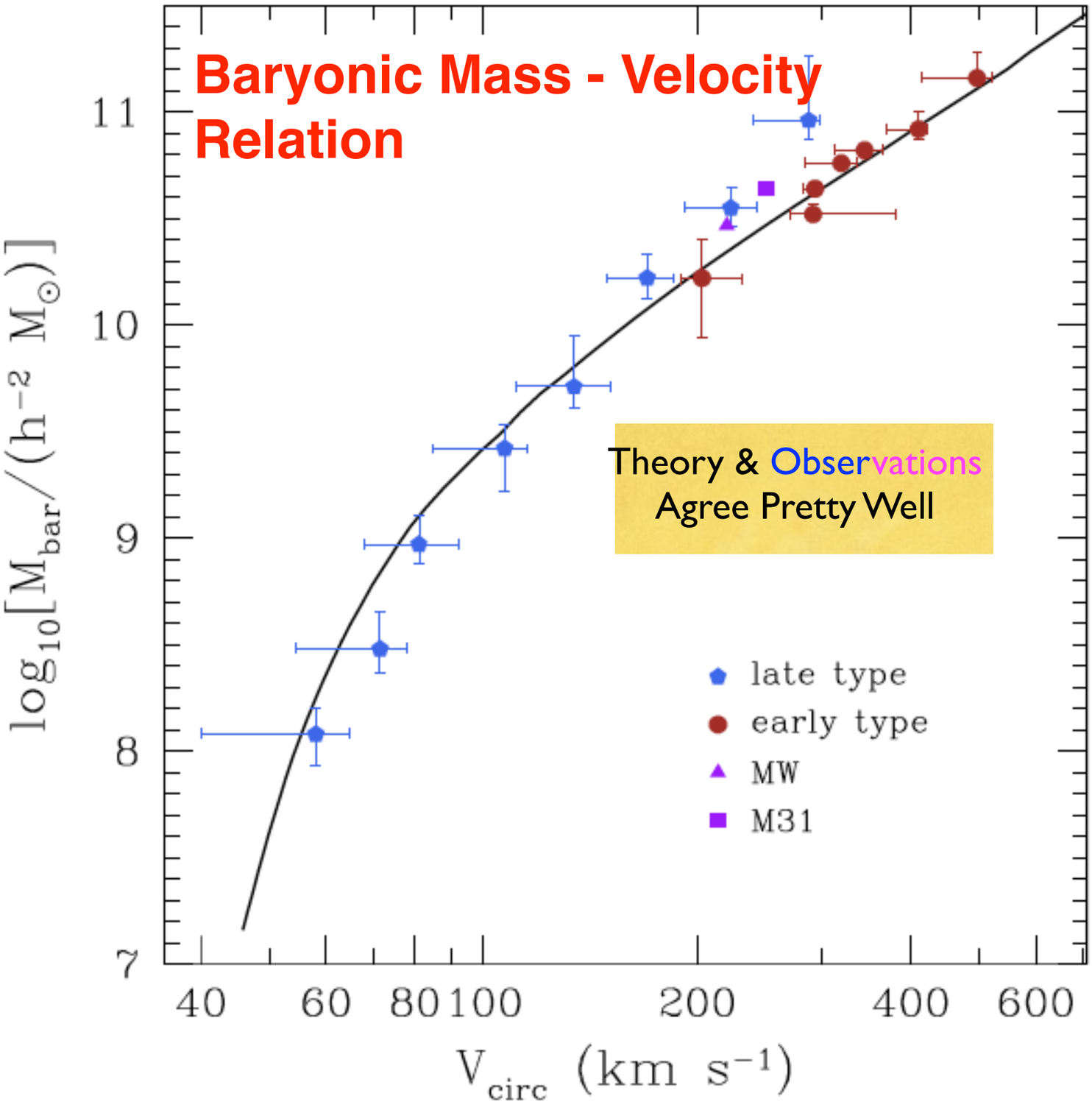

Trujillo-Gomez, Klypin, Primack, & Romanowsky ApJ 2011

Fig. 10.— Mass in cold baryons as a function of circular velocity. The solid curve shows the median values for the ΛCDM model using halo abundance matching. The cold baryonic mass includes stars and cold gas and the circular velocity is measured at 10 kpc from the center while including the effect of adiabatic contraction. For comparison we show the individual galaxies of several galaxy samples. Intermediate mass galaxies such as the Milky Way and M31 lie very close to our model results.

Bolshoi Sub-Halo Abundance Matching

Discrepancy due to incomplete observations or ΛCDM failure?

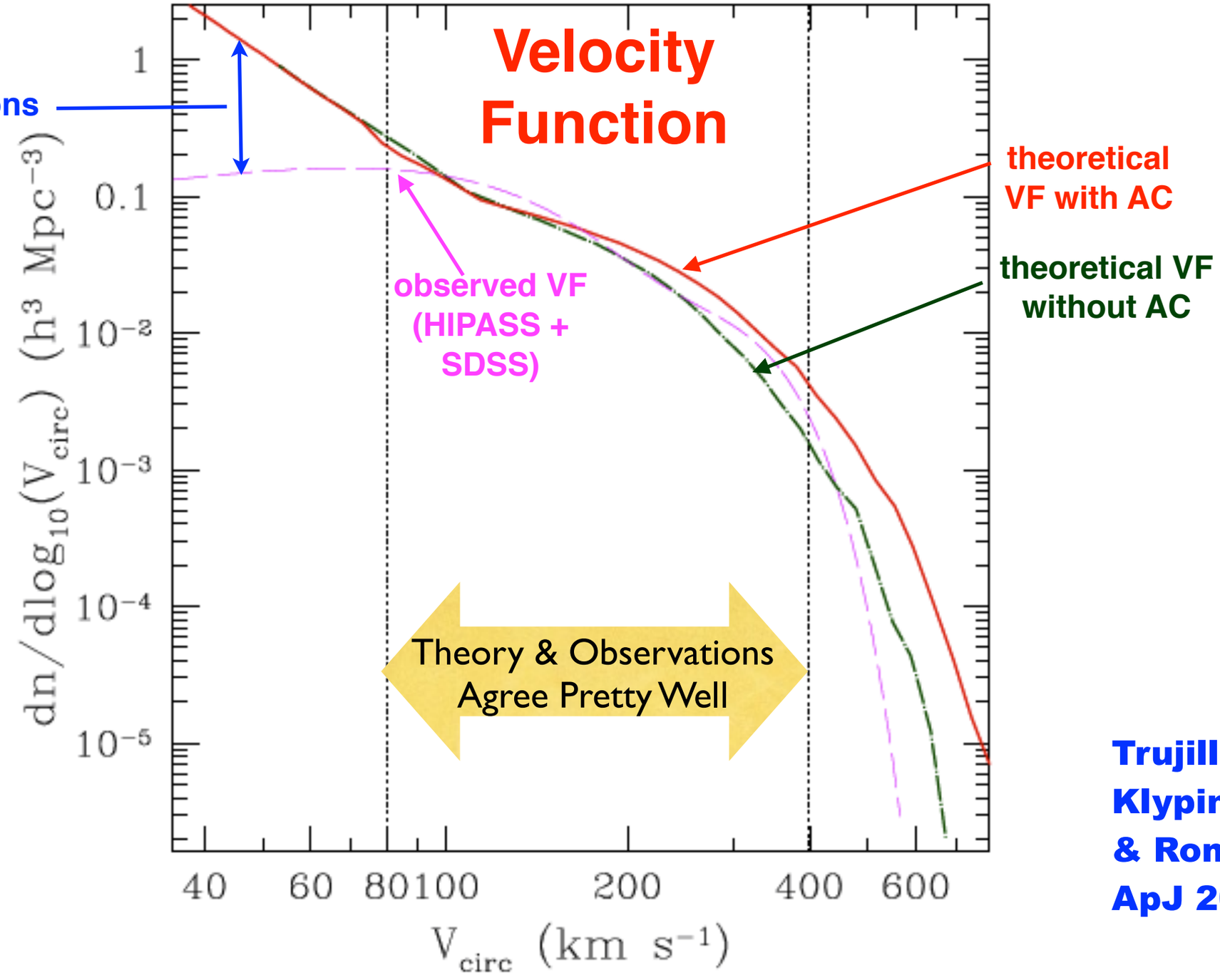

Trujillo-Gomez, Klypin, Primack, & Romanowsky ApJ 2011

Fig. 11.— Comparison of theoretical (dot-dashed and thick solid curves) and observational (dashed curve) circular velocity functions. The dot-dashed line shows the effect of adding the baryons (stellar and cold gas components) to the central region of each DM halo and measuring the circular velocity at 10 kpc. The thick solid line is the distribution obtained when the adiabatic contraction of the DM halos is considered. Because of uncertainties in the AC models, realistic theoretical predictions should lie between the dot-dashed and solid curves. Both the theory and observations are highly uncertain for rare galaxies with $V_{\rm circ} > 400$ km s^{-1}. Two vertical dotted lines divide the VF into three domains: $V_{\rm circ} > 400$ km s^{-1} with large observational and theoretical uncertainties; < 80 km s^{-1} $< V_{\rm circ} < 400$ km s^{-1} with a reasonable agreement, and $V_{\rm circ} < 80$ km s^{-1}, where the theory significantly overpredicts the number of dwarfs.

Presented at KITP Conf "First Light and Faintest Dwarfs" Feb 2012 and UCSC Galaxy Workshop Aug 2012

Klypin, Karachentsev, Nasonova 2012

Deeper Local Survey -- better agreement with ΛCDM but still more halos than galaxies below 50 km/s

Local Volume: D <10 Mpc

Total sample: 813 galaxies
Within 10 Mpc: 686
M_B<-13 N=304
M_B<-10 N=611

80-90% are spirals or dIrr (T>0)

Errors of distances are 8-10%

80% with D<10Mpc have HI linewidth

Vrot =
150x10^(-(20.5+M_B)/8.5)km/s

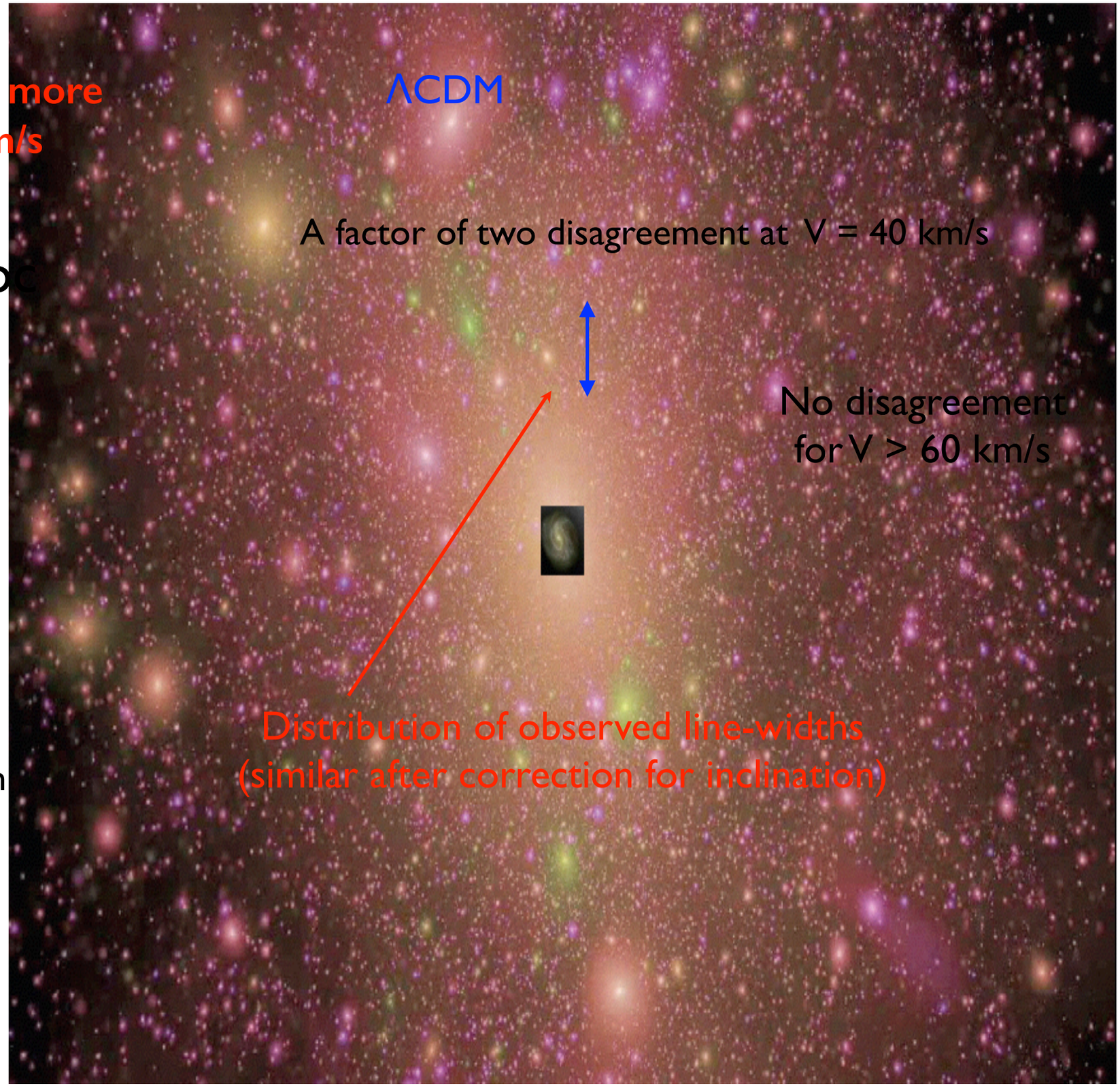

STELLAR MASS – HALO MASS RELATION

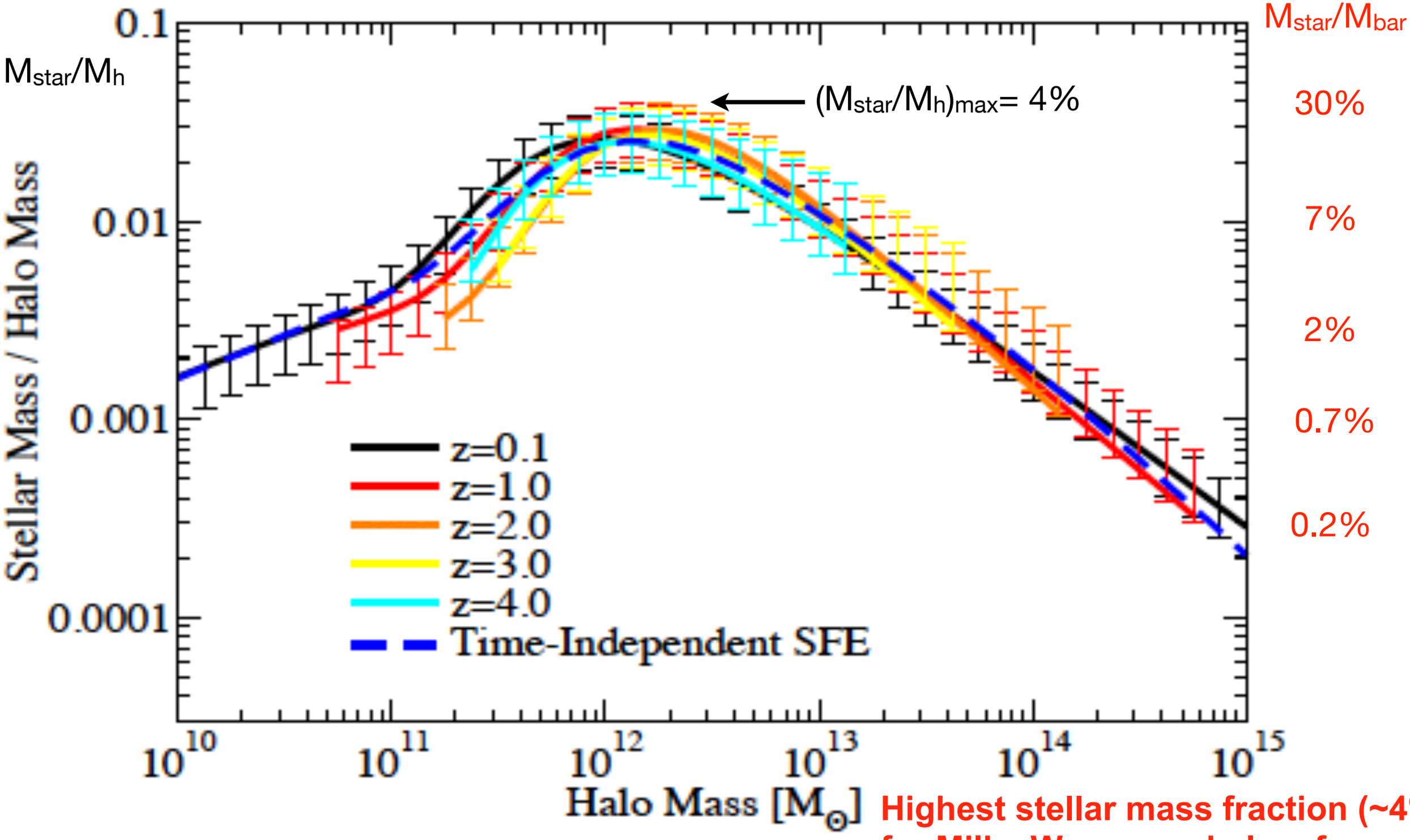

Cosmic baryon fraction = 0.045/0.31 = 14%
Milky Way M^*/M_{halo} = 0.3 x 14% = 4%

Highest stellar mass fraction (~4%) for Milky Way mass halos, for which stars are ≲30% of baryons.

Behroozi, Wechsler, Conroy ApJL, 762, L31 (2013)

Dependence of Halo Concentration on Mass and Redshift

Profiles of dark haloes: evolution, scatter, and environment

J. S. Bullock[1,2], T. S. Kolatt[1,3], Y. Sigad[3], R.S. Somerville[3,4], A. V. Kravtsov[2,5⋆], A. A. Klypin[5], J. R. Primack[1], and A. Dekel[3] 2001 MNRAS 321, 559

ABSTRACT

We study dark-matter halo density profiles in a high-resolution N-body simulation of a ΛCDM cosmology. Our statistical sample contains ∼5000 haloes in the range $10^{11} - 10^{14} h^{-1} M_{\odot}$ and the resolution allows a study of subhaloes inside host haloes. The profiles are parameterized by an NFW form with two parameters, an inner radius r_s and a virial radius R_{vir}, and we define the halo concentration $c_{vir} \equiv R_{vir}/r_s$. We find that, for a given halo mass, the redshift dependence of the median concentration is $c_{vir} \propto (1+z)^{-1}$. This corresponds to $r_s(z) \sim$ constant, and is contrary to earlier suspicions that c_{vir} does not vary much with redshift. The implications are that high-redshift galaxies are predicted to be more extended and dimmer than expected before. Second, we find that the scatter in halo profiles is large, with a 1σ $\Delta(\log c_{vir}) = 0.18$ at a given mass, corresponding to a scatter in maximum rotation velocities of $\Delta V_{max}/V_{max} = 0.12$. We discuss implications for modelling the Tully-Fisher relation, which has a smaller reported intrinsic scatter. Third, subhaloes and haloes in dense environments tend to be more concentrated than isolated haloes, and show a larger scatter. These results suggest that c_{vir} is an essential parameter for the theory of galaxy modelling, and we briefly discuss implications for the universality of the Tully-Fisher relation, the formation of low surface brightness galaxies, and the origin of the Hubble sequence. We present an improved analytic treatment of halo formation that fits the measured relations between halo parameters and their redshift dependence, and can thus serve semi-analytic studies of galaxy formation.

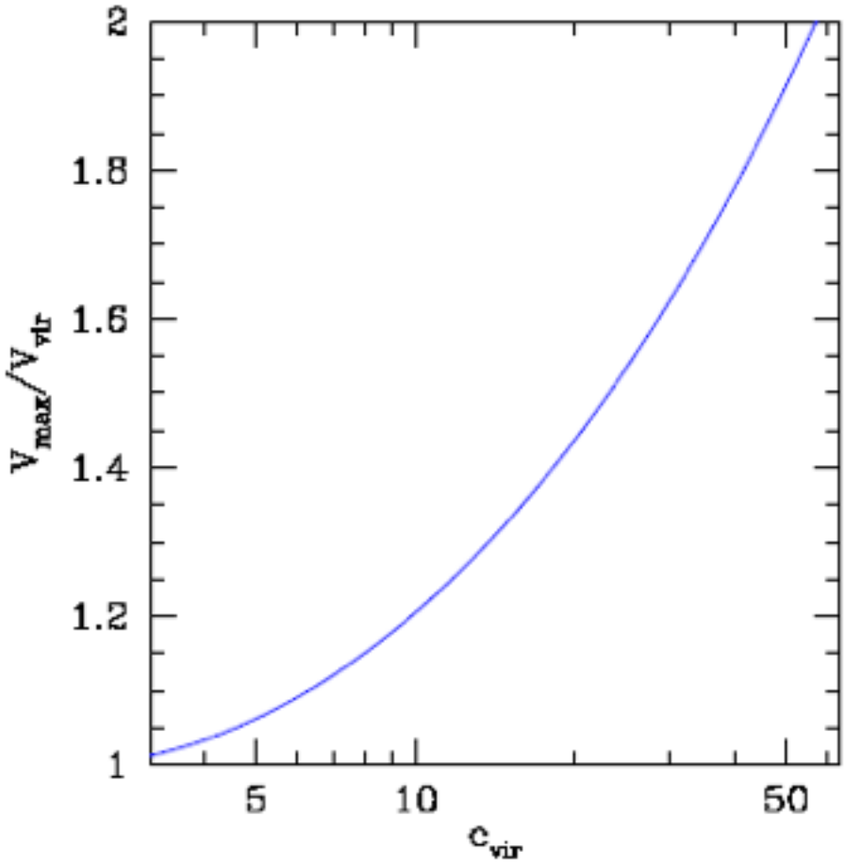

Figure 1. Maximum velocity versus concentration. The maximum rotation velocity for an NFW halo in units of the rotation velocity at its virial radius as a function of halo concentration.

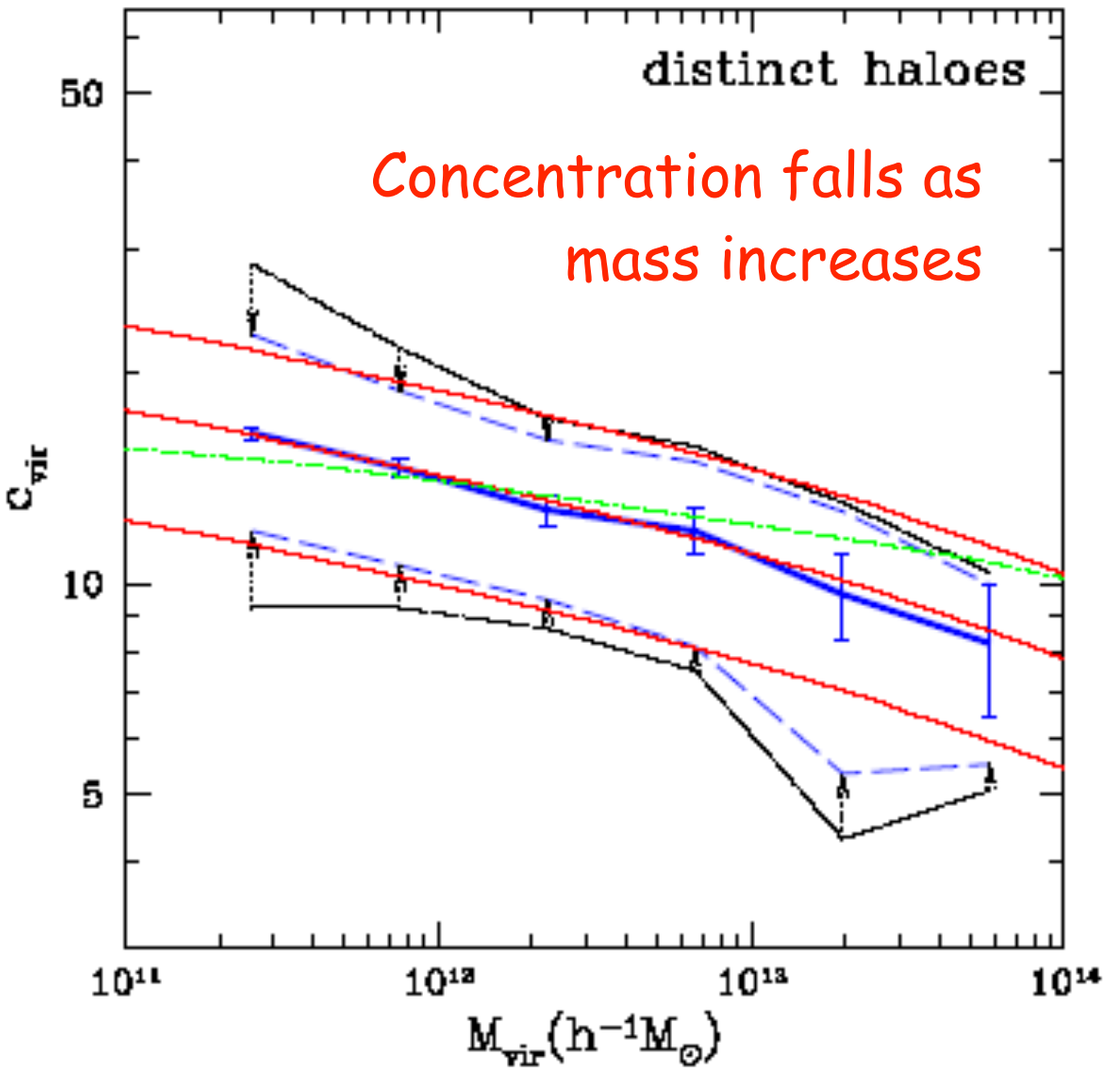

Figure 4. Concentration versus mass for distinct haloes at $z = 0$. The thick solid curve is the median at a given $M_{\rm vir}$. The error bars represent Poisson errors of the mean due to the sampling of a finite number of haloes per mass bin. The outer dot-dashed curves encompass 68% of the $c_{\rm vir}$ values as measured in the simulations. The inner dashed curves represent only the true, intrinsic scatter in $c_{\rm vir}$, after eliminating both the Poisson scatter and the scatter due to errors in the individual profile fits due, for example, to the finite number of particles per halo. The central and outer thin solid curves are the predictions for the median and 68% values by the toy model outlined in the text, for $F = 0.01$ and three different values of K. The thin dot-dashed line shows the prediction of the toy model of NFW97 for $f = 0.01$ and $k = 3.4 \times 10^3$.

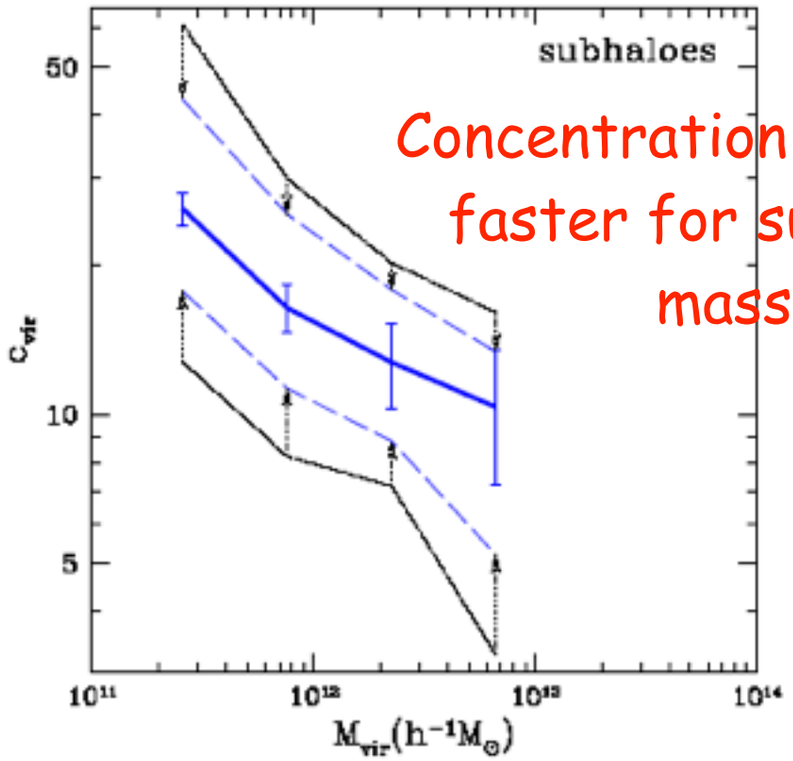

Figure 5. Concentration versus mass for subhaloes at $z = 0$. The curves and errors are the same as in Figure 4.

Bullock et al. 2001

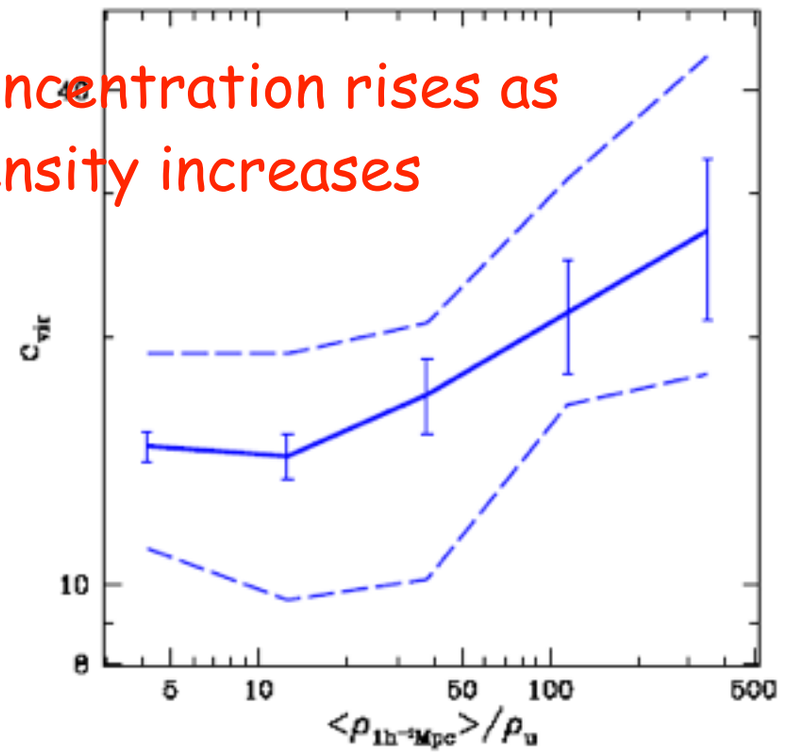

Figure 6. Concentrations versus environment. The concentration at $z = 0$ of all haloes in the mass range $0.5 - 1.0 \times 10^{12} h^{-1} M_\odot$ as a function of local density in units of the average density of the universe. The local density was determined within spheres of radius $1h^{-1}$Mpc. The solid line represents the median $c_{\rm vir}$ value, the error bars are Poisson based on the number of haloes, and the dashed line indicates our best estimate of the intrinsic scatter.

Spread of Halo Concentrations

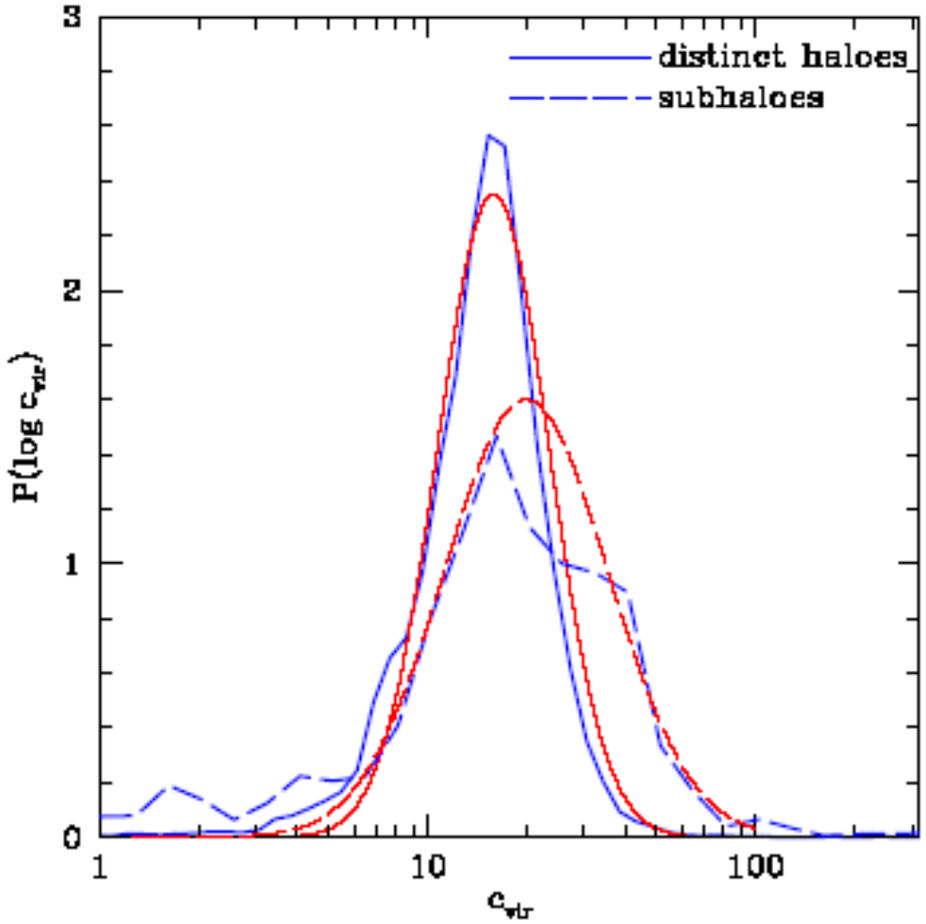

Figure 7. The probability distributions of distinct haloes (solid line) and subhaloes (dashed line) at $z = 0$ within the mass range $(0.5 - 1.0) \times 10^{12} h^{-1} M_{\odot}$. The simulated distributions (thick lines) include, the $\sim 2,000$ distinct haloes and ~ 200 subhaloes within this mass range. Log-normal distributions with the same median and standard deviation as the measured distributions are shown (thin lines). Subhaloes are, on average, more concentrated than distinct haloes and they show a larger spread.

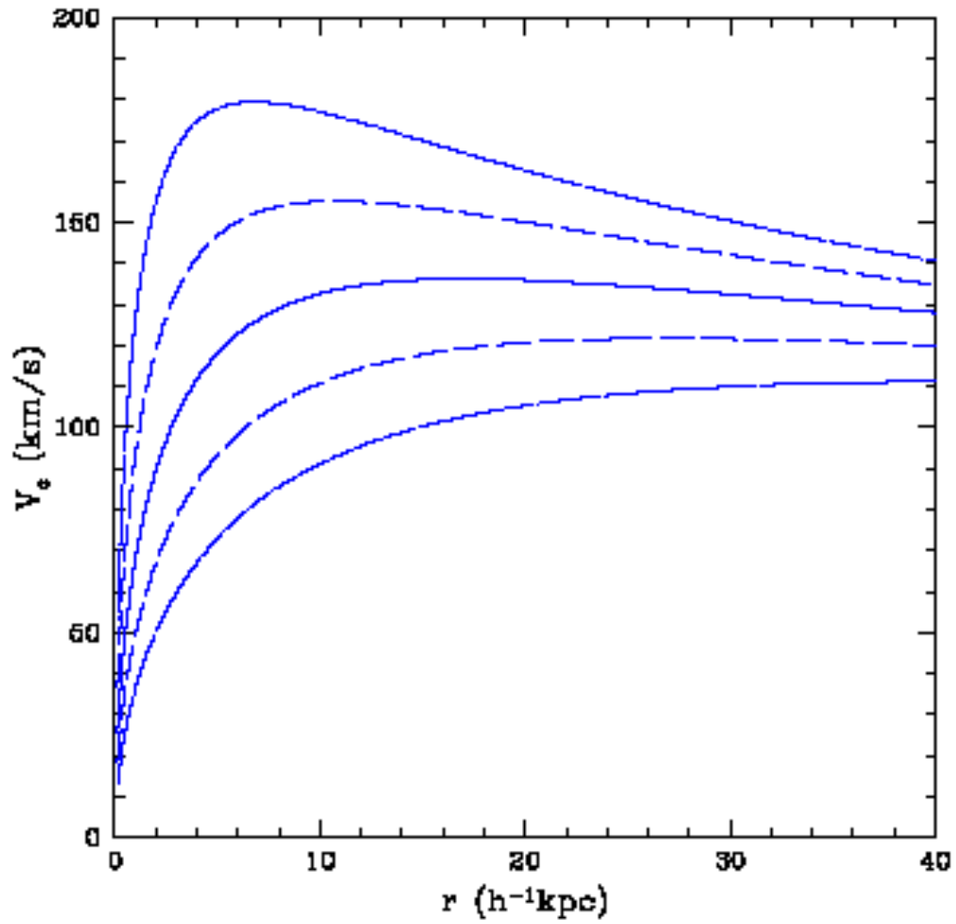

Figure 8. The spread in NFW rotation curves corresponding to the spread in concentration parameters for distinct haloes of $3 \times 10^{11} h^{-1} M_{\odot}$ at $z = 0$. Shown are the median (solid), $\pm 1\sigma$ (long dashed), and $\pm 2\sigma$ (dot-dashed) curves. The corresponding median rotation curve for subhaloes is comparable to the upper 1σ curve of distinct haloes.

Bullock et al. 2001

Evolution of Halo Concentration with Redshift

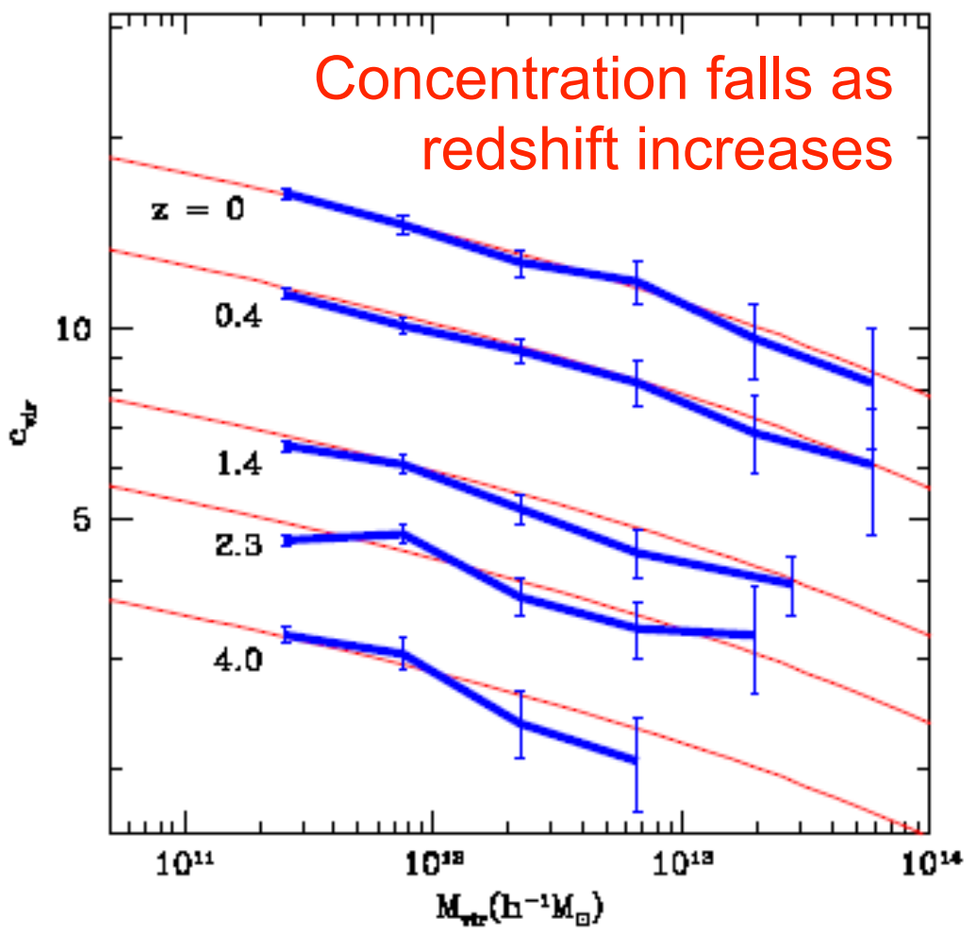

Figure 10. Median $c_{\rm vir}$ values as a function of $M_{\rm vir}$ for distinct haloes at various redshifts. The error bars are the Poisson errors due to the finite number of haloes in each mass bin. The thin solid lines show our toy model predictions.

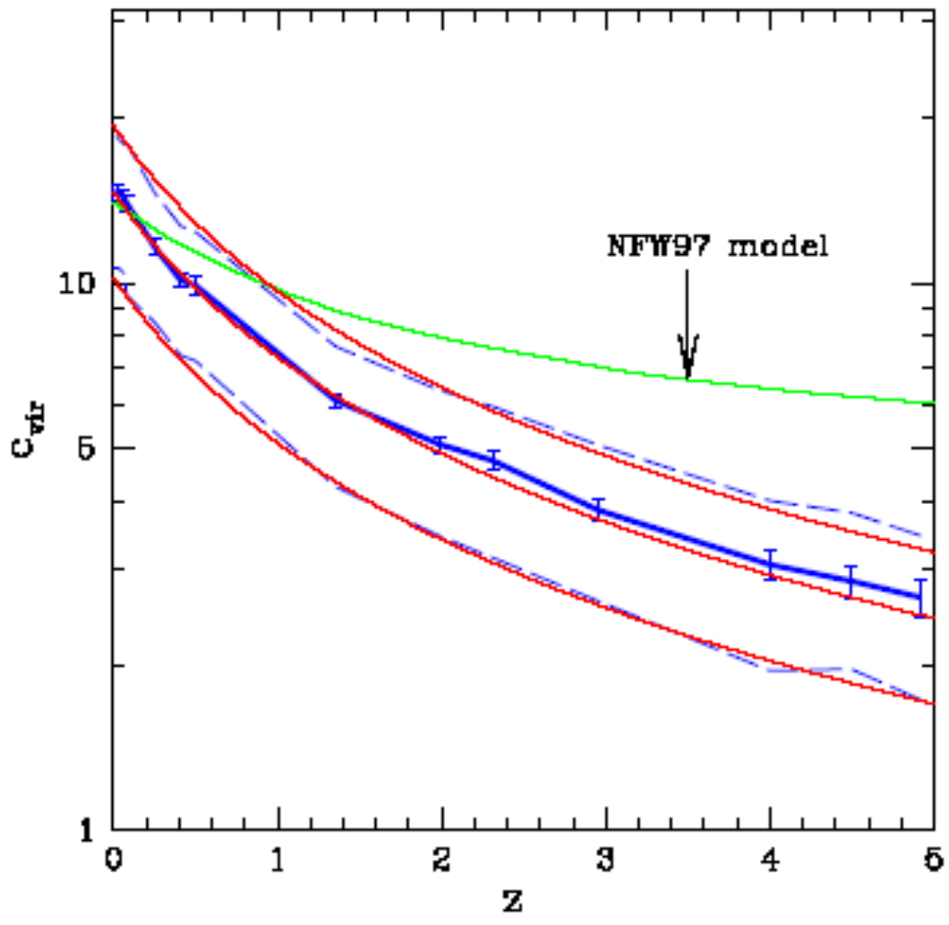

Figure 11. Concentration as a function of redshift for distinct haloes of a fixed mass, $M_{\rm vir} = 0.5 - 1.0 \times 10^{12} h^{-1} M_\odot$. The median (heavy solid line) and intrinsic 68% spread (dashed line) are shown. The behavior predicted by the NFW97 toy model is marked. Our revised toy model for the median and spread for $8 \times 10^{11} h^{-1} M_\odot$ haloes (thin solid lines) reproduces the observed behavior rather well.

$C_{vir} \propto 1/(1+z)$
at fixed mass

Bullock et al. 2001

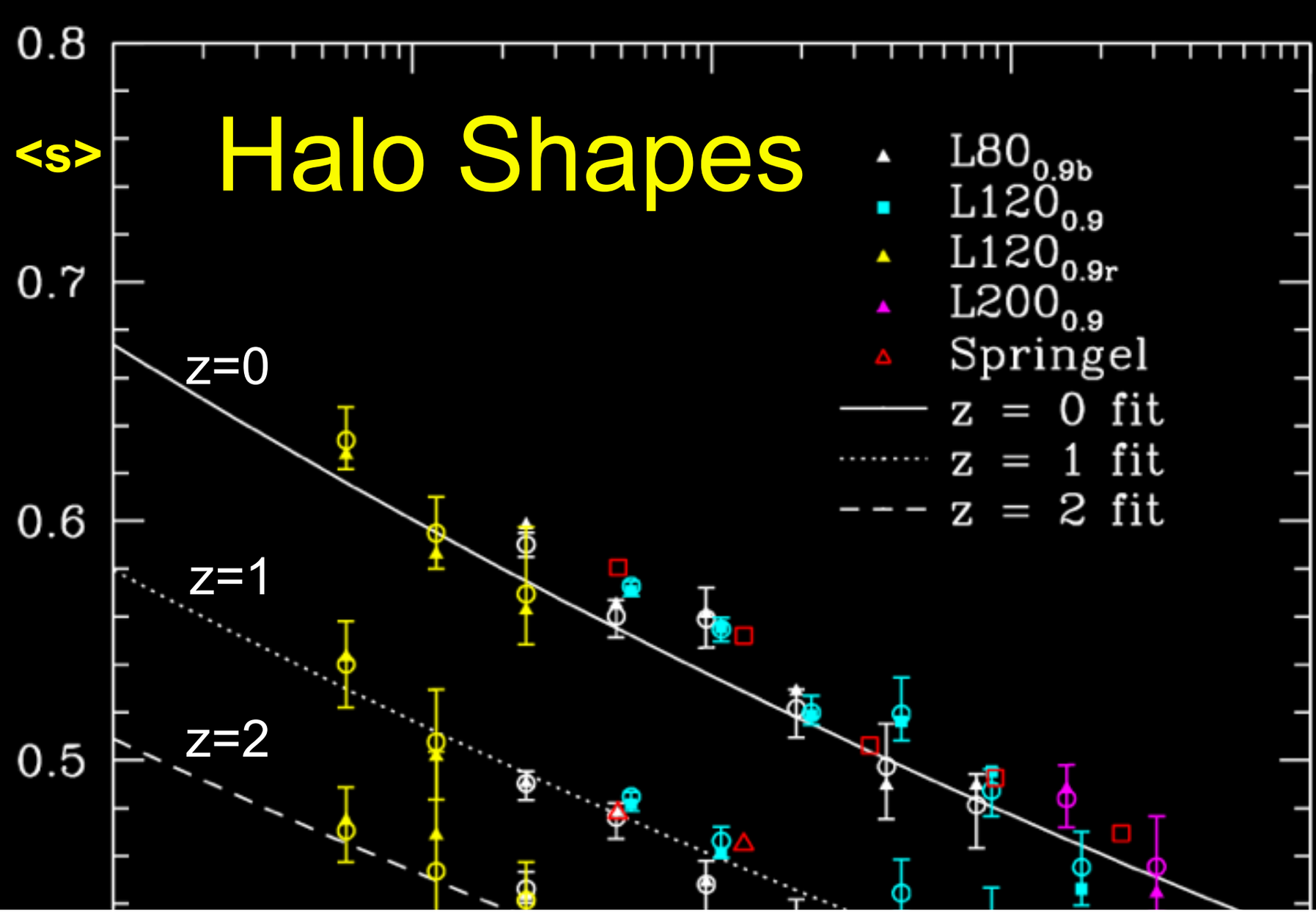

A simple formula describes these results, as well dependence on epoch and cosmological parameter σ_8 :

$$\langle s \rangle (M_{\rm vir}, z = 0) = \alpha \left(\frac{M_{\rm vir}}{M_*} \right)^{\beta}$$

with best fit values

$$\alpha = 0.54 \pm 0.03, \ \beta = -0.050 \pm 0.003.$$

<s> = short / long axis of dark halos vs. mass and redshift. Dark halos are more elongated the more massive they are and the earlier they form. We found that the halo <s> scales as a power-law in Mhalo/M*. Halo shape is also related to the Wechsler halo formation scale factor a_c.

Allgood+2006

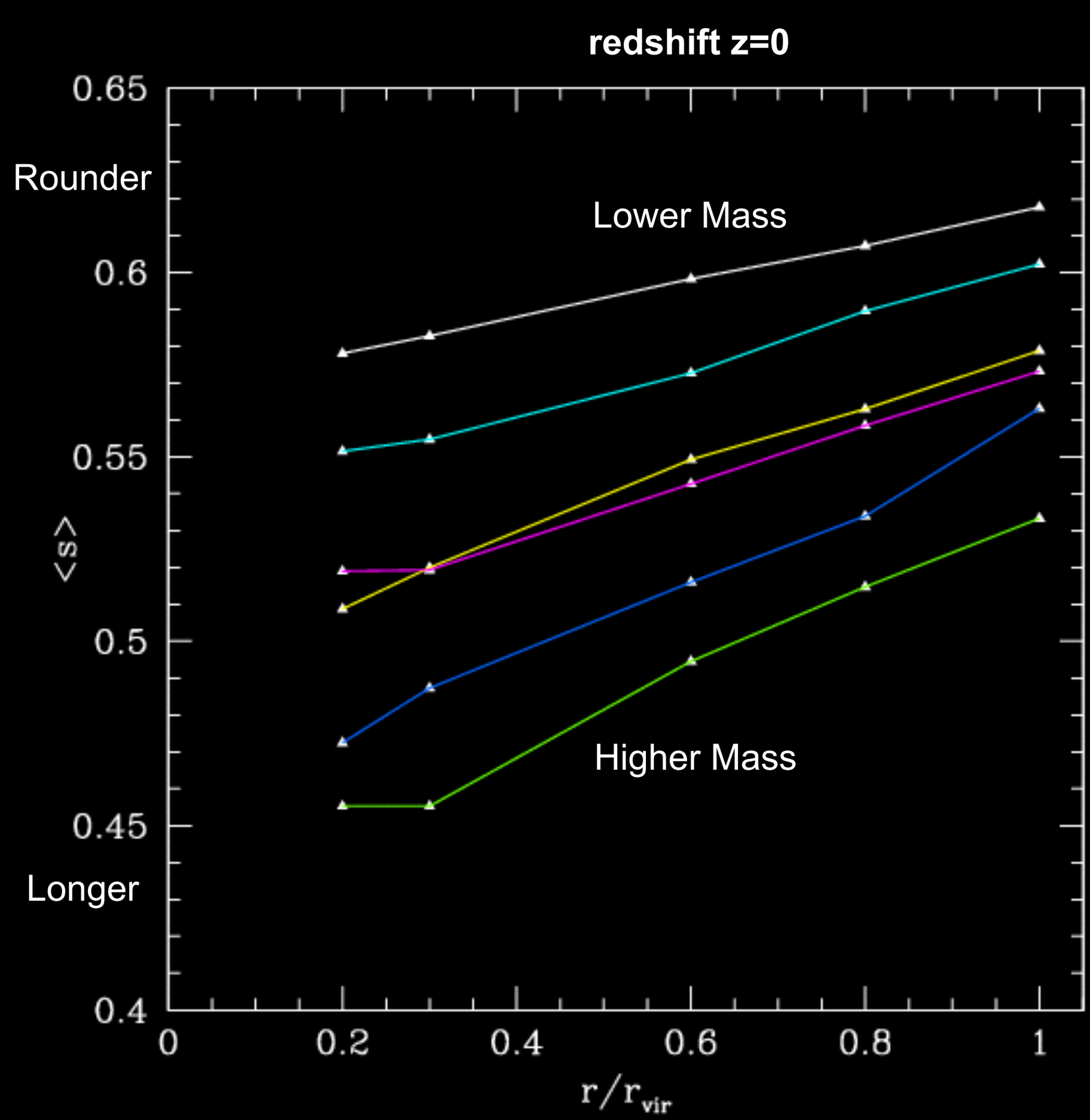

Halos become more spherical at larger radius and smaller mass. As before,

$$s = \frac{\text{short axis}}{\text{long axis}}$$

These predictions can be tested against cluster X-ray data and galaxy weak lensing data.

Allgood+2006

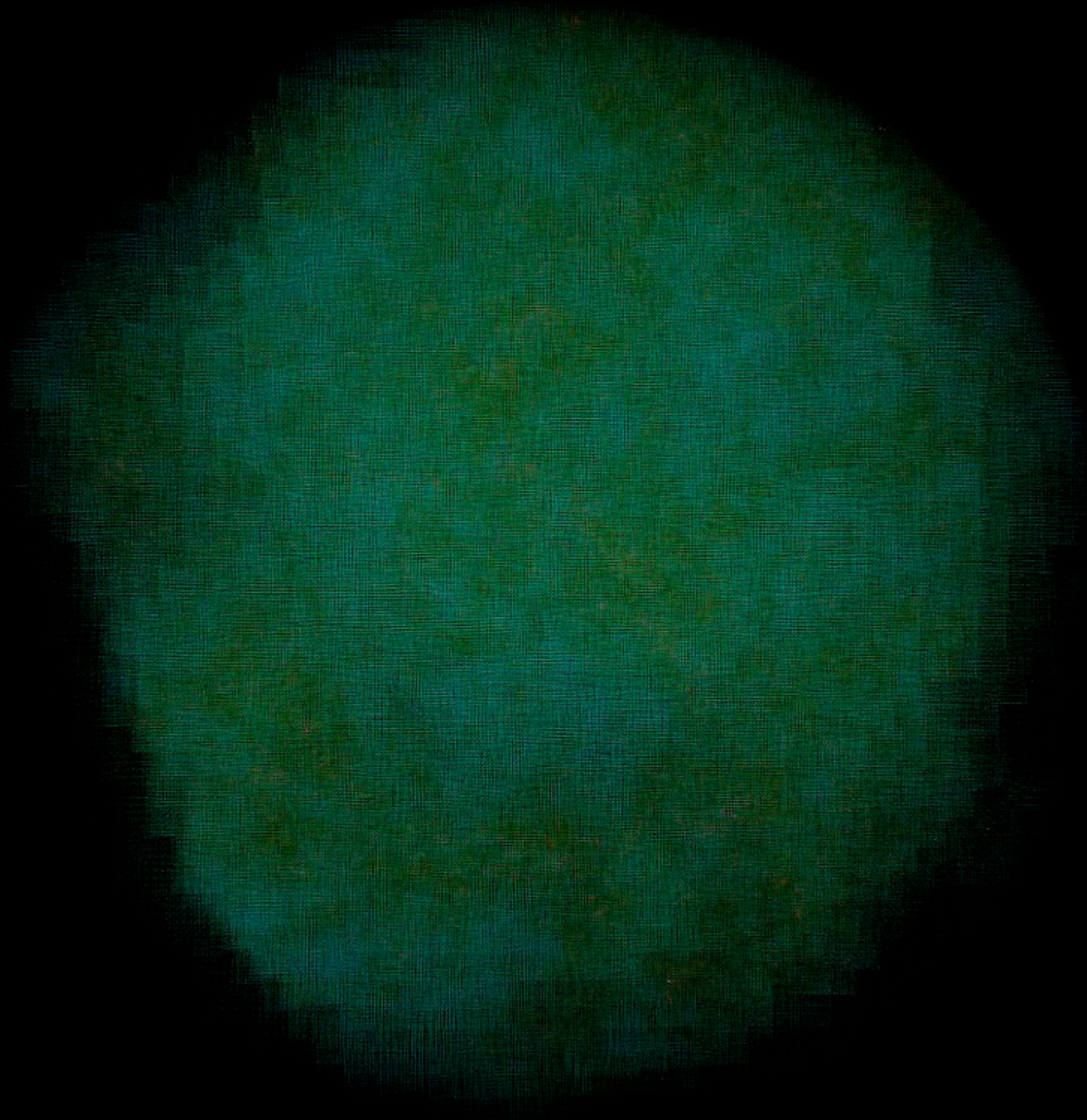

Columbia
Supercomputer
NASA Ames
2005

Simulation:
Brandon
Allgood &
Joel Primack

Visualization:
Chris Henze

(rotation to
show 3D)